Modular Wireless Trackside Signalling System – Towards Rail Internet of Things (RIoT)



Thesis submitted to the University of Nottingham to obtain the degree of

Doctor of Philosophy

in Electrical and Electronic Engineering

by

Armando Méndez Villalón, B.Sc., M.Eng.

Supervised by

Dr. Steve Greedy and Prof. Dave W.P. Thomas

George Green Institute for Electromagnetics Research - GGIEMR
Department of Electrical and Electronic Engineering

The University of Nottingham, University Park, UK

November, 2019

Abstract

Railway operations are becoming increasingly automated and integrated through the use of Information and Communication Technology. Advance signalling systems efficiently handle the traffic among a railway network providing the ability to increase the population of rolling stock on the same track with a precise time slot for each of them, as well as diminishing risks by human error.

Recently, wireless signalling systems are being accepted as a feasible option to overcome wired infrastructure, aiming to create a cheaper system yet with a high level of reliability. Lower installation and maintenance costs would result in significant savings that could be passed on to the service provider and ultimately the users through a reduction in costs and travel time for passengers and freight transportation. However, there exist a greater number of variables to consider in order to have a stable communication link, such as weather conditions, terrain configuration, interference and noise.

Given the recent tendency of utilising decentralised networks and the use of Internet-of-Things (IoT), railway infrastructure manufactures are moving towards the development of a signalling network system to control and monitor railway traffic remotely and wirelessly, with the use of modular sensors, and sending the data through cloud computing systems. This is known as Rail Internet-of-Things (RIoT) due to its application for railway.

Candidate wireless systems were investigated, ZigBee was chosen and proven through this work to be robust within an increasingly complex environment and tested under extreme conditions in laboratory so as proofed against future sources

of interference.

Motivated by this, in this work a ZigBee-protocol-based wireless signalling system is presented as an alternative to current infrastructure, that ultimately will require a less arduous implementation in terms of labour, and simultaneously being low cost whilst considering its performance within the complex environment found in and around rail infrastructure.

A portion of this work is dedicated to studying and implementing the set ups within laboratory facilities to recreate certain realistic environments given by the nature of the scenarios or by multiple sources of interference or noise, aiming to develop a benchmark for testing performance of wireless devices within a laboratory facility.

The complete system is demonstrated to operate within a real-world rail environment supporting observation on robustness seen in the laboratory-based scenarios. The rail tests along with meetings and demonstrations held with rail operators concluded that the wireless solution developed through this work to be a candidate for wide area signals control, but also for more localised applications in and around level crossing installations or applications requiring rapid deployment for example in and around rail works that require temporary or ad-hoc signalling to be deployed.

Publications

Angelo Gifuni, Gabriele Gradoni, Christopher Smartt, Steve Greedy, Armando Mendez-Villalon, Luca Bastianelli, Franco Moglie, Valter Mariani Primiani, Stefano Perna, and Dave W.P. Thomas, "Latest developments on the Shielding Effectiveness Measurements of Materials and Gaskets in Reverberation Chambers". *IET Science, Measurement & Technology.* (Accepted) 2019.

Armando Mendez-Villalon, Dave W.P. Thomas, and Steve Greedy, "Performance Study of ZigBee Networks in a Rail Environment for Signalling Systems". *IEEE International Conference on Models and Technologies for Intelligent Transportation Systems.* Naples, Italy, 2017.

Armando Mendez-Villalon, Stephen Greedy and Dave W. P. Thomas, "Robustness Study of ZigBee Networks in an EM Environment for Railway Signalling Systems". *IEEE International Conference on Intelligent Rail Transportation.* Birmingham, 2016.

Mohamed Samra, Shiemaa Sidahmed, Stephen Greedy and Armando Mendez-Villalon, "Feasibility Analysis and Novel Implementation of Wireless Technologies for Railway Signalling". *IEEE International Conference on Intelligent Rail Transportation.* Birmingham, 2016.

Dedication

I dedicate this work to my parents Irma and Adolfo, and my brother Fito.

Declaration

This work has been carried out by Mr. Armando Méndez Villalón under the supervision of Dr. Steve Greedy and Prof. Dave W. P. Thomas in the George Green Institute for Electromagnetics Research - GGIEMR, part of the Department of Electrical and Electronic Engineering, The University of Nottingham, University Park, U.K.

Acknowledgment

I am highly thankful for all the patience and support provided unconditionally by my supervisors Dr Steve Greedy and Prof. Dave W.P. Thomas. Additionally, to my internal assessor Dr Ana Vukovic, for the discussion and her valuable suggestions during the annual reviews.

I am also thankful to Dr Chris Smartt for his advices and help during the realisation of my experiments in the laboratory. Thanks to my friends and colleagues Mir, Hafiz and Michael for all the memories and experiences we shared together during all this time.

This project was possible to a partnership established between the University of Nottingham, led by Dr Steve Greedy, and Thales Ground Transportation Systems, led by Richard Carr, Ben Pritchard, Ken Peters.

Finally, the realisation of my PhD studies was supported in full by the National Mexican Council of Science and Technology (Consejo Nacional de Ciencia y Tecnología) through the grant 250828/372910.

List of Figures

1.1 Example of coupling mechanisms. 27

1.2 Example of coupling mechanisms in a railway infrastructure.[5] 28

2.1 Wolfson Building location denoted by the yellow rectangle and the tram track by the red line 35

2.2 EMCO 6404 Helmholtz Coil. 36

2.3 NET2 EMI threat analysis graph with threats up-to-date at 22 November 2013 [8] 38

2.4 Antenna locations inside the Pharmacy Building of the University of Nottingham. 40

2.5 Loop antenna set-up the Pharmacy Building 41

2.6 Log-periodic antenna set-up the Pharmacy Building 41

2.7 Data logged across time before activation of the OHL 42

2.8 Data logged across time following activation of the OHL 43

2.9 Maximum values comparison, before and after the power lines went on. The outgrowths observed correspond to GSM mobile and TV broadcasting services . 44

2.10 Emissions before the activation of the OHL. 45

2.11 Emissions following the activation of the OHL. 46

2.12 Maximum values comparison measured before and after the lines were in operation. 47

2.13 Aerial view of the Long Marston test track 49

3.1 Interior of an anechoic chamber 57

3.2 Pyramidal absorbers used. The section has 81 pyramids of 21 cm height and square base of 6.5 cm of length 58

3.3 Example of a ferrite tile 59

3.4 Internal reflection and phase cancellation method used in the Salisbury screen . 60

3.5 Gigahertz Transverse Electromagnetic Cell schematic 61

3.6 Inside of a RC displaying the metallic walls and with an antenna array set-up [22] 62

3.7 Stirrers of a RC. When in operation, they modify the internal geometry of the chamber [22] 63

3.8 RC diagram 64

3.9 External and internal dimensions 65

3.10 Working volume dimensions 65

3.11 Total number of modes as a function of frequency 66

3.12 Mode density per MHz 67

3.13 Typical immunity test set-up in RC 70

3.14 Emissions test set-up in RC 71

3.15 Working volume 75

3.16 Standard deviation of data for E-field components of 8 probes and field uniformity. 78

3.17 Chamber Calibration Factor 79

3.18 Insertion Loss of an unloaded RC 80

3.19 Chamber Q-factor using S_{21} measurements 81

3.20 Chamber Q-factor up to 2 GHz using S_{21} measurements 82

3.21 Strong direct coupling measured in the RC. The centroid (black dot) is displaced (black arrow) from the centre of the plane (red square), meaning that the average is not located in 0 88

3.22 Little direct coupling measured in the RC. The centroid is now located at the centre of the plane in 0 (red square) 89

3.23 Antennas and absorbers set-up inside the RC 90

3.24 Comparison of resultant K-factor by modifying the loading levels in RC 91

3.25 Comparison of resultant K-factor by modifying the loading levels in RC 92

3.26 Comparison of resultant K-factor by modifying the antenna polarisation in RC with 8 absorbers 93

3.27 Cubic absorber in the RC elevated 2m from the ground plane 94

3.28 Comparison of resultant K-factor by modifying the loading levels in RC 95

3.29 Pantograph producing a spark as it moves along the power line 96

3.30 Typical and representative waveform of the output current produced by the ESD generator [44] 97

3.31 ESD gun set-up screen. 99

3.32 Schematic of table-top set-up for ESD laboratory test 100

3.33 Schematic of circuit closed loop for the ESD table-top test. 100

3.34 Contact discharge set-up for RF emission on the a vertical coupling plane (VCP). 101

3.35 Air discharge projected onto a PCB. 102

3.36 Contact discharge configuration. 103

3.37 Contact discharge set-up for RF emission. 104

4.1 FHSS spectra occupancy . . . 108
4.2 FHSS scheme . . . 109
4.3 DSSS transmission scheme. a) Tx, b) Rx . . . 110
4.4 Narrow Band to a Spread Spectrum signal schematic. . . . 110
4.5 Example of DSSS modulation. a) Original signal, b) PN code, c) Resultant signal 111
4.6 CSK transmitter block . . . 114
4.7 CSK receiver block . . . 115
4.8 Fixed-block scheme. The train footprint and braking curve are constant. . . . 120
4.9 Moving-block scheme. The train footprint, safety distance and braking curve are calculated based on the track occupancy and train speed. . . . 120
4.10 Braking curves variation at low speed a) and high speed b) in moving block scheme . . . 121
4.11 Train-ground communication in CBTC . . . 122
4.12 Eurobalise installed on the track . . . 125
4.13 ETCS Level 1 [56] . . . 125
4.14 ETCS Level 2 [56] . . . 126
4.15 ETCS Level 3 [56] . . . 126
4.16 TWPS Loop Sensor . . . 128
4.17 TWPS Schematic [52, 58] . . . 128
4.18 On-board and track elements of AWS [52] . . . 129

5.1 Example of channels available for XBee use, and its current, maximum and average transmitting powers during a test. . . . 138
5.2 Default and total frequency occupancy of XBee: all channels active . . . 139

5.3 Channel Mask Band 1 occupancy 140

5.4 Channel Mask Band 2 occupancy 141

5.5 Channel Mask Band 3 occupancy 142

5.6 LBT+AFA deactivated: only 868.95 MHz band available 143

5.7 Frame division 144

5.8 Network topologies. a) Star b)Peer-to-peer 145

5.9 Point-to-point topology 146

5.10 Repeater topology 146

5.11 Mesh topology 147

5.12 RFID schematic 148

5.13 Network elements 149

5.14 Time delay measured with multiple packet sizes. 155

5.15 Spectrum occupancy at the test track. The ellipse in the graph contains the frequency occupancy of GSM mobile services 157

5.16 Interference generated. Half of XBee bandwidth, equivalent to 50% of the XBee channels dedicated to transmit on. 160

5.17 Interference generated. Three quarters of XBee bandwidth, equivalent to 75% of the XBee channels dedicated to transmit on. 161

5.18 Spectrum occupancy by the inference signal generated, aiming to block 50% of the available XBee channels to transmit 162

5.19 Spectrum occupancy by the inference signal generated, aiming to block 75% of the available XBee channels to transmit 163

5.20 Throughput reached by XBee at specific stirrer positions in one rotation with 30 channels (black line), 15 channels (red line) and 8 channels (blue line) available for communication 164

5.21 Emissions generated by the ESD gun in the RC. 166

5.22 Emissions caused by the ESD gun in the RC centred in the XBee bands. . . . 167

5.23 ESD test set-up in RC for immunity testing 168

5.24 Spectrum occupancy by the ESD and the XBee radio 169

5.25 Throughput obtained whilst the spark generator is in operation. 170

5.26 RSSI measured whilst the spark generator is in operation. Red line is the Tx and green line is Rx 170

5.27 Spectrum occupancy by the ESD and the XBee radio with LBT+AFA disabled. 171

5.28 Throughput obtained whilst the spark generator is in operation. 172

5.29 RSSI measured whilst the spark generator is in operation. Red line is the Tx and green line is Rx 172

5.30 XBee signal with LBT+AFA enabled and -30dBm noise signal. 174

5.31 XBee signal with LBT+AFA disabled and 0 dBm noise signal 175

5.32 XBee signal with LBT+AFA disabled and 20 dBm noise signal 176

5.33 XBee and arduino interconnection. 177

5.34 Signalling system prototype with traffic lights. 178

5.35 On-Board unit and Light Node in the background. 180

5.36 Tx-Rx RSSI measurements 182

5.37 Quadratic approximation 183

5.38 RSSI detection areas 184

5.39 RSSI as function of the distance 184

5.40 RFID antenna located at the trackside. 186

5.41 One of the two RFID tags placed at the front and rear of the train 187

6.1 Redundancy action 192

A.1 Control Centre Interface 194

A.2 On-board Unit Interface 195

List of Tables

2.1 Frequency allocation in the UK 44

2.2 Electromagnetic emissions limits for signalling systems apparatus 53

3.1 Field deviation limits of the DO 160 standards 69

3.2 Samples and turn positions recommended 74

3.3 Standard deviation limits set by the standard BS EN 61000-4-21 for RC calibration 77

3.4 Test voltages specified in the IEC 61000-4-2 standard 98

3.5 Test voltages specified in the IEC 61000-4-2 standard 98

4.1 ISM bands in Europe 107

4.2 Logic table for DSSS modulation 111

4.3 Bluetooth classes 117

4.4 Comparison between Wireless PAN technologies [49] 118

4.5 Grades of Automation [54] 123

5.1 Frequency bands and data rates for the 802.15.4 standard 134

5.2 Channel frequencies available for the XBee module 136

5.3 Channel Mask bands 140
5.4 RFID Channel frequencies 148
5.5 Current consumed by XBee with a power source of 12V DC 153
5.6 Average throughput achieved in a unloaded RC. 158
5.7 Average throughput achieved in a loaded RC with different k-factor 158
5.8 Throughput and success rate measured in the RC 165
5.9 Throughput and success rate measured in the RC in presence of the ESD . . . 172
5.10 Throughput and success rate measured in the RC in presence of noise. 173
5.11 Photographs taken during the rail test 179

List of Abbreviations

AFA ..... Automatic Frequency Agility

AP ..... Access Point

AWGN ..... Additive White Gaussian Noise

BER ..... Bit Error Rate

BPSK ..... Binary Phase Shift Keying

BS ..... Base Station

CBTC ..... Communications-Based Train Control

CC ..... Control Centre

CSMA ..... Carrier Sense Multiple Access

EMC ..... Electromagnetic Compatibility

EMI ..... Electromagnetic Interference

ERTMS ..... European Rail Traffic Management System

ESD ..... Electrostatic Discharge

FHSS ..... Frequency-Hopping Spread Spectrum

FH-CDMA ..... Frequency-Hopping Code Division Multiple Access

GPS ..... Global Positioning System

GSM ..... Global System for Mobile Communication

GTEM ..... Gigahertz Transverse Electromagnetic Cell

ISM ..... The Industrial, Scientific, and Medical radio band

IoT ..... Internet of Things

LBT ..... Listen Before Talk

LOS ..... Line-of-Sight

LTE ..... Long-Term Evolution

MIMO ..... Multiple Input Multiple Output

MPC ..... Multipath Component

MAC ..... Medium Access Control

NLOS ..... Non-Line of Sight

OU ..... On-board Unit

OFDM ..... Orthogonal Frequency Division Multiple Access

OHE ..... Over Head Equipment

OHL ..... Over Head Line

PAN ..... Personal Area Network

PDF ..... Probability Density Function

PDP ..... Power Delay Profile

PER ..... Packet Error Rate

PHY ..... Physical Layer

PSD ..... Power Spectral Density

QAM ..... Quadrature Amplitude Modulation

QPSK ..... Quadrature Phase Shift Keying

QoS ..... Quality of Service

RC ..... Reverberation Chamber

RF ..... Radio Frequency

RIoT ..... Rail Internet of Things

RFI ..... Radio Frequency Interference

RMS ..... Root Mean Square

SPAD ..... Signal Passed At Danger

TDMA ..... Time Division Multiple Access

TS ..... Time Slot

WCDMA ..... Wideband Code Division Multiple Access

WiFi ..... Wireless Fidelity

WLAN ..... Wireless Local Area Network

WMAN ..... Wireless Metropolitan Area Network

WPAN ..... Wireless Personal Area Network

Contents

1 Introduction **23**

1.1 Advantages and Challenges of Wireless Communications Technologies 23

1.2 Spectrum Allocation for Current Wireless Communications 25

1.3 Electromagnetic Measurements 26

1.3.1 Interference 26

1.3.2 Compatibility 28

1.3.3 Internet-of-Things 30

1.4 Project Goals 31

1.5 Thesis Structure 32

2 Electromagnetic Environment Measurements - Real Rail Scenarios **34**

2.1 Previous Emission Measurements - Simulated conditions 36

2.2 Measurements with active Overhead Lines 39

2.3 Test Track Scenario 47

2.3.1 Challenges 50

2.4 Railway Standards 52
2.5 Conclusion 53

3 Experimental Environments 55

3.1 Experimental Tools 55
3.1.1 Anechoic Chamber 56
3.1.2 Gigahertz Transverse Electromagnetic Cell 60
3.1.3 Mode Stirrer Reverberation Chamber 61
3.1.4 Standards for radiated emissions and immunity applications 68
3.2 Rayleigh & Rician environments 83
3.3 Representation of a Overhead Line within a Reverberation Chamber 96
3.4 Conclusion 104

4 Wireless Communication Technologies and Train Infrastructure 106

4.1 Wireless Communication Technologies 106
4.1.1 Modulation Techniques: Spread Spectrum 107
4.1.2 Frequency-Hoping Spread Spectrum 107
4.1.3 Direct-Sequence Spread Spectrum 109
4.1.4 CDMA 112
4.1.5 CSK 113
4.1.6 Low-power Consumption Communication Technologies . . . 116
4.2 Communication Systems for Railway Transportation 119
4.2.1 Communication-Based Train Control 119

4.2.2 European Rail Traffic Management System 124
4.2.3 Driver Assistance Systems 127
4.3 Conclusion 130

5 Towards an Alternative Solution for Railway Signalling Systems Applications 131

5.1 ZigBee Implementation 132
5.1.1 IEEE 802.15 protocol 132
5.1.2 XBee Modules 135
5.1.3 Frame format 144
5.1.4 Network Topologies 144
5.2 Radio-Frequency Identification 147
5.3 System Design and Description 149
5.4 Performance Metric Parameters 150
5.5 Performance assessment 153
5.5.1 Evaluation in Environments Simulated in a RC 157
5.5.2 Co-existence with other signals 159
5.5.3 Spark Generator 165
5.5.4 Additive Gaussian White Noise 173
5.6 Proposed prototype 176
5.6.1 Signalling system 177
5.6.2 Detection and Location System 181
5.6.3 Train Integrity 187

5.7 Conclusion 188

6 Conclusion **189**

6.1 Realistic Wireless Environments 190

6.2 Future research 191

6.3 Security 193

A LabVIEW Interface **194**

Chapter 1

Introduction

In this chapter a brief overview of the wireless communication systems, electromagnetic interference and the goals of this manuscript is presented, as well as a comparison with the wired communication systems. Wireless systems are exposed to multiple mechanisms that generate interference that can contribute to the corruption of the message being transmitted. Every commercial wireless device must comply with the spectrum allocation and emission to operate, especially in licence free bands such as the Industrial, Scientific and Medical radio band. The chapter will conclude with the project goals and the structure of this thesis.

1.1 Advantages and Challenges of Wireless Communications Technologies

Nowadays as technology, micro-controllers and semiconductors evolve, communication systems evolve rapidly as well. Having the ability of removing a physical connection to share information is highly convenient as no additional infrastructure is required other than the devices themselves. The high demand creates an increase in population of such devices. All of these devices share the same communication channel: the environment.

Digital communications over wired systems is highly reliable, but limited to the length of the wire between transmitter (Tx) and receiver (Rx). Increasing the distance between Tx and Rx implies an increment in infrastructure required. At the same time, increasing the length of the wire causes losses after a certain point. Usually for wired systems, the cable losses are not considered for a given section of the cable, and it does not disrupt the original signal. Beyond a certain length, losses should be considered, and additional hardware is advised to cope with losses and amplify the signal to a suitable delivery level.

Usually, coaxial and twisted pair cables are used for wired communication systems. As the length of the transmission line increases the loses are proportionally significant. Additionally, as the signal travels along the transmission line, it is susceptible to noise . Therefore, an amplifier usually will amplify the noise in the same proportion as the signal, having the resultant *signal + noise*:

$$y = x + n \tag{1.1}$$

where x is the original signal, n is the noise contribution and y is the received signal. The noise contribution can be reduced or corrected by simple methods at the Rx. Eq. 1.1 describes the simplest expression of a communication channel where the wire has a minor or irrelevant contribution, and does not corrupt the original signal.

Wireless systems allow mobility, flexibility, and scalability to communication links. In the wireless case scenario, the channel has a greater contribution to the original signal itself. Type of antenna, fading, reflections and obstacles have a direct impact in the transmission, modifying the amplitude and phase of the original signal. All of these factors could be summarised in one expression as follows:

$$y = hx + n \tag{1.2}$$

where x is the original signal, n is the noise contribution and h is the channel

contribution to the signal in an Single-Input Single Output (SISO) scheme or H in a multi antenna array. In some cases, these contributions could be mitigated by modern demodulation, decoding and error correction techniques, able to be performed by real-time processing. However, the more precise the modulation, the more hardware is required for retrieving the original signal, causing an increase in the RF chain at the Rx and subsequently more energy consumption.

Furthermore, wireless systems share the channel with many other wireless communication links. Lately this common environment is highly populated, making it more difficulty to identify correctly the source of the message and the message itself. This causes interference. A precise time and frequency slot allocation should be done to avoid intercommunication damage.

1.2 Spectrum Allocation for Current Wireless Communications

Since all wireless devices share the same channel it is important to have a correct spectrum allocation management for every specific RF service. This spectrum allocation varies slightly by country. However, regulations should meet the international agreements issued by the International Telecommunication Union (ITU). This regulation allocates a specific frequency band or bands for specific services, as well as the transmission power, so multiple systems can coexist without being harmful to each other in terms of interference.

Lately, overpopulation of systems demanding space in the spectrum, has created the need for spectrum reuse. This is when a system is inactive, its allocated space could be used by different services and let free when the original service requires it. Methods such as cognitive radio allow for this re-use of the available spectrum.

1.3 Electromagnetic Measurements

Many validation procedures exist and should be satisfied, as well as standards for compatibility and emissions prior to mass production of any electric and electronic device. Additionally, these measurements could help to predict the behaviour of a device when operating in certain environments as well as being drastically close to other similar devices.

1.3.1 Interference

All electronic equipment suffers from electrical and electromagnetic interference. To them, such signals constitute a serious form of pollution, which is produced by many sources. The collective term for this pollution is electromagnetic interference (EMI)[1]. The effects of EMI are extremely variable in character and magnitude. To correct EMI problems that occur after equipment is designed and already in production, is usually expensive and may cause delay. It is preferable to develop good electromagnetic compatiblility (EMC) engineering practice during the equipment design and development phase [2]. For EMI to exist there must be a source of emission, a path for the coupling of the emission and a circuit or system sensitive to the received noise. The sources of EMI are electrical, magnetic, and electromagnetic fields that emanate from wiring of transmitters, AC power mains, and anything that runs on electricity. The proximity of these radiating sources increases the probability of interference or mutual coupling between them [3]. The coupling mechanisms can be radiative, capacitive, conductive or inductive, as shown in Figure 1.1.

- Radiative coupling is direct signals from an antenna (source) to the susceptible equipment (victim).
- Capacitive coupling is present when a variation of the electrical field between two conductors exists, inducing a change in voltage or current in the victim.
- Conductive coupling arrives by the wires connected (transmission line) to

the victim. Noise is classified into two types according to the conduction mode: Common mode and Differential mode [4]

- Magnetic induction means that the two different circuits are magnetically coupled, existing a magnetic field between two parallel conductors inducing voltage along the receiver conductor [1].

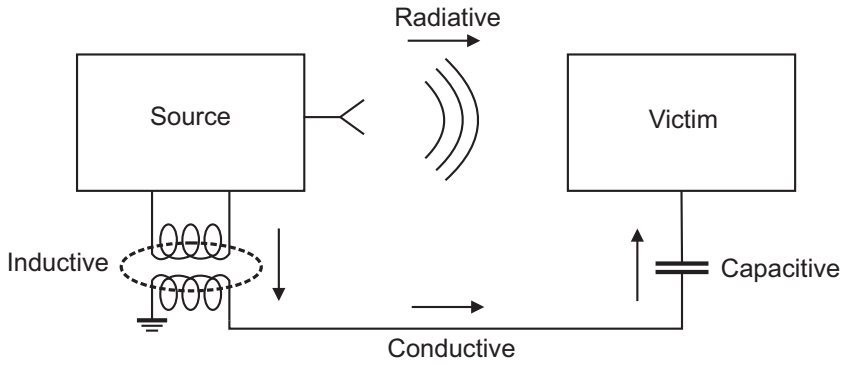


Figure 1.1: Example of coupling mechanisms.

EMI can be mitigated using one or more strategies, such as isolation, shielding, grounding, matching, filtering or redesigning the system to diminish external effects [3]. This forms of interference can be easily found in systems such as rail transportation systems. Trains are susceptible to interference caused by the lines used for power delivery using a pantograph and for the power plants in its vicinity, as shown in Figure 1.2.

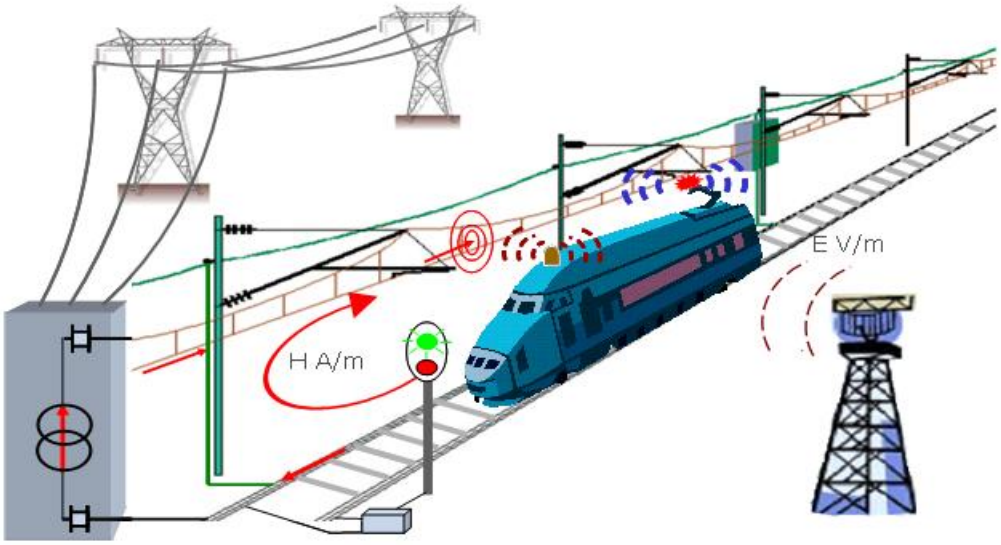


Figure 1.2: Example of coupling mechanisms in a railway infrastructure.[5]

1.3.2 Compatibility

Electromagnetic Compatibility is the ability of a system to function correctly in a given environment without introducing electromagnetic disturbance to other systems around it. According to [6], to accomplish EMC, a system must not cause interference with other systems, must not be susceptible to emissions from other systems to satisfy EMC requirements. As there are many variables and external conditions to consider, it is not possible to avoid EMI. The purpose of EMC is to keep the side effects to the minimum making it possible for a diverse type of systems to coexist and operate correctly in the same environment. It is required to test a system or device to verify if the standards are fully met. The test could be carried out in open-air test sites (OATS), by computer simulation with specialized electromagnetic simulation software, or within a specialised EMC test facility.

EMC measurements could be divided into types that provide fundamental information regarding DUT characteristics under different conditions: emissions and immunity.

Emissions

Any electronic and electric device produces certain levels of conducted or radiated field strength in its vicinity when operating under normal conditions, without any external influence. Emission measurements are useful to know the characteristics of the radiated field, mainly in terms of frequency occupancy and magnetic and electric field strength produced by the device under test (DUT).

Immunity

Immunity or susceptibility measurements could be understood as the opposite of emission tests. For this measurement, the DUT is exposed while in operation to a well known source of electromagnetic field, whilst its performance is recorded. With this, the device is tested in presence of continuous or transient RF interference (RFI) or EM pulse energy to ensure it performs as expected in the presence of interference to levels specified in appropriate measurement standards.

Environment characterisation

Depending on the application, electronic devices could be designed for indoors or outdoors purposes. Usually, indoors environments are the more likely to be highly populated or occupied by several devices using the same bands for communication given its characteristic emissions when in operation. This is a challenge to overcome in spaces reduced in size. On the other hand, in outdoor applications, usually we can encounter radiations by TV transmitters, mobile cells, cars, and power plants.

To characterise these environment a survey in multiple indoors or outdoors location points should be made. Using equipment such as spectrum analyser, electric field probes or antennas, power meter and interference analyser, various variables can be studied such as power levels and frequency occupancy in short and long term. With this data, a similar environment could be recreated in a test facility for EMC or EMI and expose any device for performance assessment before

it is deployed for the desired application and make the required modifications to avoid a decrease in efficiency and/or performance.

1.3.3 Internet-of-Things

Internet-of-Things (IoT) is an interconnection of systems (mainly embedded) for data exchange. Such systems are typically (not specifically), control units, sensors, actuators, and more sophisticated systems such as mobile phones, health monitoring systems and house appliances. All those systems are known as "smart", given the possibility of being connected to the internet and retrieve information without human interaction. From an industry point of view, IoT helps to acquire huge amounts of information from sensors from a complex system and more importantly from human behaviour or preferences. All the information gathered and processed is known as Big Data. IoT and Big Data help the industry to increase production of goods or provide services targeting a specific sector of the population where the demand is high. For example, having a huge interconnection of systems and monitoring, helps to predict when a machine will stop working due to tool wear for regular use. The information is gathered and processed in real time, allowing a maintenance team to fix it even before the failure exist.

Rail Internet of Things (RIoT) is an extension of IoT, where a smart sensor network is included in the train infrastructure, on-board and trackside. IoT on-board system can monitor the locomotive and freight carriages status and create diagnostics about the engine status, door locking and passengers, increasing security. Additionally, it can assist the trains to arrive on time and maintain a precise schedule for a more reliable traffic management. The implementation of RIoT is thought to be deployed using technology such LTE, thanks to its high speed, low latency and wide coverage [7]. However, this will imply the use of third-party infrastructure and will increase the cost of usage.

Currently, RIoT is not yet widely used but it is being adopted and developed by infrastructure manufactures, such as Thales Ground Transportation Systems (Thales-GTS), which is the sponsor of this project. This project is focused on

the signalling infrastructure, that is part of the traffic control, management and estimation and vehicle-to-vehicle communication of the total RIoT, which includes cloud services, passage and freight allocation, tickets and on-board services.

1.4 Project Goals

The aim of this project is to investigate and compare different technologies for wireless communication to implement a signalling system for commercial use, promoted by Thales Group, specifically with its Ground Transportation Systems division (Thales GTS). Thales Group is a French multinational company that designs and builds electrical systems and provides services for the aerospace, defence, transportation and security market.

At this time, most of the signalling systems, as the ones presented previously, involve a great amount of infrastructure composed by many sensors and high-power consumption transceivers, for which it is necessary to deploy a wired network to supply sufficient energy for all the devices aside the railway. Furthermore, when it is necessary to make changes in the railway lines to add or modify a route, the power lines must be modified as well (usually deployed underground), leading to a cost increase.

This work will focus on studying, proposing and implementing a feasible, low-cost and low-power consumption solution for the current signalling system, which can be reached using a technology that meets those characteristics. Principally, there are two challenges to face: coverage area and time of response. Since it is planned to have a wireless signalling system, coverage becomes a subject of interest. The area of coverage must ensure successful data transmission.

The top speed of a high-speed rail is 250km/h (155 mph), although classic main railway lines operate up to 201km/h (125mph) in the UK. Some other examples of high-speed trains in the world are the Shanghai Maglev in China, with a top speed of 431 km/h (267mph) in a 19 mile trajectory, and the Shinkansen in Japan, with a top speed of 360 km/h (224mph). The latter is know widely as the "bullet

train". Each rail route section has a published speed limit which will vary locally according to track and route features such as junctions where trains pass between different routes [9].

Additionally, the time of response or latency must be short or minimal compared to the train speed in order to locate the on-board system and send information to the drivers. For example, for every second of delay for the Shanghai Maglev train, the displacement increases for 120m. Hence it is vital to minimise the delay.

1.5 Thesis Structure

Chapter 2 addresses the emissions present in the vicinity of a tram line. These emissions are produced by the current flowing along the power lines over the tram, which generate a magnetic field that could interfere with the correct operation of electronic devices and instruments, in addition to the challenges of a realistic environment or scenario where ultimately the system will be deployed.

Every wireless system has to share the limited spectrum with many other devices. Chapter 3 addresses some facilities or rooms for electromagnetic emission tests. These chambers are used widely for equipment and instrument validation, since various conditions and communication channels can be emulated inside them, being the most important for this work the use of the RC for stress, interference, and resilience test for the DUT or equipment under test (EUT) in presence of noise and potentially disruptive signals.

Chapter 4 presents a discussion of the advantages of the wireless over the wired communications and train infrastructure. The aim of this project is to provide a wireless alternative for signalling systems. Hence, the current most used signalling protocols for train control are mentioned which have in common the use of the Industrial, Scientific and Medical radio bands (ISM) for the train-ground communication link.

Motivated by and based on the current signalling systems, the prototype previously mentioned is presented in Chapter 5. The chapter focuses on the network

and device features. Subsequently, the system as a whole is described as well as additional features for traffic management.

Finally, in Chapter 6 a final conclusion and discussion of the obtained results is presented. Moreover, future work addressing potential improvements, scenarios and challenges is also presented.

Chapter 2

Electromagnetic Environment Measurements - Real Rail Scenarios

During the past years, a new tram line in Nottingham started operations and a segment of its track layout cuts across the University of Nottingham campus area, including a flyover structure over the A52 Clifton Boulevard, as part of Nottingham Express Transit Phase 2 Project (NET2). One end of this structure is on Science Road (ramping down) on the University Park Campus and is in close proximity to Boots Science Building (BSB), Wolfson Building (WB) and Institute of Hearing (IHR), and the other end is in from of the University of Nottingham Medical School. This location is shown in a the in the below Figure 2.1

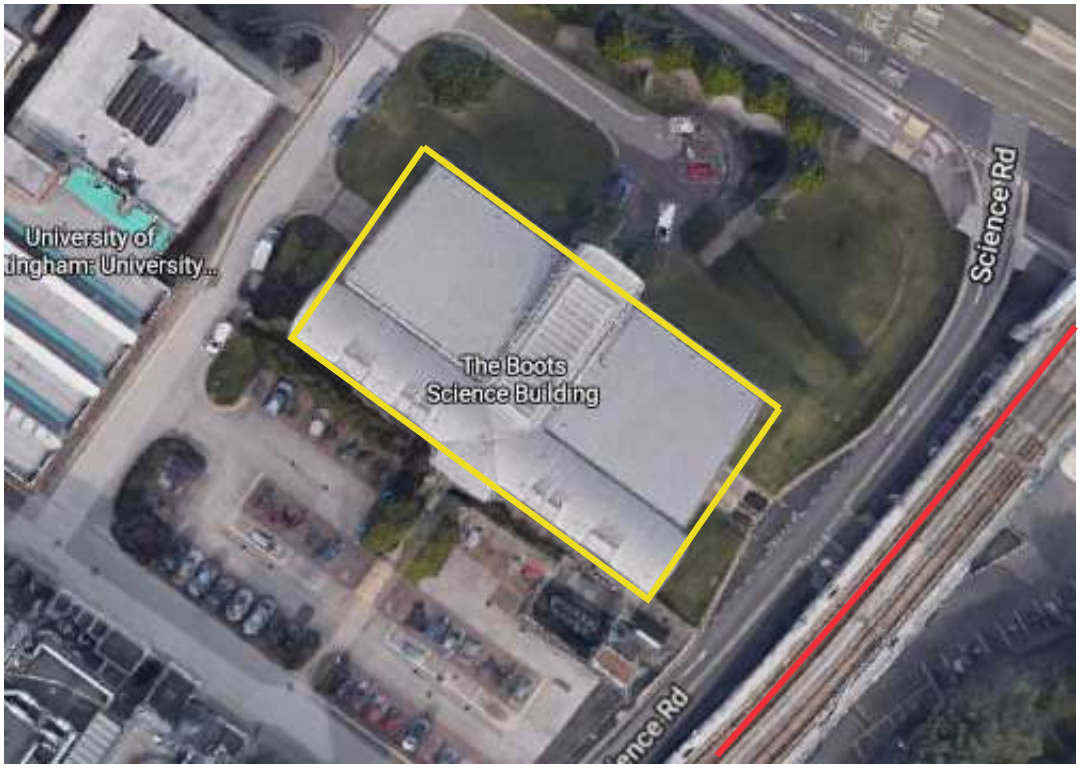


Figure 2.1: Wolfson Building location denoted by the yellow rectangle and the tram track by the red line

In particular, the potential for EM emissions and vibration were of major concern, due to the impact of these on the high-precision equipment located in the buildings mentioned above, and the possibility of interference with instrumentation that may lead to inaccurate measurements, for example Electroencephalogram (EEG), Electron Beam Instrumentation, Magnetic Resonance Imaging (MRI), X-ray and Spectroscopy (SPEC), Thermal Equipment (THERM), Chromatography (CROM), Mechanical Equipment (MECH), among others. The closest piece of equipment is located 10 m away from the OLE and is a MRI in the Institute of Hearing. Electroencephalography (EEG) is used for recording electrical activity from the brain. EEG measures voltage fluctuations resulting from ionic current flows within the neurons of the brain. In this case the signals from individual stem cells are monitored using electrodes from the subject under test (small mammal).

This chapter covers an evaluation of the EM environment pre and post tram

line installation and energisation. The pre installation study was carried out by Alstom SA and their work will be only mentioned as a precedent as well as their conclusions. The post installation and energisation measurements were carried out as part of the work described in this thesis and a discussion of the spectral occupancy in the vicinity of the tram lines based on these measurements is addressed in this chapter, either produced by the lines themselves or by the wireless services the Wolfson Building.

2.1 Previous Emission Measurements - Simulated conditions

At the beginning of this study, the NET2 tram line was not in operation and therefore an engineer from Alstom body set up an experimenting test to simulate the electromagnetic presence of the line using a Helmholtz coil with a signal generator and power amplifier to generate a magnetic field.

The equipment under test (EUT) was a neurophysiological subject, consisting on an EEG measurement using electrodes, at the distance from only one coil from the EMCO 6404 Helmholtz Coil, shown in Figure 2.2.



Figure 2.2: EMCO 6404 Helmholtz Coil.

This test's frequency covered a range from DC to 5kHz, but also 2.5 kHz and 4.6 kHz frequencies were considered, to try to determine the susceptibility to "chopper noise" from the tram's traction power converters, which have switching (chopping) frequencies between 2 and 2.5kHz. All the previous was generated using an Arbitrary Waveform Generator Agilent 33250A, 1kW VLF Amplifier Techron 7560 and the EMCO 6404 Helmholtz Coil.

With this test, the external body (Alstom) concluded that the performance of the instrument used for the neurophysiology EEG's should not decrease from detectable degradation due to low frequency magnetic fields emitted by NET2 over the frequency range 0Hz to 290Hz at distances of 10m or more from the centre of the tram line, assuming the peak magnetic field level of 4μT at 2400A. However, they mentioned that there may be problems at the 300Hz harmonic due to the traction current, and possibly also at higher frequencies, due to traction rectifier noise.

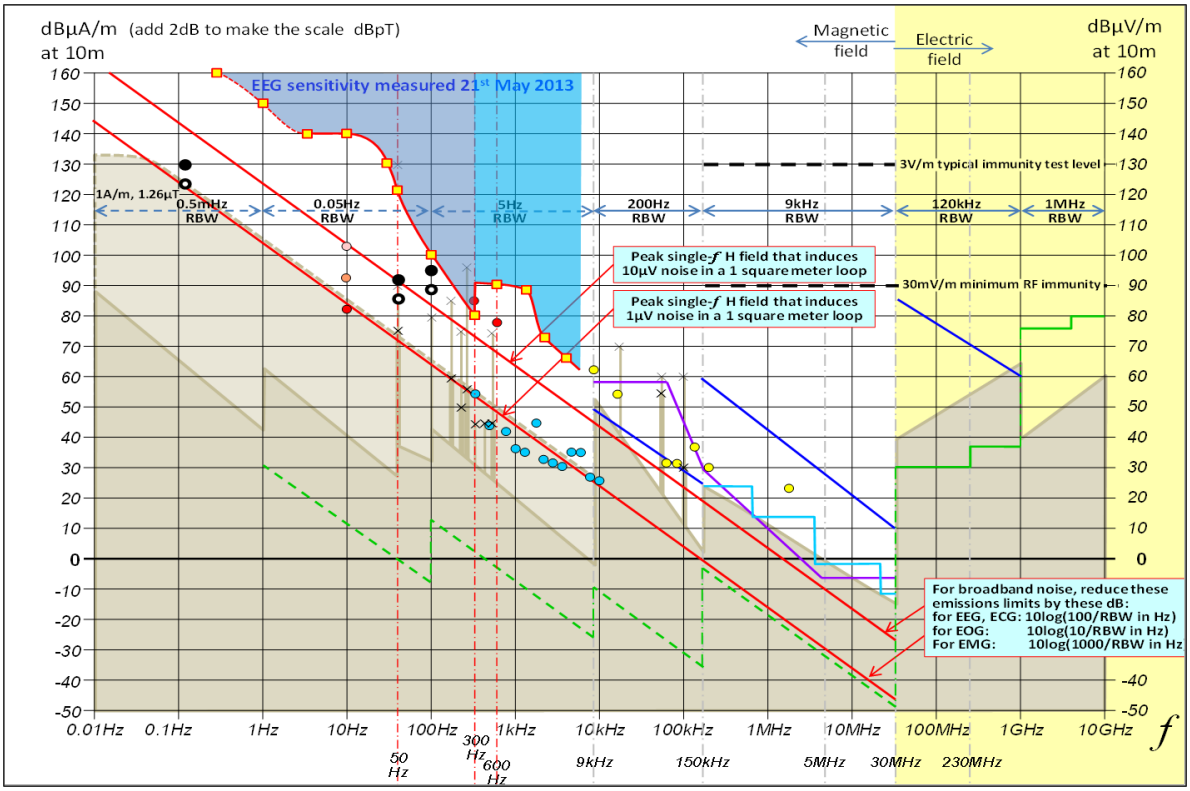


Figure 2.3: NET2 EMI threat analysis graph with threats up-to-date at 22 November 2013 [8]

On a previous work similar to the one mentioned in this section, a representative tram test track was tested and measured in La Rochelle, France carried out by Alstom as well. Alstom conducted a series of measurements with an operating tram and they are presented in the Figure 2.3. Alstom claimed that the tram is very similar in terms of length, engine and power to the projected to be in operation in Nottingham[8].

The Figure 2.3 plots this test in light blue dots. It shows that 300Hz emissions at 25dB less than the level that the test conducted in the University of Nottingham show to be just acceptable, and emissions at 600Hz and above to be 30-40dB lower.

Furthermore, a latter low frequency EMC survey conducted over the Nottingham Express Transit Phase 1 (NET1) in July 2009 (red dots in Figure 2.3) found NET1's 300Hz emissions to be 5dB higher than the La Rochelle tests found to

be acceptable, and at 600Hz NET1's emissions were only 12dB less. NET2 trams draw more current than NET1. Therefore, it could be assumed that NET2 has even higher emissions than NET1 when run on NET1's line. The levels of harmonics from the NET2 traction substations is therefore an important concern. Additionally, these measurements do not consider the possibilities for NET2 interfering with any other equipment or experiments at the Medical School.

2.2 Measurements with active Overhead Lines

The concerns raised previously meant that a survey was necessary before and after the Overhead Line (OHL) went into operation. Motivated by this, the EM spectrum readings were taken before and after the power overhead lines were powered on, in order to visualise its occupancy in the frequency domain. The spectrum was monitored from 30 MHz to 1 GHz. Since this project focuses on the operation of ZigBee technology for signalling systems, the ISM bands were a matter of concern for the survey. The antenna was placed at a 9m distance from the tram tracks, which complies with the most used worldwide standards for High-Voltage (HV) substations or transmission lines measurements where the maximum distance is established, mentioned below.

- ANSI Std 430-1986. IEEE Standard Procedures for the Measurement of Radio Noise from Overhead Power Lines and Substations. The procedure applies in the frequency range of 0.010 MHz–1000 MHz. Maximum distance: 15m.
- AS/NZS 2344:1997. Limits of Electromagnetic Interference from Overhead A.C. Power Lines and High Voltage Equipment Installations in the Frequency Range 0.15 to 1000 MHz. Maximum distance: 20m.
- CISPR 11. The International Standard for electromagnetic emissions (disturbances) from Industrial, Scientific and Medical (ISM) Equipment. Frequency range of 0.15 MHz–1000 MHz. Maximum distance 30m.

The undertaken data will be used to analyse the spectrum and record the

magnitude of the emissions at the scene. Furthermore, such data may be used to assess the electromagnetic interference with the equipment located inside the building, which is a main concern by researchers located in BSB.

Three locations were required to take measurements from, as shown in Figure 2.4. The distance from the nearest track centre to the different points marked to the tramlines (or power lines) is 18.5m, 28.5m and 38m.

For each location, and according to the antenna range, measurements were taken from 9 kHz to 150 kHz, and 200 MHz to 1GHz, recording data from the SA with the set-up shown in Figures 2.5 and 2.6.

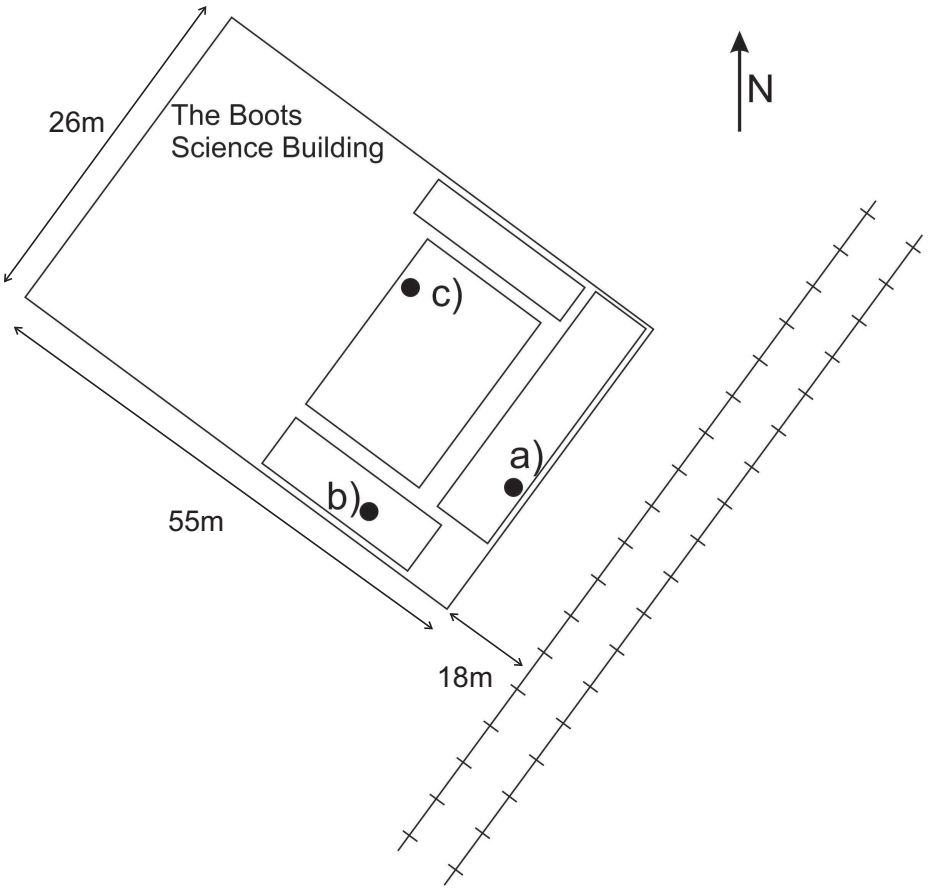


Figure 2.4: Antenna locations inside the Pharmacy Building of the University of Nottingham.

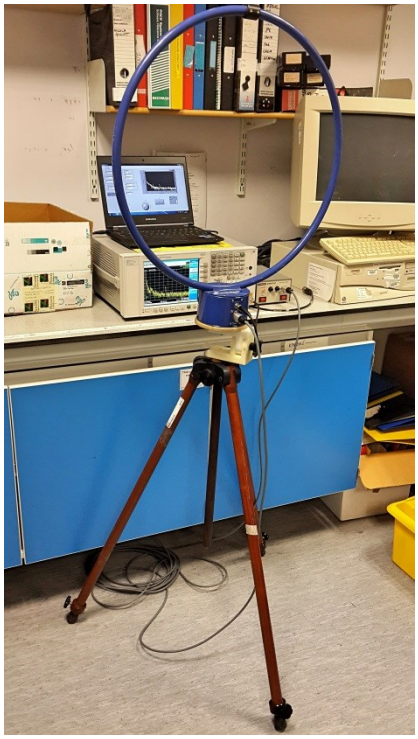


Figure 2.5: Loop antenna set-up the Pharmacy Building

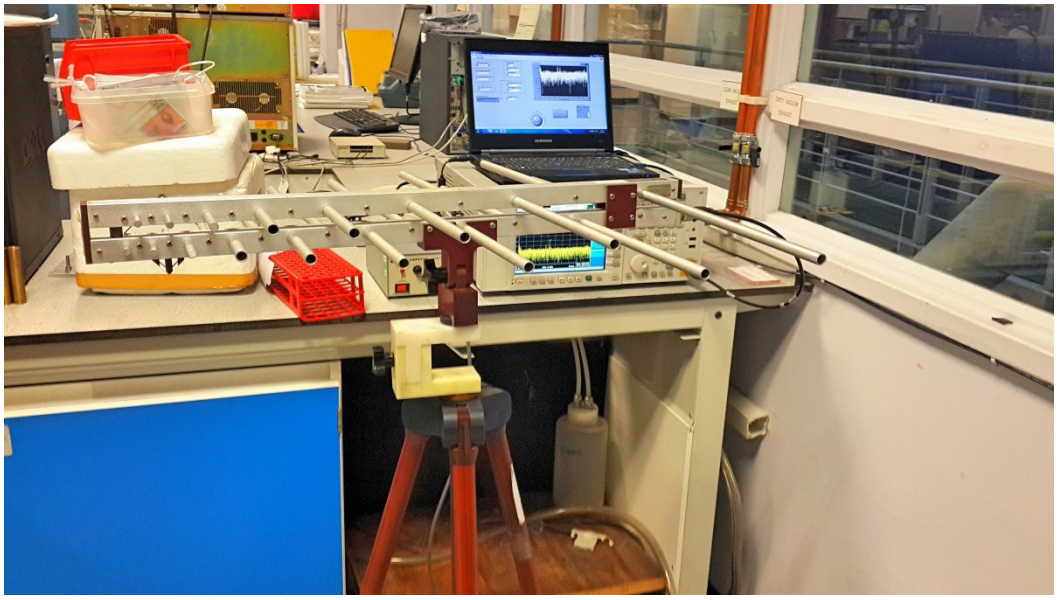


Figure 2.6: Log-periodic antenna set-up the Pharmacy Building

Initially, the spectrum was monitored in a period of time before the OHL lines

started operations. Hence, the equipment was positioned inside the laboratories to gather the data. The results obtained are shown in Figure 2.7. In that Figure, a compilation of several measurements logged at different moments is presented. With this, it is possible to stablish a regular spectrum occupancy from diverse sources, such as TV and radio stations, as well as equipment using the ISM band. The purpose of this is to then be compared with the measurements conducted once the OHL are active.

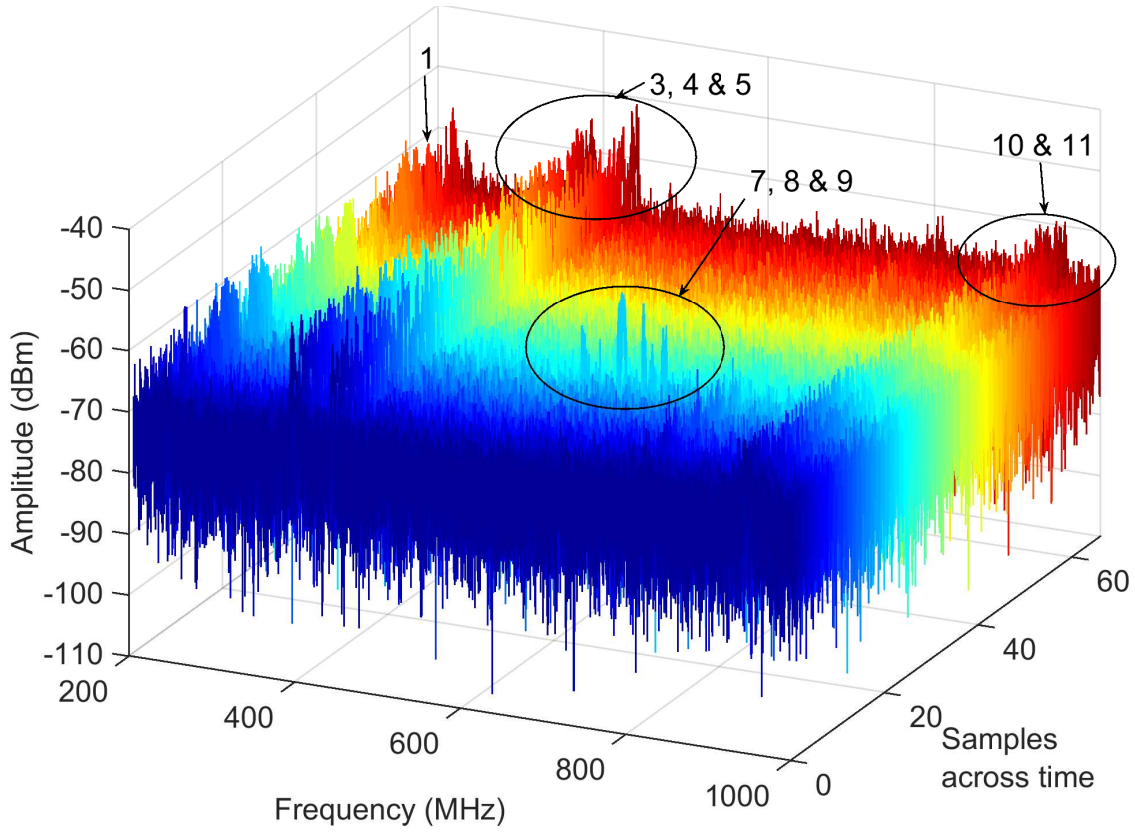


Figure 2.7: Data logged across time before activation of the OHL

Approximately three months after the previous measurements, the set-up was put in place again once the OHL started were set to operate. It is worth to note that the tram was not operational at the time. The emissions observed in the spectrum are shown in Figure 2.8.

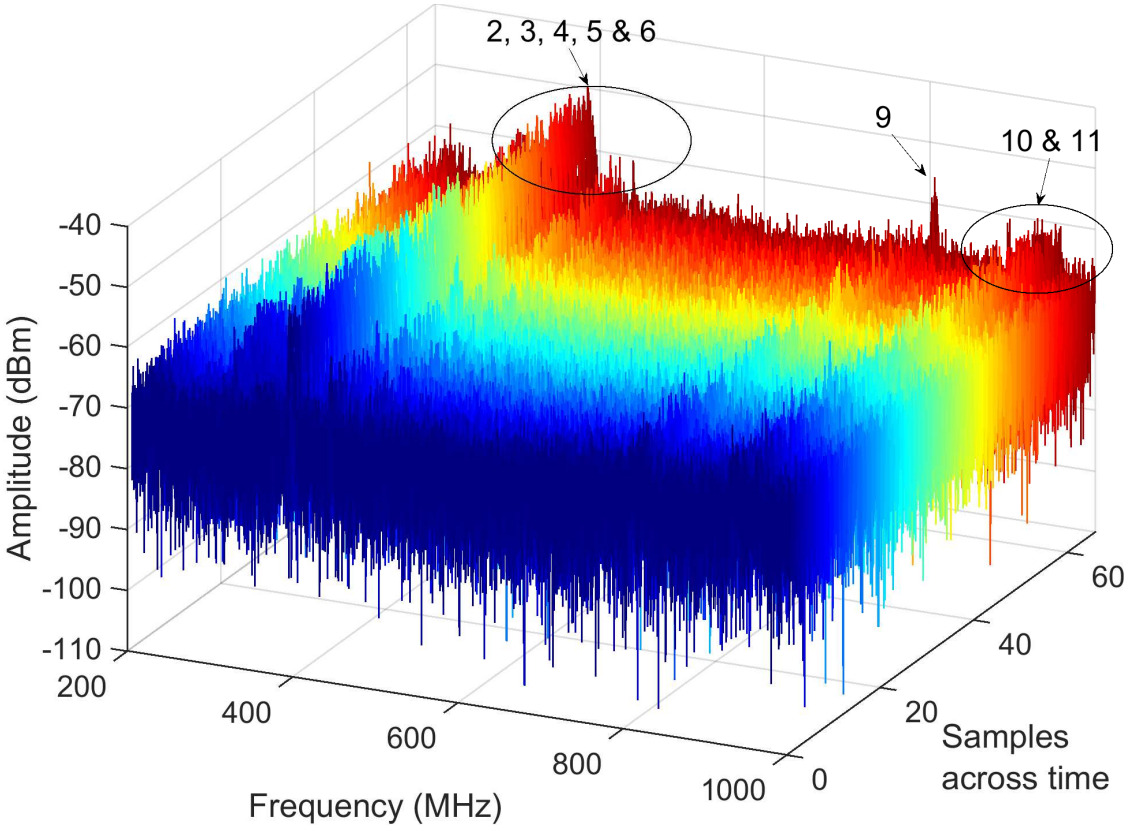


Figure 2.8: Data logged across time following activation of the OHL

The colour grading present in the plots from Figures 2.7 and 2.8 serve no other purpose that make a visual differentiation from sample to sample across time.

It was worth to compare the maximum values received before and after the electrification of the lines, in order to observe if a difference in the power level registered exists. Hence a comparison is shown in Figure 2.9 where the maximum and the minimum amplitude levels observed through the duration of the experiment (period of two weeks) are plotted. Excluding the area of interest of this experiment (863-870MHz) the other outgrowths observed correspond to other different services continuously present, such as mobile communication (GSM)and TV broadcasting. A list of these identified services are presented in Table 2.1 and they match with the indexing shown in the figures 2.7 and 2.8.

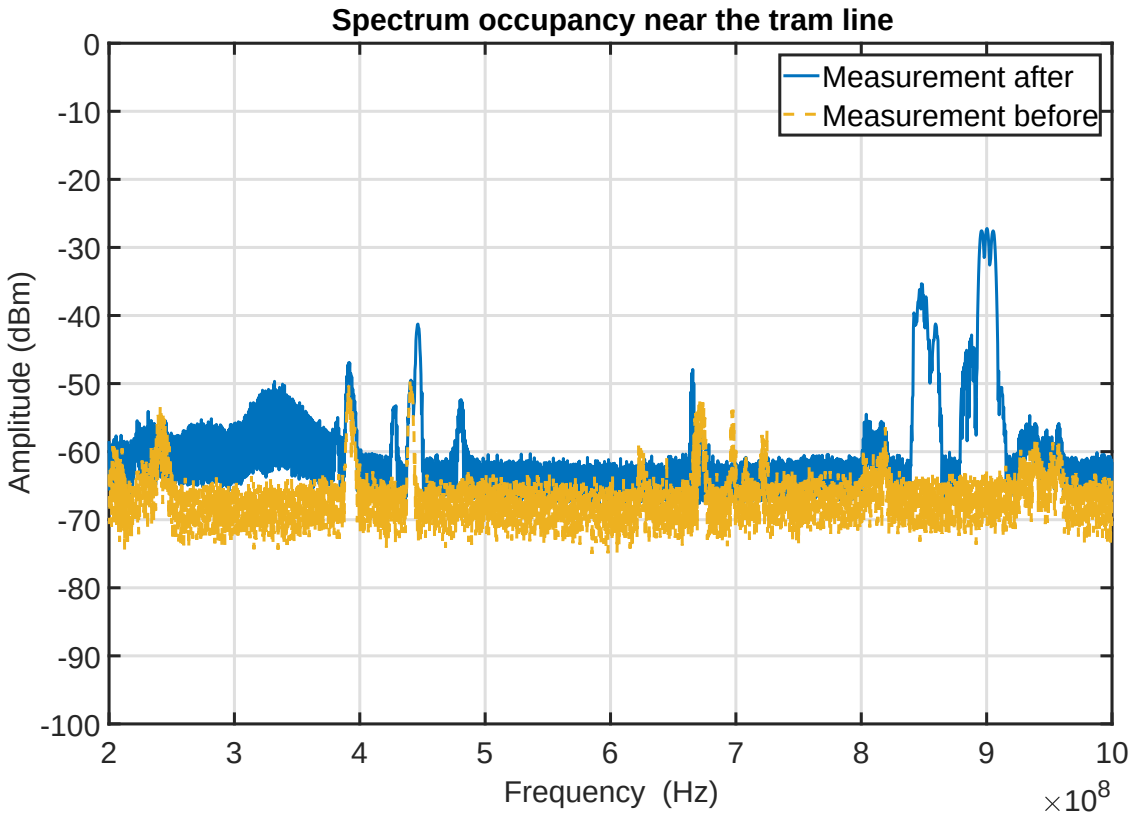


Figure 2.9: Maximum values comparison, before and after the power lines went on. The outgrowths observed correspond to GSM mobile and TV broadcasting services

Table 2.1: Frequency allocation in the UK

Index	Frequency	Service
1	241MHz	BROADCASTING
2	332MHz	AERONAUTICAL RADIONAVIGATION
3	392MHz	AERONAUTICAL RADIONAVIGATION
4	428MHz	AERONAUTICAL RADIONAVIGATION
5	472MHz	BROADCAST & MOBILE
6	481MHz	BROADCAST & MOBILE
7	671MHz	BROADCAST & MOBILE
8	697MHz	BROADCAST & MOBILE
9	725MHz	BROADCAST & MOBILE
10	810MHz	BROADCAST & MOBILE
11	947MHz	MOBILE & RADIO LOCALISATION

According to the data obtained and shown in Figures 2.7 and 2.8, some of those services are constantly in use, such as the bands corresponding to Aeronautical radio-navigation and Broadcast & Mobile. But, some others are transient, specifically the Mobile and Radio localisation.

The focus of this survey is to investigate the occupancy in the 800-950 MHz band, since the study of the capabilities and resilience of ZigBee radios is fundamental for this research work. The occupancy in the 800-950 MHz band before and after the OHL energisation are shown in Figure 2.10 and 2.11, respectively.

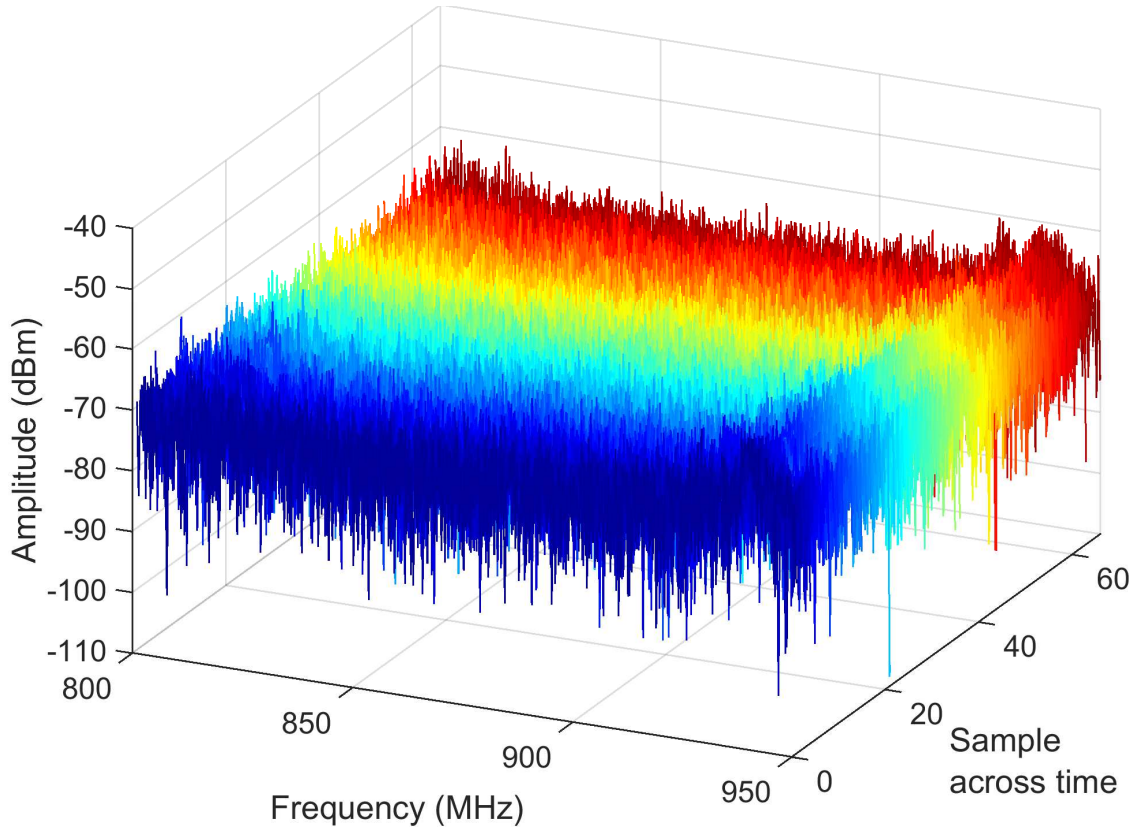


Figure 2.10: Emissions before the activation of the OHL.

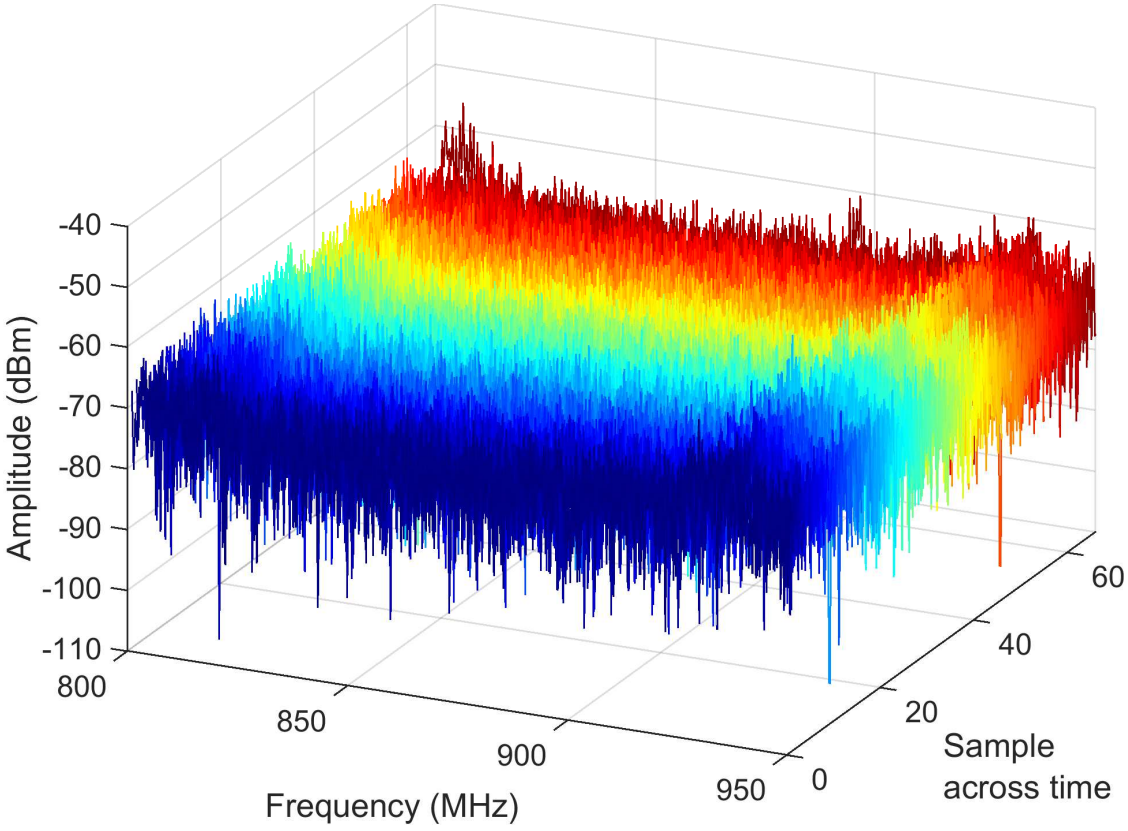


Figure 2.11: Emissions following the activation of the OHL.

The colour grading present in the plots from Figures 2.10 and 2.11 are solely to make a visual differentiation from samples. Interestingly, between the 863 - 864 MHz band some emissions exist, as shown in Figure 2.12. These emissions are likely to be produced by a cellular phone call in the surroundings during the measurements, since one of the bands used for GSM mobile communication operates at 850MHz and it was not continuous throughout the entire measurements. However, the transmission power level produced by the XBee is higher and should not be affected by this disturbance, as both technologies share and comply with the ISM emissions requirements.

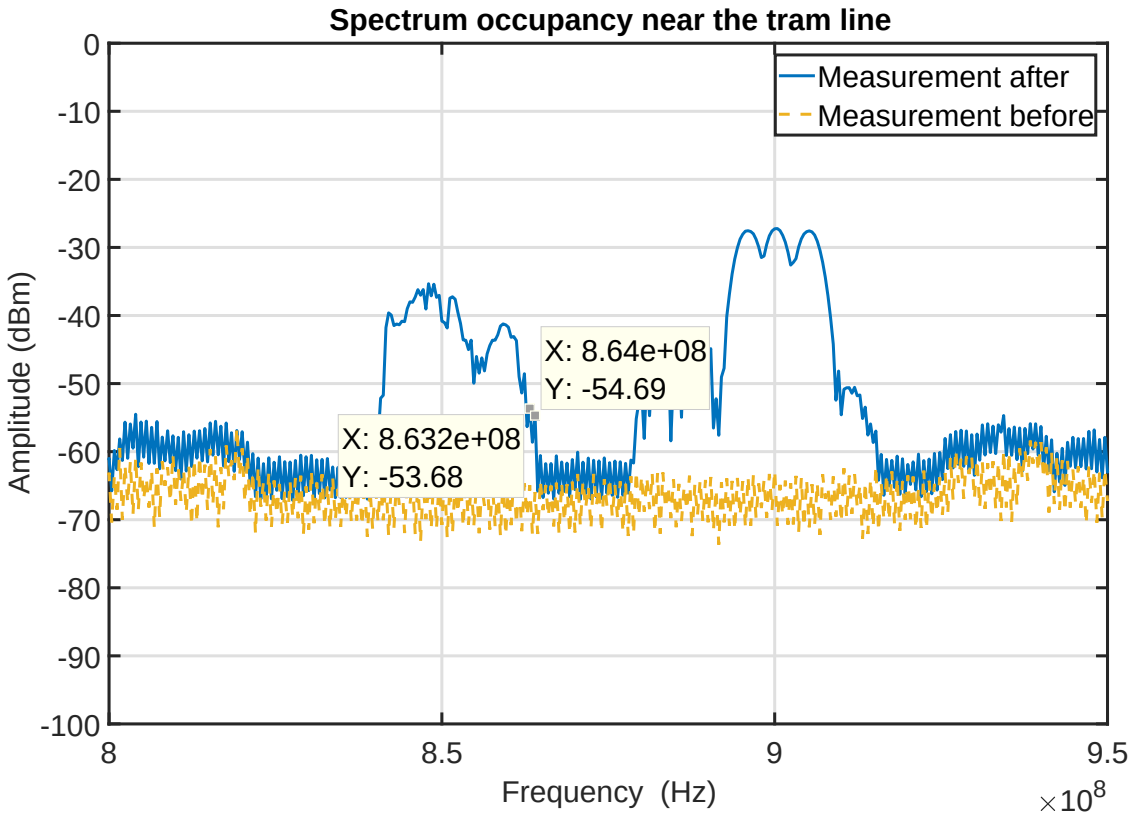


Figure 2.12: Maximum values comparison measured before and after the lines were in operation.

In average, the received signal increased by 3dB across the frequency monitored. However, it was observed that the increase would not interfere with any equipment utilised for research in the facilities.

2.3 Test Track Scenario

Aside from the laboratory tests or set ups, the real-life environment is the ultimate challenge to face and considered to evaluate the characteristics provided by any communication system. In railway, the signalling system is the overall controllable to deliver instructions to the driver from the main control centre in the far field, as well as coordinate the movement of each of the trains (locomotive and carriages),

as well as monitor the geographic position, speed and operational status of them for traffic management. Furthermore, alerts and in some occasions overdrives the driver decisions in order to keep safe the passengers or the goods it transports. Currently, the signalling is mainly wired. Although, it could be more reliable in terms of error and noise susceptibility, the costs of implementation are costly.

For a realistic evaluation, the scenario selected should provide features to replicate the environment present in the surroundings of a train track, such as power stations, power lines, curves, stationary and moving rolling stock. Therefore, the Long Marston test track in at the Quinton Rail Technology Centre (QRTC) in Warwickshire was proposed to carry out these proof of concept. Mainly, it consisted of a closed loop of 3.8km, where the maximum straight line available is nearly 1km, with live overhead power lines. The test facility is shown in Figure 2.13.

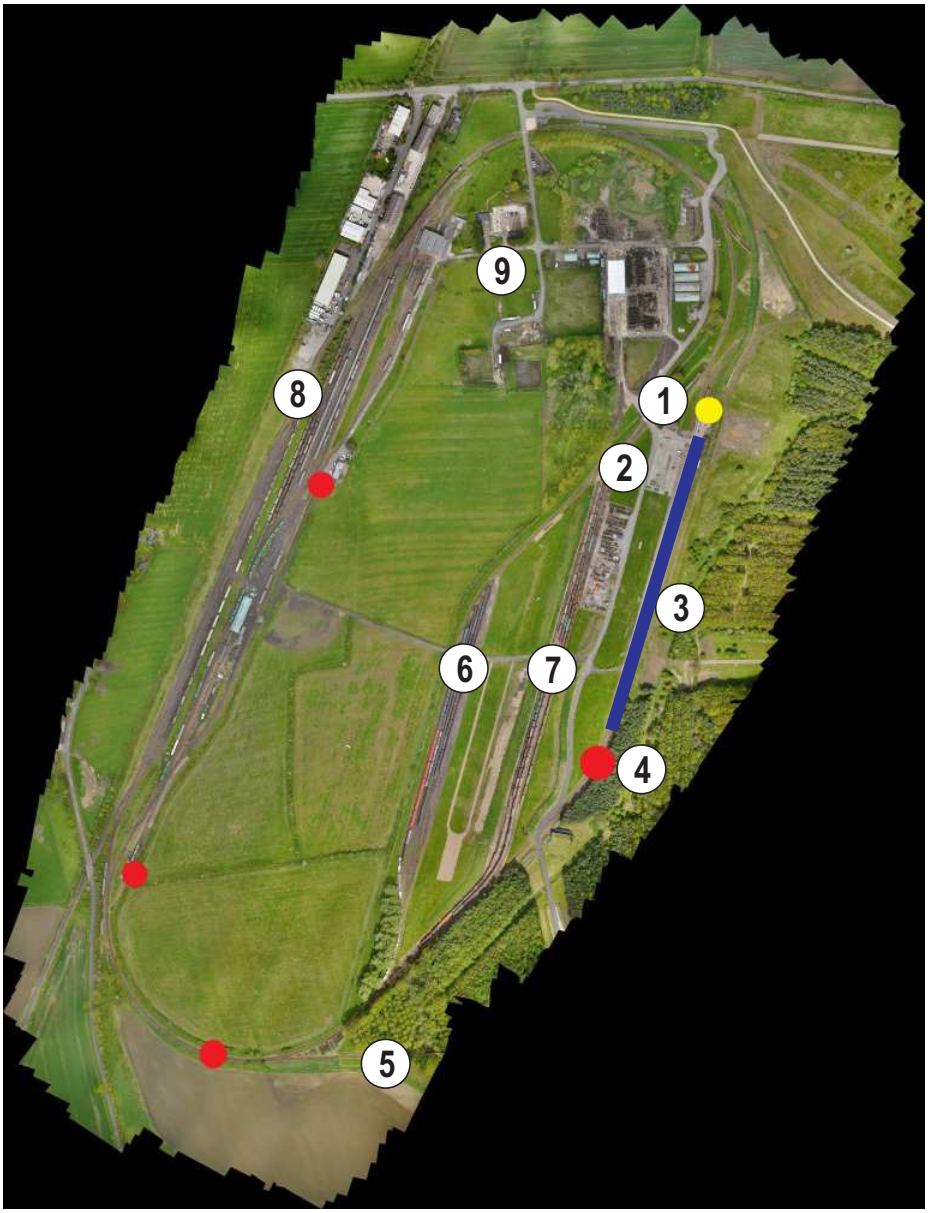


Figure 2.13: Aerial view of the Long Marston test track

From Figure 2.13, we can mention the following elements according to the nomenclature:

- **1**: Control centre location (yellow dot).
- **2**: Board platform.

- **3**: Overhead Line (purple line) along a track section.
- **4**: Signal nodes are marked with a red dot.
- **5**: Big area with trees, blocking LOS.
- **6**: Rolling stock infrastructure.
- **7**: Rolling stock infrastructure.
- **8**: Rolling stock infrastructure.
- **9**: Fixed infrastructure

Test Design

The experiment was designed to cover three fundamental communication scenarios: point-to-point link, multipoint link and train to ground link. For the point-to-point scenario, a Tx and Rx set up should utilised in a direct link communication, sending a continuous data frame at while while varying the distance between them. Secondly, a multipoint scenario is addressed where a repeater is included in the communication scheme as a transparent module, therefore the message is transmitted to the destination without begin analysed. Thirdly, a moving Rx is introduced to the network, as the OU will be placed inside the locomotive to display information sent by the CC to the driver. These components will be explained in detail further in the following chapters.

2.3.1 Challenges

For the study, the experimental procedures must address the following challenges.

Coverage Area

Since the main goal of this alternative solution is to replace the current wired systems, the coverage area provided for a single node should be wide enough to

maintain a constant communication link with low error rate. It is well know that high quality link could be ensured by reducing the distance between Tx and Rx. However, increasing the number of nodes across the network would be counter-productive to the principle of "low cost" solution. Therefore, it is important to find the balance between low error rate and distance between nodes. Furthermore, the Tx power levels cannot interfere with other services in the ISM in order to coexist with other technologies using the same bands.

Additionally to this, a degree of redundancy should be considered, in case one or more nodes fail.

Autonomy

The aim of this system is to reduce the amount of infrastructure and wire currently utilised in order to decrease implementation and maintenance costs. Because of this, wire for communication and power delivery is no longer considered and should be substituted by another type of power supply. Therefore, batteries, renewable energy and solar panels are being considered. Nowadays, energy harvesting is being widely explored as well as high capacity batteries. Nevertheless, this is still limited. Hence, the system must be low power consuming and energy efficient.

Moving Rolling Stock

An important factor to consider is that the OU is moving across the rail network and will be changing from the coverage area from $Node_{n-1}$ to $Node_n$, i.e. from the previous to the current node. This transition should be transparent and the network should provide continuity. However, a pairing time $t_{pairing}$ must be considered and be minimum compared to the train displacement done in that same $t_{pairing}$.

2.4 Railway Standards

The European Standard series EN 50121 is a set of standards for electromagnetic compatibility. It defines the criteria for integration of wireless functions and system into the railway environment [9]. This standard was porposed in 1995, adopted in 2000 and fully effective in 2009 [10]. The EN 50121 is divided into 5 parts covering different aspects of the railway environment:

- EN50121-1 General
- EN50121-2 Emission of the whole railway system to the outside world
- EN50121-3-1 Rolling stock – Train and complete vehicle
- EN50121-3-2 Rolling stock – Apparatus
- EN50121-4 Emission and immunity of signalling and telecommunications apparatus
- EN50121-5 Emission and immunity of fixed power supply installations and apparatus

The EN50121-1 General describes the multiple noise sources of electromagnetic interference present in a railway environment. The sources considered as internal are static and mobile elements, power converters, track-side equipment and traction return current. The external sources are track-side radio stations, neighbouring railway systems and industrial plants that disturb the electricity supply network [11], [12], as well as the coupling mechanisms previously mentioned in Chapter 1.

The most relevant section for the work described in this document, is the EN50121-4 Emission and immunity of signalling and telecommunications apparatus, which specifies the limits for emissions and immunity tests for apparatus in relation to electormagnetic disturbances likely to be present in a reilway environment, that applies for vital equipment such as interlocking or command and control separated by 3m or more from the centre of the nearest track [13]. This

standard is highly based on the Electromagnetic Compatibility (EMC) — Part 6-4: Generic standards — Emission standard for industrial environments [14]. The emission limits are defined in the below Table 2.2:

Table 2.2: Electromagnetic emissions limits for signalling systems apparatus

Environmental phenomena	**Specification**	**Limit**
Radio-frequency electromagnetic field. Amplitude modulated	80 MHz to 800 MHz	10 V/m
Radio-frequency electromagnetic field.	80 MHz to 1000 MHz 1 400 MHz to 2 000 MHz 2000 MHz to 2700 MHz 5100 MHz to 6000 MHz	20 V/m 10 V/m 5 V/m 3 V/m
Electrostatic discharge	Contact discharge Air discharge	± 6 kV ± 8 kV

These limits will define if any signalling device would be suitable for railway purposes and fit to be deployed within the railway network.

2.5 Conclusion

The survey conducted by Alstom mentioned at the beginning of this chapter, concluded that the OHL and the NET2 would not affect the correct operation of a "victim" instrumentation at distances greater than 10m directly. On the other hand, the latter survey conducted, shows that some services are in the ISM bands where many low-cost communication devices operate, specifically sensor nodes such as ZigBee modules, that will be matter of investigation and discussion further in the following chapters as this technology will be the base for a proposed prototype for a signalling system. These services do not operate continuously and, since are in a free licensing band, they are obliged to meet compatibility criteria as well as emission levels not to interfere with other devices and instruments.

Furthermore, part of the tram infrastructure consists on a pantograph which makes contact with the OHL as it travels across the tram track. Under certain

circumstances, a phenomenon occurs where the pantograph does not make strong contact with the lines and a high current arc is produced, due to natural age of the line, icing or not enough tension. It should be taken into account that the discharge generated may produce interference with nearby devices. Hence, this phenomenon will be addressed in the next chapters.

Chapter 3

Experimental Environments

3.1 Experimental Tools

Before its final implementation, any electronic device should go through a validation process where its performance is analysed under certain circumstances, in order to stablish the optimum conditions in which its features reach maximum efficiency and stability. Additionally, it is worth knowing the conditions in which that given device could fail.

When using wireless devices, interference is one of the main problems to face, given that the channel is highly populated by many adjacent signals, plus objects that could reflect and scatter the radiated signal.

Thus, the use of experimental tools like anechoic and reverberation chamber can provide realistic performance metrics of an electronic device, particularly in presence of noise and interference.

3.1.1 Anechoic Chamber

General Features

An anechoic chamber is a metallic cavity designed to absorb reflections of sound or electromagnetic waves, where the walls, ceiling and floor are populated by an Radiation absorbent materials (RAM). For RF measurement, the walls are constructed to absorb electromagnetic radiation. The purpose of the absorbent material is to minimize the reflection of the incident multipath components and reflect a minimum fraction of them. Therefore, the link between the Tx and Rx is the Line-of-Sight (LOS) path, which is the highest link in amplitude. Having this strongest component in terms of amplitude, will benefit the communication link as the scattering and reflected components are despised. This effect will be discussed further in this chapter.

This chamber emulates an free open field where reflection is not present. Furthermore, as the interior is isolated by the absorbers and contained by a Faraday cage, no external signals are present, allowing maximum transfer from Tx to Rx without any additional influence.

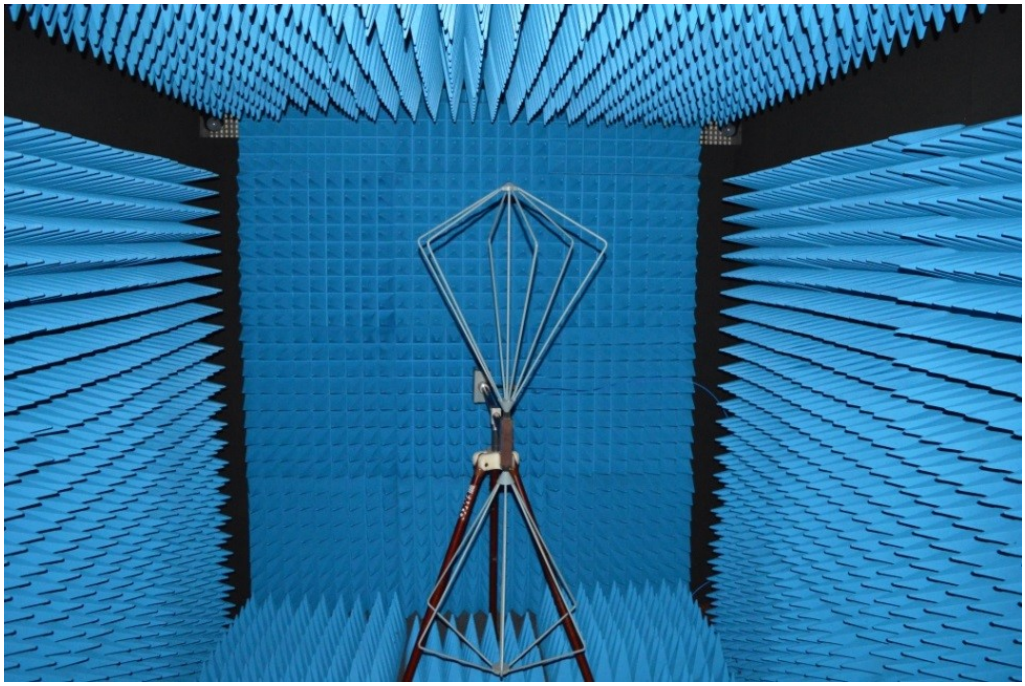


Figure 3.1: Interior of an anechoic chamber

When the six walls of the chamber are covered by RAM, it is said to be full anechoic, and when at least one of the walls lacks of RAM, it is said to be semi-anechoic and such a wall can be conductive and some of the radiation could escape.

Radiation-absorbent Materials (RAM)

As the name depicts, RAM is used to absorb partially or totally emitted RF radiation. This material is widely use for EM measurements to avoid reflected signals coming from the known source or undesired emissions from an external entity. With this, the effective radiation pattern and the maximum power transferred can be measured accurately inside a testing facility, reducing the error.

Pyramidal absorbers

One of the most effective types of absorbers are pyramidal shaped, as shown in Figure 3.2. The performance of pyramidal-shape absorber is the result of mul-

tiple reflections that occur between the pyramids, as well as absortion from the material. Each of them is bigger in comparison to the wavelength, so the sides of the pyramids reflect the incident signal which gets reflected several times by the adjacent, to be minimized or absorbed by the material [15], to ensure that the signal received at Rx is directly from the transmitter.

To be effective, the pyramids must be at least one half wavelength long at the lowest frequency of interest. The wavelength of the radio frequency signal as it passes through the absorber is reduced by a factor of:

$$\lambda = \frac{1}{\sqrt{\epsilon_r}} \tag{3.1}$$

where λ is the wavelength within the absorber, and ϵ_r is the permitivity relative to free space [16], defined as:

$$\epsilon_r \approx 8.8542 \times 10^{-12} \frac{F}{m} \tag{3.2}$$

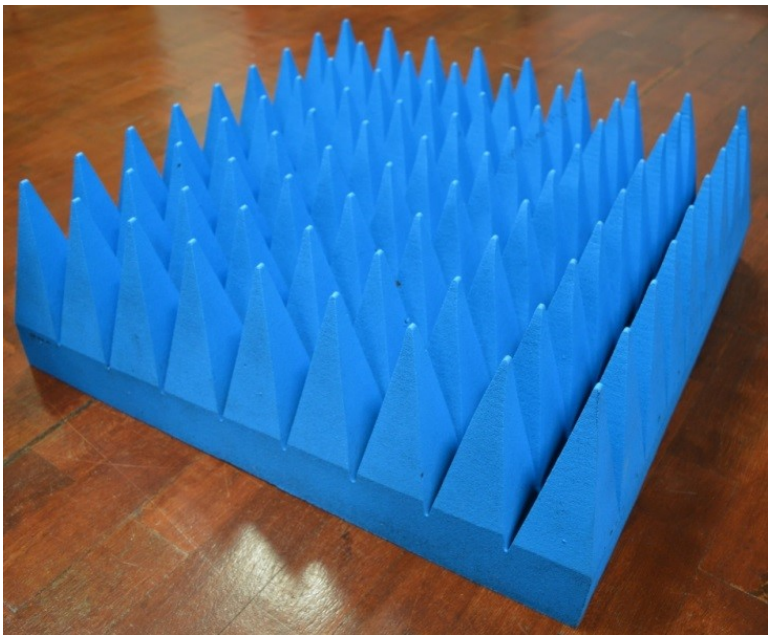


Figure 3.2: Pyramidal absorbers used. The section has 81 pyramids of 21 cm height and square base of 6.5 cm of length

Ferrite tile

Ferrite tiles shown in Figure 3.3 are a absorbent material also used to cover the walls of a anechoic rooms. This material is more compact than the usual pyramidal foam absorber and can be used in conjunction with the pyramidal absorvers to increase the attenuation. Ferrite tile is less effective at higher frequencies, specifically it works best below 100MHz. Its impedance must be equal to 377Ω. Nevertheless, this will not stop the reflection of the incident wave. The principle is that the thickness of the tile is tuned so the phases of the incident an reflected wave cancel to form a resonant condition within the material [17].



Figure 3.3: Example of a ferrite tile

Salisbury screen

Another type of EM absorber is the Salisbury screen, as shown in Figure 3.4. It consists in a single thin resistive sheet placed at a distance of $\lambda/4$ from the conducting ground plane, and a low-loss dielectric substrate is placed within these two layers.

When resonance exists, the impedance of the conducting ground plane is turned into a open circuit at the resistive sheet and it presents an impedance $Z_0 = 377\Omega$, identical to free space [18]. If the incident signal passes through the resistive screen, it is reflected by the conducting plane back to the restive screen, with a phase change of 180° which subsequently leads to a 180° phase difference with the incident signal, resulting in a destructive interference causing no reflection or phase cancellation [19].

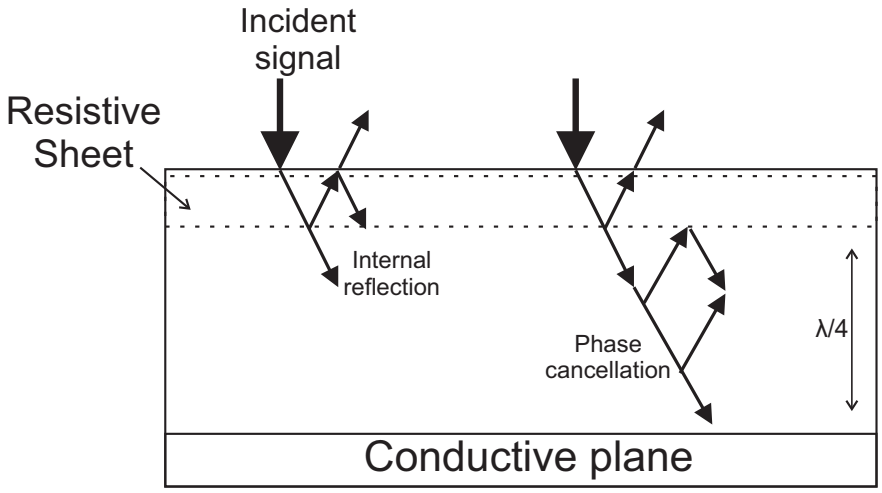


Figure 3.4: Internal reflection and phase cancellation method used in the Salisbury screen

3.1.2 Gigahertz Transverse Electromagnetic Cell

Transverse electromagnetic (TEM) cells are testing environments for EM emission and immunity tests in a shielded environment. Essentially, they are expanded versions of a coaxial transmission line big enough to place a EUT inside. The TEM cell consists of a section of rectangular coaxial transmission line with a uniform central section between two tapers. The discontinuity between the one of the tapers and the central section limits the upper operating frequency because non-TEM modes are excited, degrading the field uniformity [20]. Wave propagation travelling through the cell has a characteristic impedance of 377Ω, which replicates the effect of far-field propagation in free-space [21].

GTEM are a pyramidal-shaped single metallic taper structure of a characteristic

impedance of 50Ω, with an absorber at the end, as shown in Figure 3.5. It can be seen as a combination of an anechoic chamber and a TEM, although is a low cost alternative to semianechoic chambers.

Being a single taper and the lack of discontinuity allows high operation frequencies in the order of Gigahertz, with the walls acting as a wave guide.

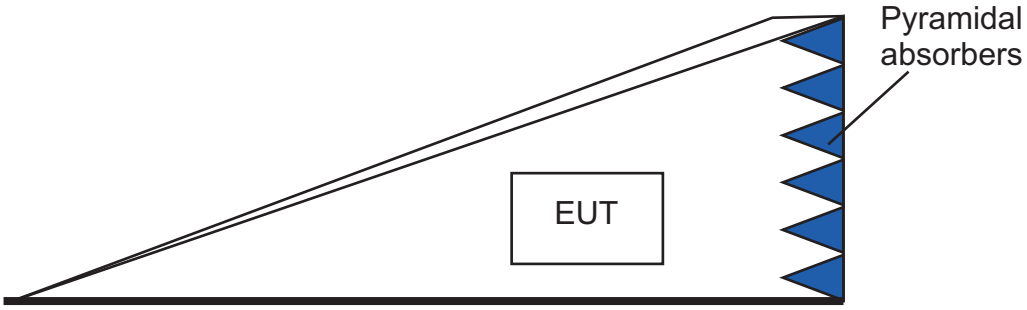


Figure 3.5: Gigahertz Transverse Electromagnetic Cell schematic

This device was not used for EM test through this project. Thus, is not investigated further throughout this document.

3.1.3 Mode Stirrer Reverberation Chamber

A Mode Stirrer Reverberation Chamber (MSRC or RC) is an environment facility for EMC testing, consisting of a screened room or cavity (typically aluminium) that blocks external static and non-static electric fields to isolate electrical devices excited by a source, (typically, a wide band antenna). RC's are able to provide a flexible and repeatable test environment, highly used for commercial, military, aerospace and automotive testing.

The metallic walls reduce the coupling of radio waves, electromagnetic fields and electrostatic fields. Furthermore, they are able to recreate a real scattering environment where multipath conditions exist due to the metallic walls.

When the cavity is excited at a single frequency, resonance modes can be excited as well. The number of modes is directly proportional to the dimensions of the chamber.



Figure 3.6: Inside of a RC displaying the metallic walls and with an antenna array set-up [22]

A RC can create very high field strength with moderate input power. Existing chambers make use of a paddle wheel or stirrer to change the resonant modes in the chamber in order to obtain a field that is considered statistically isotropic and homogeneous, making possible to carry out immunity and emission tests [23]. As the stirrer rotates, the internal geometry changes and it modifies the distribution of the electromagnetic field. The interior of an RC is shown in Figure 3.6, and Figure 3.7 shows the detail of a stirrer. The typical arrangement for an RC experiment system is shown in Figure 3.8.



Figure 3.7: Stirrers of a RC. When in operation, they modify the internal geometry of the chamber [22]

RC's can be used to measure antenna radiation efficiency, absorption and heating properties of materials, shielding characterisations of cavities, cables, connectors and materials, diversity gains, capacity of multiple-input multiple-output systems, total radiated power (TRP) and total radiated sensitivity (TRS) of active wireless devices [24].

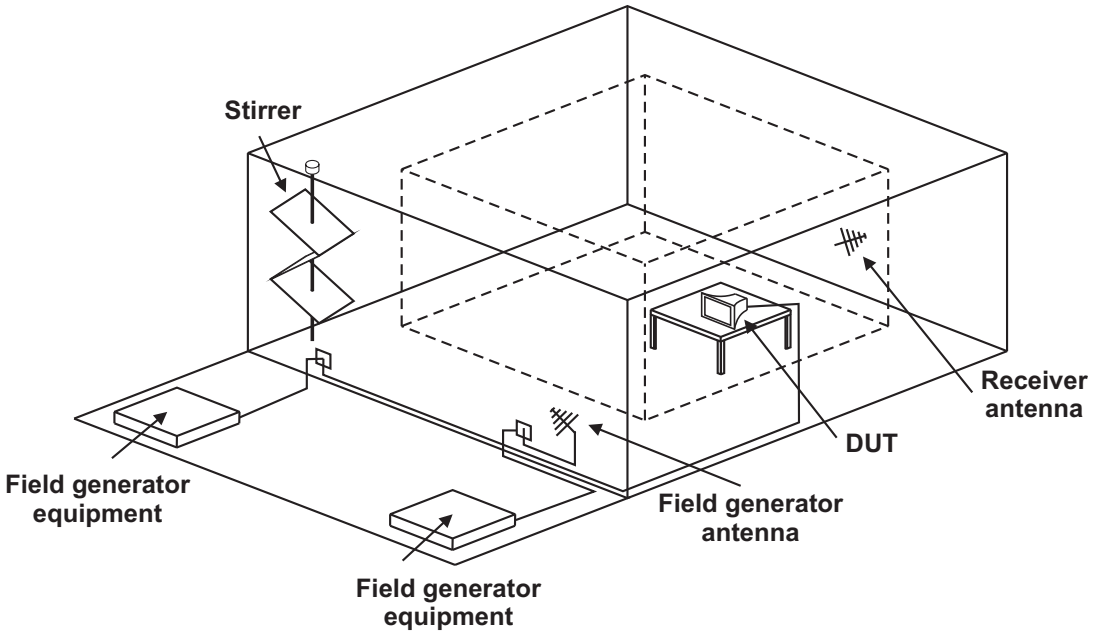


Figure 3.8: RC diagram

Siepel Eole 200: Reverberation Chamber

The George Green Institute for Electromagnetics Research holds a RC for EM testing. The cavity was supplied by French manufacturer Siepel and made out of galvanised steel. The lowerst usable frequency LUF of a RC is the frequency at which the cavity meets operation conditions to excite up to the 60^{th} of the source at the input [25]. The cavity's LUF is 200 MHz and its dimensions are:

- **External** - Height (H) of 3.23m, Width (W) of 3.76m and Length (L) of 4.88m.
- **Internal** - $H = 3.11$m, $W = 3.72$m and $L = 4.84$m.

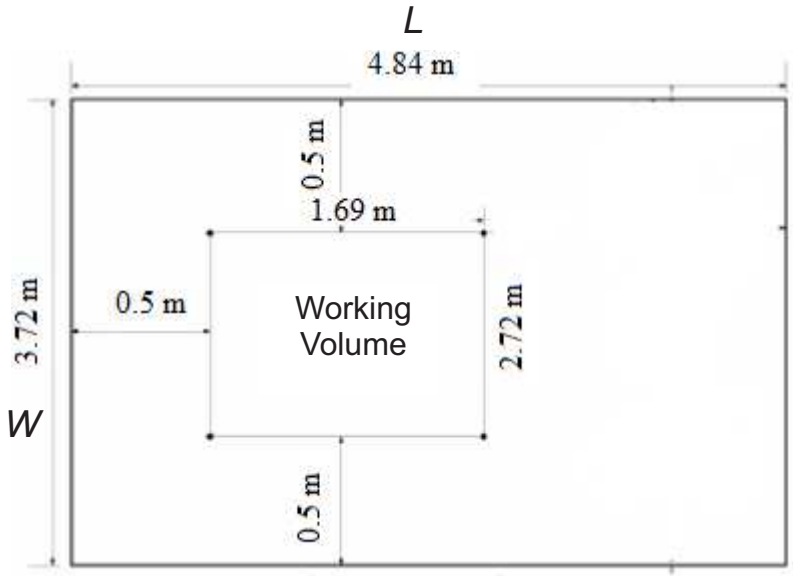


Figure 3.9: External and internal dimensions

with a defined working volume of dimensions: $H = 2.11$m, $W = 2.72$m and $L = 1.96$m, as shown in figures 3.9 and 3.10. This working volume is defined by the vendor as the space where the conditions for statistical uniformity are met.

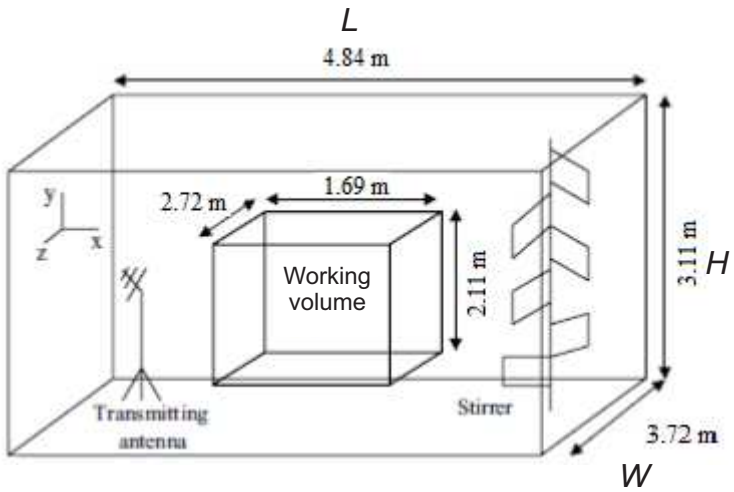


Figure 3.10: Working volume dimensions

As mentioned previously, the bigger the chamber, the more modes may be excited simultaneously. The resonance frequencies or modes are defined as:

$$F_{mnp} = \frac{c}{2}\sqrt{\left(\frac{m}{L}\right)^2 + \left(\frac{n}{W}\right)^2 + \left(\frac{p}{H}\right)^2} \tag{3.3}$$

where m, n and p are positive integers and represent the mode number or modes indices, with the restriction that only one can be equal to zero simultaneously [26]. c is the speed of light (2.998×10^8 m/s), L, W and H are the RC's length, width and height respectively. The first frequency of resonance or eigenmode for the RC is when $m = 1$, $n = 1$, and $p = 0$, which is 51.7MHz. The total number of modes can be approximated using Weyl's formula [27]:

$$N = \frac{8\pi}{3}(L \times W \times H)\frac{f^3}{c^3} \tag{3.4}$$

This is shown in Figure 3.11 for the RC.

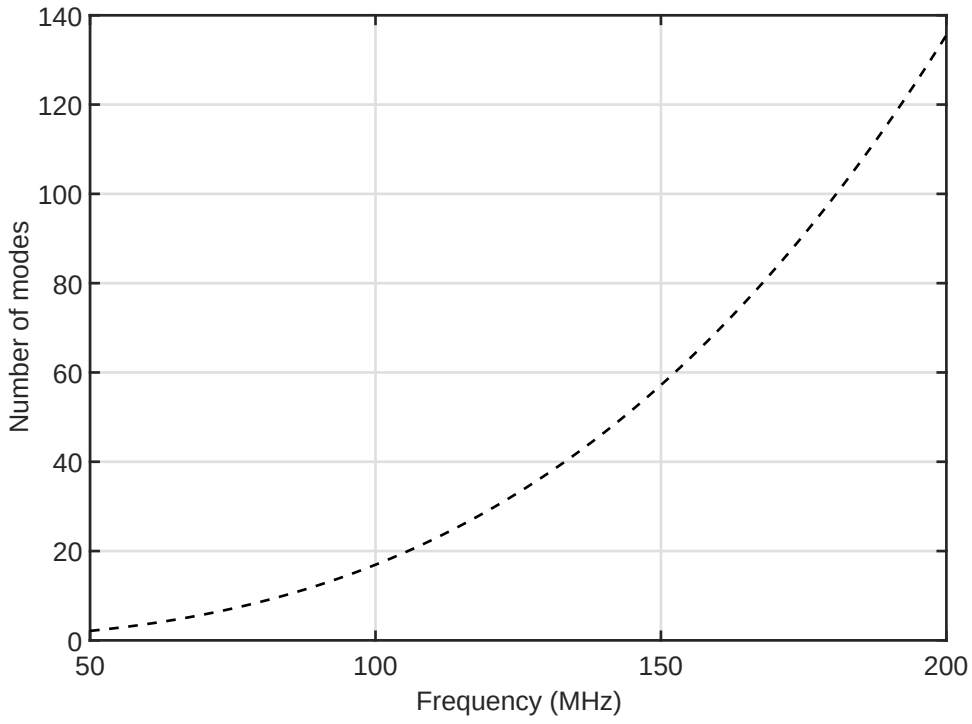


Figure 3.11: Total number of modes as a function of frequency

Additionally, another calculation is the mode density, which is the amount of modes available in a small bandwidth about a certain frequency. Low mode density means that the cavity or RC will not have adequate performance, as the mode density is too small to obtain spatial field uniformity [27]. Mode density is given by:

$$D_s(f) = 8\pi(L \times W \times H)\frac{f^2}{c^3} - \frac{L+W+H}{c} \tag{3.5}$$

and the mode density of the RC is shown in Figure 3.12.

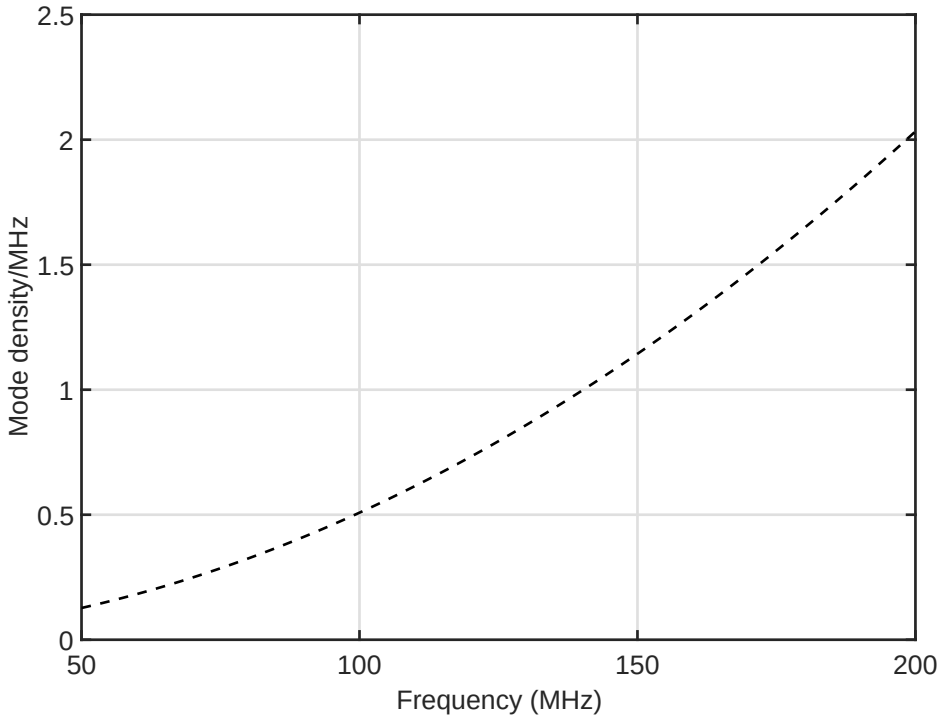


Figure 3.12: Mode density per MHz

3.1.4 Standards for radiated emissions and immunity applications

MIL-STD 461 F

MIL-STD 461 F is a United States standard that establishes the testing requirements for conducted and radiated emissions and immunity, utilised by the Department of Defence for military applications. It provides guidelines and principles for shielding, abortion, measurement procedure and tolerances for the frequency range of 30 Hz to 40 GHz [28, 29].

RTCA DO 160

The Environmental Conditions and Test Procedures for Airborne Equipment is a standard published by the Radio Technical Commission for Aeronautics (RTCA), which covers the procedures for testing airbone electrical and electronic equipment and mechanical systems RTCA DO 160 [30]. The standards establishes a calibration procedure for RC, where firstly the chamber is calibrated when empty in order to determine the normalised field, insertion loss and constant of the chamber. Subsequently, the chamber is loaded and the calibration is performed once more. This determines the loading factor of the chamber [28].

The calibration procedure consists of taking field measurements in multiple positions, each in one of the edges of the working volume (similar to Figure 3.8) with a three axis electric field probe for frequencies below 10 times the lowest working frequency F_s ($10F_s$), and 3 positions for frequencies above that over. The tolerance levels of the total field deviation to meet the requirements for this standard are:

Table 3.1: Field deviation limits of the DO 160 standards

Frequency range	**D0 160 D limit**	**D0 160 E, F, G limit**
100MHz	4 dB	6 dB
100 to 400 MHz	Linear decrease from 4 dB at 100MHz to 3 dB at 400 MHz	3 dB
400 MHz to 18 GHz	3 dB	3 dB

In terms of testing, the standard provides guidelines for emissions and immunity tests, similar to the IEC EN 61000-4-21 standard.

IEC EN 61000-4-21

The International Electrotechnical Commission (IEC) published the EN 61000-4-21 standard that establishes the procedures for measuring radiated emissions and immunity in a RC [28] to evaluate the performance of electric and electronic equipment in the presence of intentional and unintentional levels of emissions [31]. The tolerance level for the calibration procedure is the same as the DO 160 D standard, seen in Table 3.1. This standard is the followed in this document for the calibration process, as well as EM testing. Specifically one calibration procedure will be addressed further in this document.

Immunity Tests

In EM, immunity is the ability to perform thoroughly demonstrating resilience against harmful factors or environments. Both RTCA DO 160 and IEC EN 61000-4-21 standards depict the same set-up for this test. It involves the use of the following essential devices and instruments:

- Signal Generator
- Power meter to monitor the incident signal fed into the RC and the P_R at the receiver
- Tx and Rx antennas

- 3-axis E-field probe
- EUT operational equipment

The EUT is placed within the working volume and the stirrer is set to operate, either in step or continuous mode, depending on the experiment, as seen in Figure 3.13.

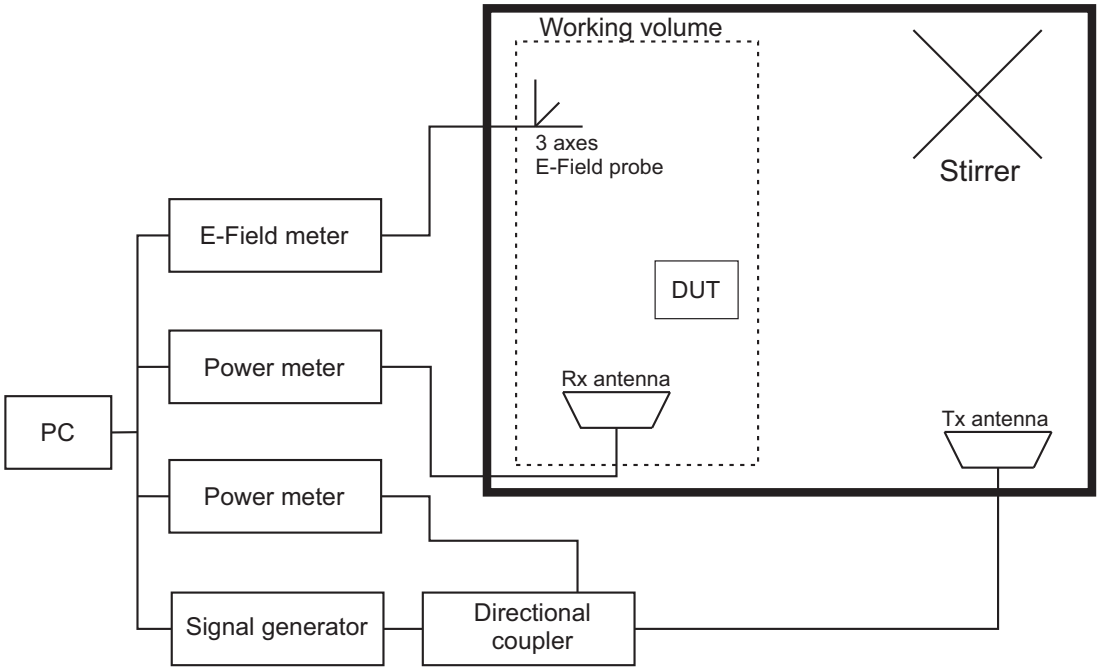


Figure 3.13: Typical immunity test set-up in RC

It is desired that the Tx antenna is pointing towards the stirrer, and the Rx towards one edge of the chamber. In this way, direct coupling is avoided and, furthermore, the receiving signal consists essentially of reflected and stirred components. Ideally, the Rx should be within the working volume. In other words, the purpose is to expose the EUT and evaluate its performance with multiple metrics.

In some cases, when the device is unable to handle with harmful signals, it is necessary to use additional tools to allow and reach the desired performance. Hence, it is necessary to use techniques such as shielding to avoid or reflect undesired emissions. This involves an enclosure (typically metallic) to protect the EUT from external sources of interference.

Emission Tests

Opposite to the the previous, this procedure focuses on measure all the resultant emissions produced by the EUT. By revolving the stirrer, the incident signal is reflected and scattered across the RC, exciting multiple modes in function of the operation frequency. The instruments required are the following:

- Power meter to monitor the received signal strength P_R
- Rx antennae
- 3-axis E-field probe
- EUT operational equipment
- Spectrum analyser

The basic configuration is shown in Figure 3.14.

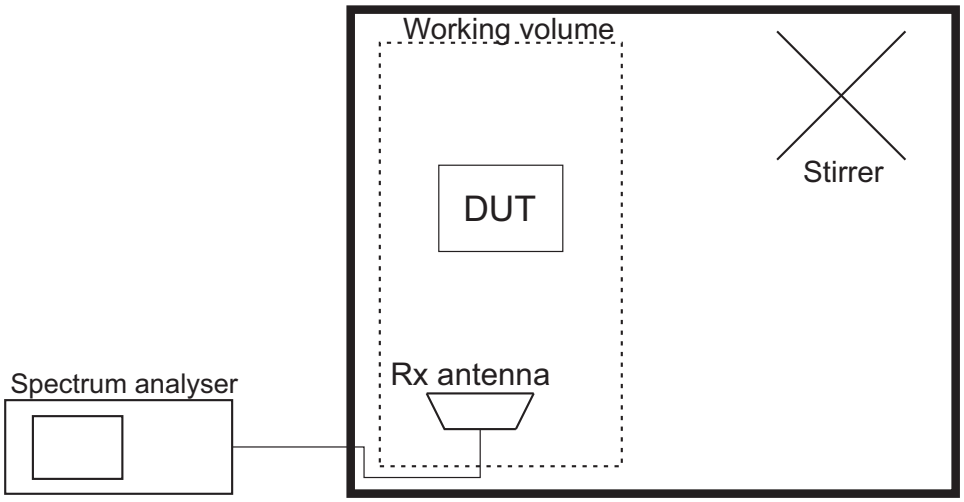


Figure 3.14: Emissions test set-up in RC

This test allows for the evaluation of the total emissions. Usually the EUT will be installed within other similar devices. Therefore, this assessment will note if the emissions exceed limits and could harm any instrument or device in its vicinity when in operation.

Quality Factor of Chamber

The statistical uniformity of the interior field is given by the quality (Q) factor. It indicates the cavity's ability to store energy which will affect the field's amplitudes and was introduced in [32] to find an expression for the average power transfer function in the chambers. It is the ratio of the stored cavity energy to the dissipated power, defined as:

$$Q = \frac{\omega U_c}{P_d} \tag{3.6}$$

where ω is the angular frequency of operation ($\omega = 2\pi f$), U is the steady-state energy in the cavity and P_d is the dissipated power.

The steady-state energy U is expressed as:

$$U = \frac{\varepsilon}{2} \int_0^c \int_0^b \int_0^a |E|^2 dxdydz \tag{3.7}$$

where ϵ is the permittivity of the propagation medium, a, b, c are the cavity dimensions in the x, y, z directions respectively, and $|E|$ is the magnitude of the total electric field vector [33]. Thus, substituting Eq. 3.7 into Eq. 3.6, Q-factor can be written as

$$Q = \frac{\omega\varepsilon \int_0^c \int_0^b \int_0^a |E|^2 dxdydz}{2P_d} \tag{3.8}$$

The chamber transfer function f_x is the statistical average of the ratio of the received power to transmitted power. From the wave perspective, the transfer function can be deduced as follows

$$f_x = \frac{P_R}{P_T} = \frac{\lambda^3 Q \eta_{Tx} \eta_{Rx}}{16\pi^2 V} \tag{3.9}$$

where P_R and P_T are the received and the transmitted powers respectively, λ is

the wavelength, V is the cavity volume, η_{Tx} and η_{Rx} are antenna efficiencies for the Tx and the Rx antenna respectively. Ideally, the transfer function is independent of the location of the antennas. Rearranging eq. 3.9, the Q-factor can be expressed as:

$$Q = \frac{16\pi^2 V}{\lambda^3 \eta_{Tx} \eta_{Rx}} \frac{P_R}{P_T} \tag{3.10}$$

The EUT is placed in the chamber and exposed to an electromagnetic field while the stirrer revolves. The average response of the EUT to the field is found by integrating the response over the time period of one revolution of the stirrer. As the stirrer rotates, the internal geometry changes and, hence the modes excited by the frequency of the incident signal. This causes the signal to resonate differently in the receiver antenna, even with small changes, and its polarisation and amplitude changes as well. This modifies directly the Q-factor and it fluctuates drastically in some cases.

The metal walls of the chamber allow a large field to be built up inside the chamber. The EUT is therefore exposed to a high field level consisting of several different polarizations [34].

The objective of the shielded walls is to add up to maximum of as many standing waves as practically possible in the usable test volume [35].

In some research documents, an alternative Q-factor calculation is addressed, known as fast calculation of Q-factor [36, 37]:

$$Q = \frac{1}{2} \omega \epsilon V \left\langle |\overline{E}|^2 \right\rangle \tag{3.11}$$

and additionally, can be caculated by measiuring the linear gain or S_{21} parameter:

$$Q = \frac{16\pi^2 V}{\lambda^3 \eta_{Tx} \eta_{Rx}} \left\langle |S_{21}|^2 \right\rangle \tag{3.12}$$

Calibration

Calibration is a procedure to be conducted in the RC before utilising it. It should be done only once in the RC lifespan, unless the geometry chances drastically, i.e. modifying the wall's dimensions. The standard used for the calibration was the EN 61000-4-21.

Calibration is an extensive process where E-field data is gathered by a 3-axis probe or sensor in multiple points inside the RC, specifically in the 8 edges of the working volume. The E-field received is the sum of the stirred and unstirred components [38].

Additionally, a receiving or reference antenna is placed within this working volume to record P_R, whilst the transmitting antenna remains outside the working volume pointing towards a wall, in order to avoid direct coupling between both antennas, and only reflected and stirred components are present[31].

The data samples are collected over a full rotation of the stirrer. The number of samples match the number of stirrer positions, which vary in function of the frequency band required and the number of frequencies are logarithmically spaced starting from the minimum working frequency f_s.

Table 3.2: Samples and turn positions recommended

Frequency range	Number of samples	Number of frequencies
f_s to $3f_s$	50	20
$3f_s$ to $6f_s$	18	15
$6f_s$ to $10f_s$	12	10
Above $10f_s$	12	20/decade

Having a reference antenna, an estimation of the E-field (E_{Est}) is possible using the recorded P_R for each turner position.

$$E_{Est} = \left\langle \frac{8\pi}{\lambda} \sqrt{5 \frac{P_{MaxRec}}{\eta_{Rx}}} \right\rangle_n \tag{3.13}$$

where P_{MaxRec} is the maximum received power over the total of turner positions and η_{rx} is the gain of the reference antenna.

Electric Field Measurements

To begin with the process, the E-field probe will be placed in each of the edges of the working volume, as shown in Figure 3.15. The order of measurements is irrelevant as the values will be averaged once the process ends.

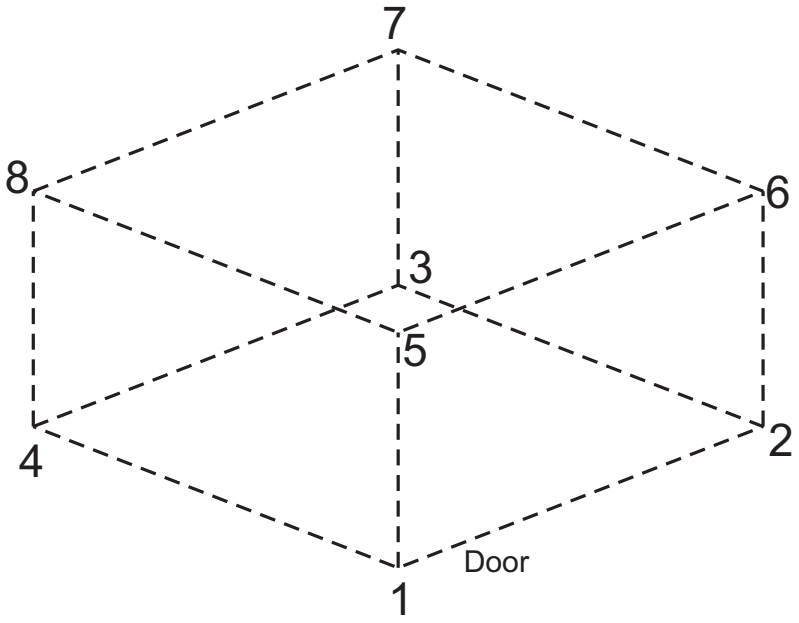


Figure 3.15: Working volume

Each sample contains the three field components E_x, E_y and E_z, and will be computed as the arithmetic mean of each axis and each frequency from the eight positions:

$$\left\langle \overleftrightarrow{E}_x \right\rangle_8 = \frac{(\sum \overleftrightarrow{E}_x)}{8} \tag{3.14}$$

$$\left\langle \overleftrightarrow{E}_y \right\rangle_8 = \frac{(\sum \overleftrightarrow{E}_y)}{8} \tag{3.15}$$

$$\left\langle \overleftrightarrow{E}_z \right\rangle_8 = \frac{(\sum \overleftrightarrow{E}_z)}{8} \tag{3.16}$$

for which it is necessary to normalise each of the maximum E-field measurement to the square root of the average input power:

$$\overleftrightarrow{E}_{x,y,z} = \frac{E_{Maxx,y,z}}{\sqrt{P_{Input}}} \tag{3.17}$$

where, $E_{Maxx,y,z}$ is the maximum value measured from each probe axis and P_{Input} is the input power.

Then, the average of the normalised maximum of all the edges is calculated. This is to give equal weight to each axis:

$$\left\langle \overleftrightarrow{E} \right\rangle_{24} = \frac{(\sum \overleftrightarrow{E}_{x,y,z})}{24} \tag{3.18}$$

Field uniformity is then calculated. It is the normalised mean of the normalised maximum values of each of the 8 edges of the working volume, and is calculated independently for each axis:

$$\sigma = \sqrt{\frac{\sum(\overleftrightarrow{E}_i - \left\langle \overleftrightarrow{E} \right\rangle)^2}{n-1}} \tag{3.19}$$

Finally, the 3-axis field uniformity is denoted by:

$$\sigma_{24} = \sqrt{\frac{\sum_{m=1}^{8}\sum_{n=1}^{3}\left(\overleftrightarrow{E}_{m,n} - \left\langle \overleftrightarrow{E} \right\rangle_{24}\right)^2}{24-1}}$$

The total of the E-field calculations mentioned previously, are plotted on Figure 3.16, as well as the limit proposed by the standard EN 61000-4-21.

There exists a possibility that these values exceed the limit proposed by the standard. This means that the chamber cannot operate at the lower desired frequency. In case the excess is minimum, reducing the working volume dimensions could lead to a reduction of the field uniformity. Once this is done, the calibration procedure must be repeated.

Calibration Results

After having processed the data gathered during the calibration exercise, it was found that the field uniformity meets the limit proposed to be adequate for EM measurements, as seen in Figure 3.16.The tolerance limits for the E-field are shown in the Table 3.3 below:

Table 3.3: Standard deviation limits set by the standard BS EN 61000-4-21 for RC calibration

Frequency range	**Tolerance requirements for standard deviation**
80 MHz to 100 MHz	4 dB
100 MHz to 400 MHz	4dB at 100MHz decreasing linearly to 3 dB at 400 MHz
Above 400 MHz	3 dB

Meeting the requirements noted in Table 3.3, it is said that the chamber is considered uniform if the standard deviation is within the limits established.

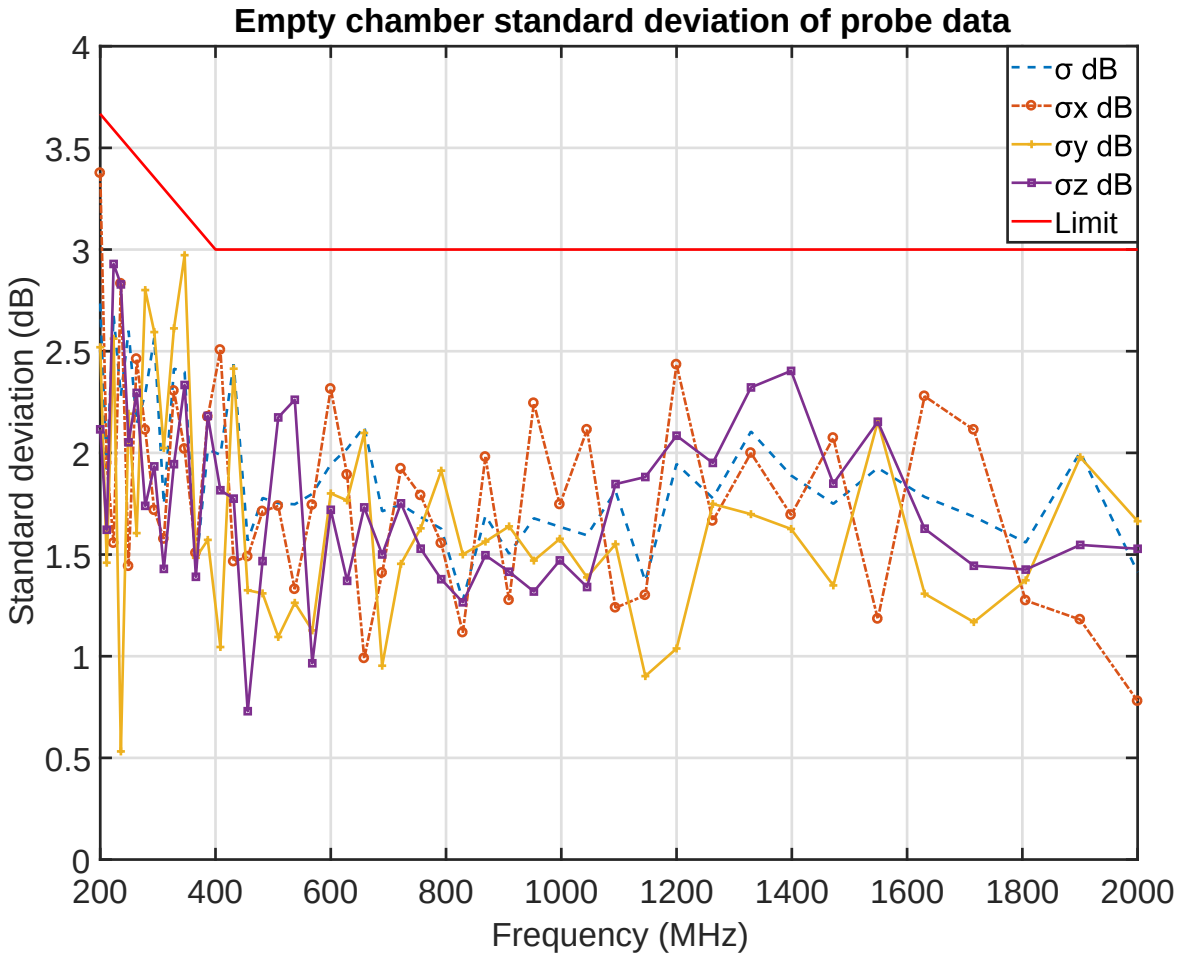


Figure 3.16: Standard deviation of data for E-field components of 8 probes and field uniformity.

The red continuous line denotes the limit and the 3-axis values are expected to be below this threshold. Orange, yellow and purple lines from Figure 3.16 denote the standard deviation from axis x, y and z, respectively. Leading to the total standard deviation or field uniformity, shown as a blue dotted line. Henceforth, the cavity is suitable for emissions and immunity testing.

A parameter needed to obtain during the calibration is the Chamber Calibration Factor CCF, essential for the RC's Q-factor calculation. It is defined as:

$$CCF = \left\langle \frac{P_{AveRec}}{P_{Input}} \right\rangle_8 \tag{3.20}$$

being P_{AveRec} the average power received and P_{Input} the average power received in all 8 probe positions. This is shown in Figure 3.17

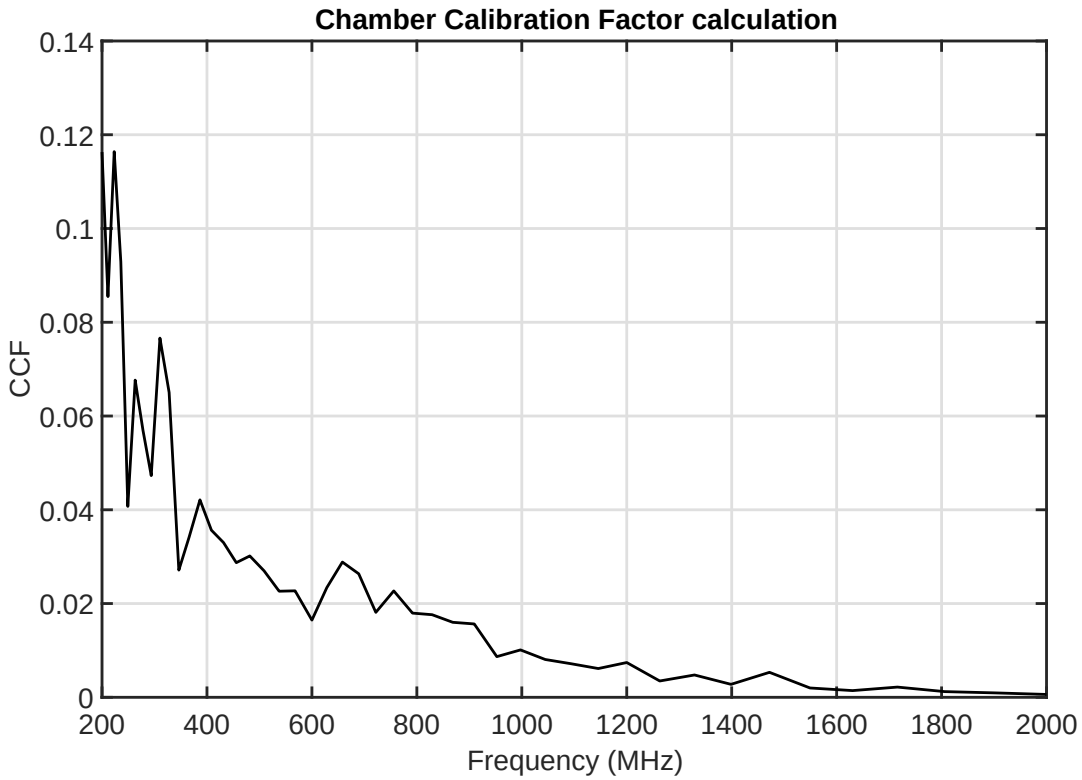


Figure 3.17: Chamber Calibration Factor

On the other hand, the ratio bewteen the output and the incident signal is know as defined as Insertion Loss, which is the total of power loss generated by the cavity itself when empty, or the summation of the chamber plus the EUT when in place.

$$IL = \left\langle \frac{P_{MaxRec}}{P_{Input}} \right\rangle_8 \tag{3.21}$$

being P_{MaxRec} the average power received in all 8 probe positions.In this case, the measurement has been performed with an empty chamber, with contribution only by the antennas, cables and non-metallic stands. This is shown in Figure 3.18.

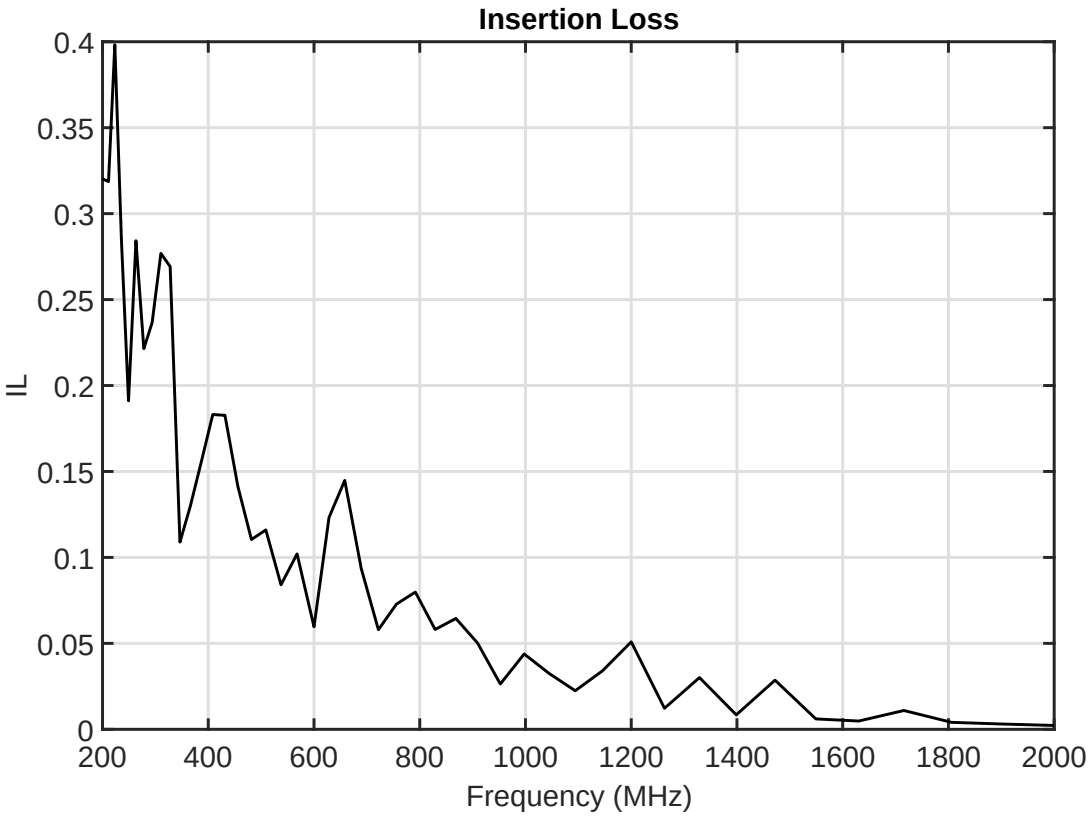


Figure 3.18: Insertion Loss of an unloaded RC

Finally, the RC's Q-factor has been calculated using S_{21} of an empty cavity, and with two different absorbers. The result is shown in Figure 3.19.

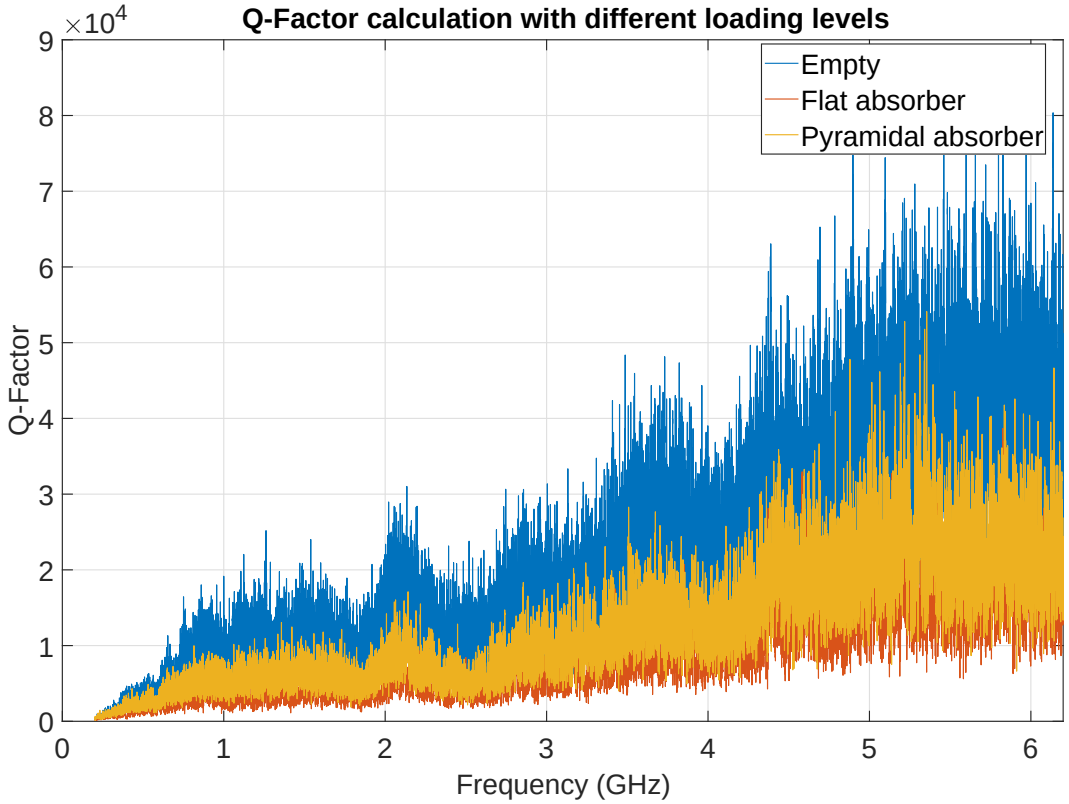


Figure 3.19: Chamber Q-factor using S_{21} measurements

As mentioned before, the combination of frequency variations and stirrer position causes the excitation of different modes. This changes the amplitude of the received signal, originating abrupt peak variation.

Furthermore, the behaviour of the Q-factor near the XBee channels is shown in 3.20.

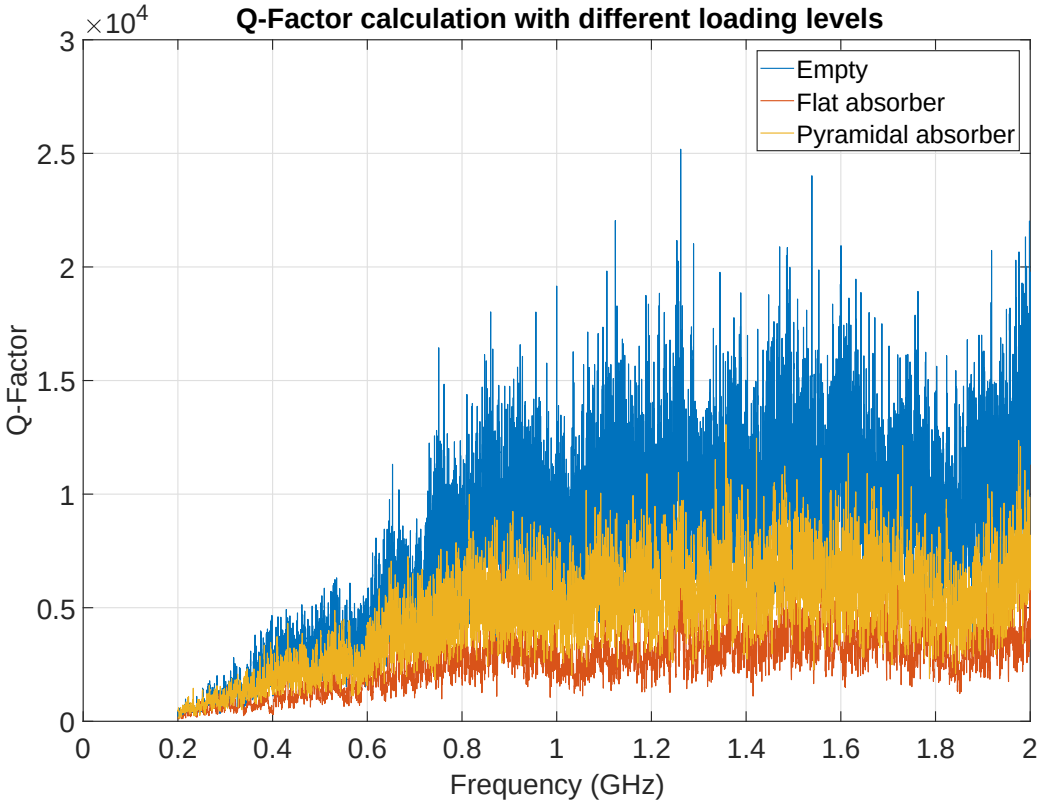


Figure 3.20: Chamber Q-factor up to 2 GHz using S_{21} measurements

In wireless communication systems, Rayleigh fading is a propagation environment model caused by multipath reception, that follows a Rayleigh distribution. The received signal is a summation of a large number of reflected and scattered waves. Rician fading is essentially a Rayleigh fading propagation with a strong dominant component caused by the presence of Line-of-Sight. In this chapter, the replication of external EM environments with the the use of a RC is presented, with the purpose of establish a laboratory setting for wireless devices or equipment testing.

3.2 Rayleigh & Rician environments

In a Tx and Rx set-up inside the RC, the received signal is comprised by a summation of many components produced inside due to the nature of the cavity's material and operation mode. Assuming that the antennas are pointing towards each other, the incident signal at Rx is comprised by two components: the LOS produced by the direct or antenna-to-antenna coupling from Tx to Rx and the reflection caused by the walls of the chamber. The second component is caused by a portion of the scattered signal reflected by walls and directed towards the stirrers which eventually reach the Rx. These two components are known as stirred and unstirred energy, respectively, as defined in [38]. Hence, the total electric field E_θ inside the RC can be defined as:

$$E_\theta = E_{s\theta} + E_{d\theta} \tag{3.22}$$

where $E_{s\theta}$ is the sum of the stirred energy components or amplitude and $E_{d\theta}$ is the sum of unstirred energy components, which at the same time can be written as the sum of the real and the imaginary components:

$$E_{s\theta} = E_{s\theta r} + jE_{s\theta i} \tag{3.23}$$

Following the assumption that the electromagnetic field in a well-operating RC is a circular complex Gaussian field, as in [39], the electromagnetic field can be expressed by two real independent Gaussian fields, with zero-mean and variance σ^2

$$\left\langle E_{s\theta r}^2 \right\rangle = \left\langle E_{s\theta i}^2 \right\rangle = \sigma^2 \tag{3.24}$$

Then, the amplitude of the complex generated E-field satisfies a Rayleigh distribution and the phase is uniformly distributed.

$$f(|E_\theta|) = \frac{|E_\theta|}{\sigma^2} \exp\left(- \frac{|E_\theta|^2}{2\sigma^2}\right) U(|E_\theta|) \tag{3.25}$$

where U is the unit step function

$$U(|(E_\theta|) = \begin{cases} 1, & |E_\theta| > 0 \\ 0, & |E_\theta| < 0 \end{cases} \tag{3.26}$$

and σ^2 is the variance of two Gaussian fields composing E_θ

Consider the excistance of an unstirred component. This implies that the deterministic component that is superimposed on the stochastic electromagnetic field due to the unstirred field should be considered, resulting in two real independent Gaussian fields with the same variance and mean values different from zero[39]. Combining them to determine an amplitude expression, the resultant expression is

$$f(|E_\theta|) = \frac{|E_\theta|}{\sigma^2} I_0\left(\frac{|E_\theta||E_{d\theta}|}{\sigma^2}\right) \times \exp\left(- \frac{|E_\theta|^2| + E_{d\theta}|^2}{2\sigma^2}\right) U(|E_\theta|) \tag{3.27}$$

where I_0 is the modified Bessel function of zero order. The resultal expression shown in Eq.3.27 is a Rician probability density function (pdf), derivered by Rice in [40].

In the occasion when direct coupling is insignificant, it is expected to have a Rayleigh distribution of the electric field. For this to happen, is necessary that

$$|E_{d\theta}|^2 \ll 2\sigma^2 \tag{3.28}$$

and Eq.3.27 reduces into Eq 3.25. This means that the unstirred or direct component is very small compared to the stirred, which can be written using 3.24 as

$$|E_{d\theta}|^2 \ll 2\langle |E_{s\theta i}^2| \rangle \tag{3.29}$$

Then, the inequality from Eq. 3.29 defines Rician K-factor in [41, 42] as

$$K = \frac{direct\ component}{scattered\ component} \tag{3.30}$$

or expressed as

$$K = \frac{|E_{d\theta}|^2}{2\sigma^2} \tag{3.31}$$

If no direct coupling exist, $K = 0$ ($K = -\infty$), the field magnitude is Rayleigh, and when no multipath is present, $K = \infty$ ($\sigma = 0$). In practice, this means that the antennas are adjusted to face each other (co-polarised) so the existence of LOS is possible. Then, the transfer is expressed as the sum of the direct coupling or LOS and the stirred energy or multipath scattering

$$S_{21} = S_{21_d} + S_{21_s} \tag{3.32}$$

where the direct component is therefore the LOS link, $S_{21_{LOS}}$. On the other hand, the real and imaginary elements of the stirred component are independent and normally distributed with zero mean and identical variances, equally to Eq.3.24. This is

$$\langle |S_{21_s}| \rangle = 0 \tag{3.33}$$

with standard deviation measured in the RC

$$var[Re(S_{21_s})] = var[Im(S_{21_s})] = \big[[Re(S_{21_s})]^2\big\rangle = \big[[Im(S_{21_s})]^2\big\rangle = \sigma_R^2 \tag{3.34}$$

Differently, the direct component measured in the RC has a nonzero mean d_R

$$\left\langle |S_{21_d}| \right\rangle = d_R \tag{3.35}$$

and zero variance

$$var[Re(S_{21_d})] = var[Im(S_{21_d})] = \left[[Re(S_{21_d})]^2 \right\rangle = \left[[Im(S_{21_d})]^2 \right\rangle = 0 \tag{3.36}$$

Considering the variance of the real and imaginary elements and using Eq.3.34 and 3.36, the variance of S_{21} can be expressed as

$$var[Re(S_{21})] = var[Im(S_{21})] = \left[[Re(S_{21})]^2 \right\rangle = \left[[Im(S_{21})]^2 \right\rangle = \sigma_R^2 \tag{3.37}$$

which can be rewritten as

$$2\sigma_R^2 = \left\langle |S_{21} - \left\langle S_{21} \right\rangle|^2 \right\rangle \tag{3.38}$$

Based on the summation of direct and stirred components deduced in Eq. 3.33 and 3.35, the mean value of the direct component of S_{21} can be expressed as

$$d_R = |\left\langle S_{21} \right\rangle| \tag{3.39}$$

Finally, a relationship among Eq. 3.24, 3.38 and 3.39 can be established which is directly related to the S_{21} measurements in the RC as

$$K = \frac{d_R^2}{2\sigma_R^2} = \frac{\left(|\left\langle S_{21} \right\rangle|\right)^2}{\left(\left\langle |S_{21} - \left\langle S_{21} \right\rangle|^2 \right\rangle\right)} \tag{3.40}$$

In [38], it has been demonstrated that the variance σ_R is not affected by the configuration of the antennas. On the other hand, the variance is affected by the

loading level or Q-factor of the chamber.

Subsequently, an experimentation set up was installed to compute the K-factor of the RC mentioned previously. Initially, the S_{21} parameter were measured with an empty chamber, in order to verify the concept stated in Eq. 3.28, where the direct coupling has little contribution in comparison with the reflected or scattered components. The antennas were configured allowing direct strong coupling in a LOS position with 1m separation connected to a Agilent Series Network Analyser E8350, with a range of 700MHz to 3 GHz for this first test and with purposes of illustration, the frequency of is 2GHz in order to compare results with the obtained in [38]. The lower frequency was limited to the horn antenna lowest working frequency. Having a strong coupling, the scattered components are relatively weak or have little contribution in amplitude compared with the LOS. Having less reflected contribution components exciting the walls and the stirrer reflections in the chamber, the environment is barely isotropic or not isotropic at all, hence the average or centroid of the real and imaginary components are not located in 0 for the real and imaginary plane. The measurement is shown in Figure 3.21.

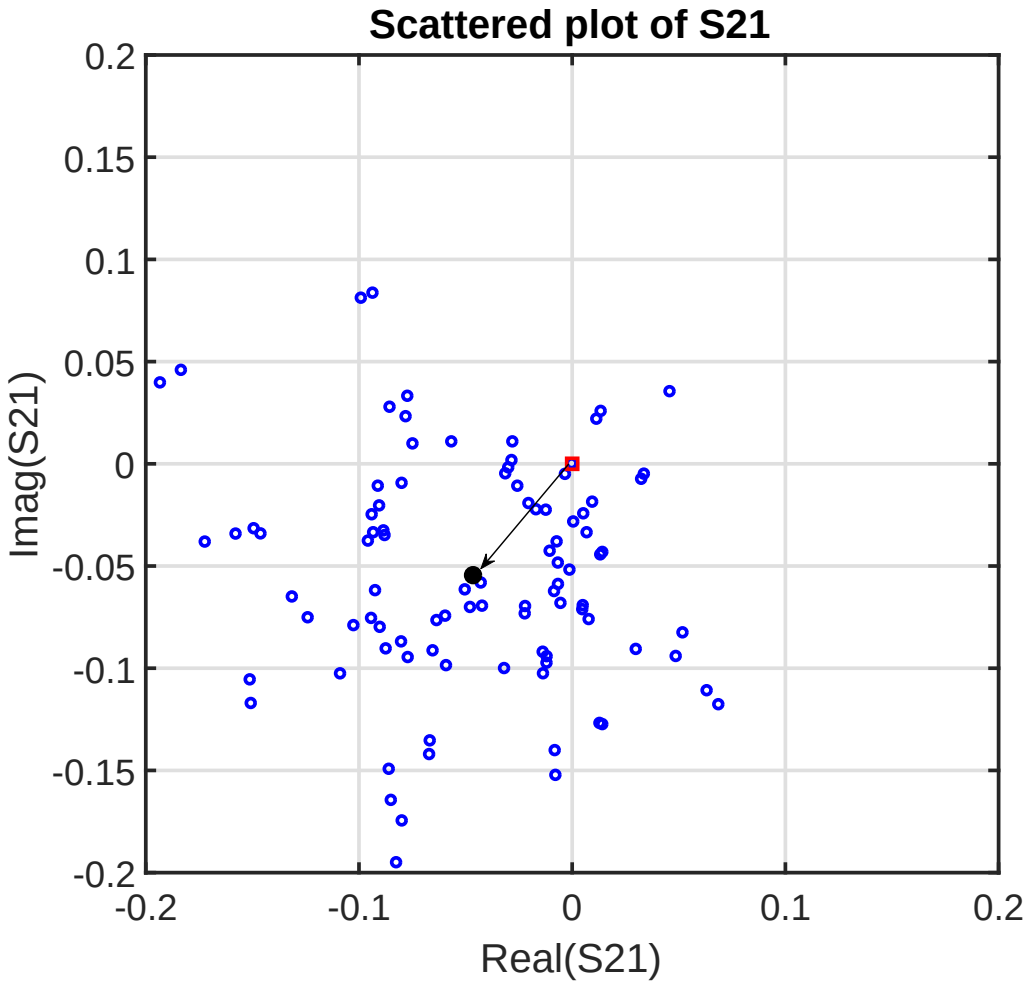


Figure 3.21: Strong direct coupling measured in the RC. The centroid (black dot) is displaced (black arrow) from the centre of the plane (red square), meaning that the average is not located in 0

In order to avoid direct coupling, the antenna configuration was changed, forcing the reduction of direct components (reduction of K) by pointing the Rx antenna to the walls, allowing the reception of more stirred components into the antenna.

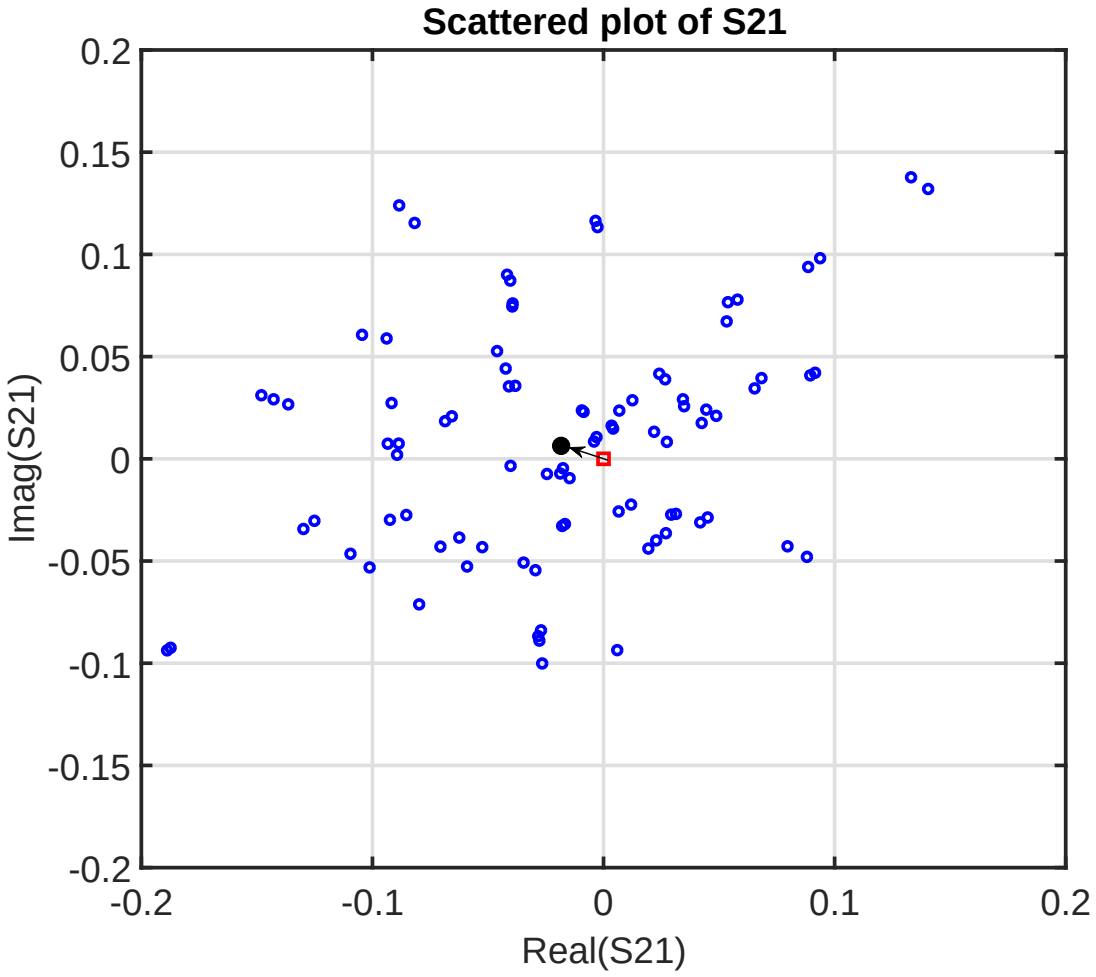


Figure 3.22: Little direct coupling measured in the RC. The centroid is now located at the centre of the plane in 0 (red square)

As a result, the stirred components have zero mean in a well stirred chamber with no direct coupling, meeting the Eq.3.33 and shown in Figure 3.22, where is possible to observe that the real and imaginary components are in a red square or dot in the vicinity of 0, where the mean is located. This allows an isotropic environment in the RC, more precisely in the working volume.

Comparing figures 3.21 and 3.22, is possible to visualise that the centroid of the points measured are displaced from 0 in case of presence of LOS, which means that

the direct components have a nonzero mean agreeing with Eq.3.35. On the other hand, when stirred components prevail and exists absence of LOS (NLOS), the centroid moves towards 0, where the mean is expected to be allocated, according to Eq.3.33, and this means that the environment has isotropic conditions.

According to the K-factor approximation shown previously and reduced to Eq.3.40, the loading factor of a RC and the antenna orientation are the predominant modifying elements of said variable. Thus, for this measurement, different loading factors have been considered, placing pyramidal absorbers inside. Each absorber has 81 square pyramids of 21cm heigh and square base of 6×6cm, similar to the one shown in Figure 3.2, the set-up is shown in Figure 3.23.



Figure 3.23: Antennas and absorbers set-up inside the RC

The VNA was configured to perform a swipe from 700MHz to 6GHz in 6401 points of resolution. Then, the RC was set to 50 steps per rotation for the stirrer.

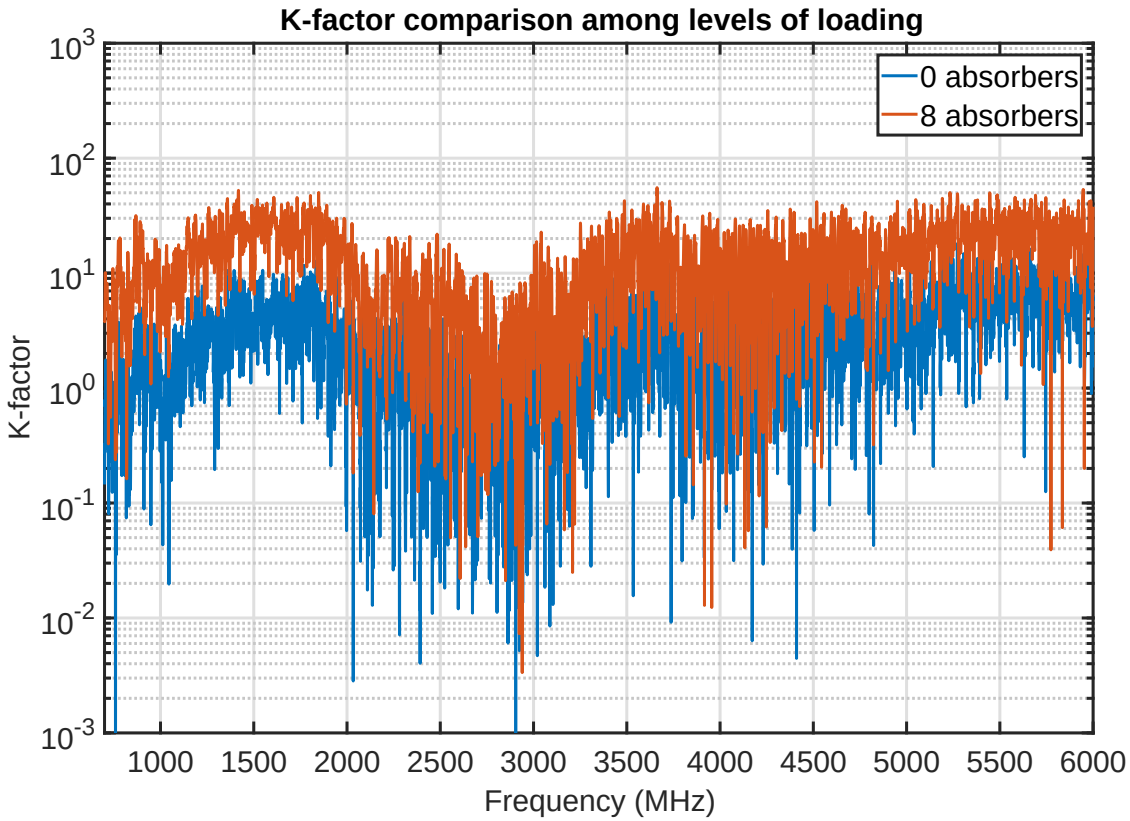


Figure 3.24: Comparison of resultant K-factor by modifying the loading levels in RC

The blue line in Figure 3.24 indicates the K-factor in function of the S_{21} measurements without any absorbers in the RC. Subsequently, 8 of these absorbers were placed inside the chamber and the measurement was conducted again resulting in the red line of Figure3.24. As expected, the absorbers reduce the contribution of the multipath or scattered components created inside the chamber, allowing the LOS component to be the greatest in magnitude which leads to increase the value of K, as in Eq.3.30. Being the bandwidth of interest from 863 to 868 MHz, it is worth noticing that around these frequencies, the K factor had an increase of around 4 times in its value from 0 to 8 absorbers, as shown in Figure 3.25. Hence, it could be assumed that the communication would be improved by this absorber configuration as the main component is greater in amplitude than the scattered components.. The frequencies of interest will be addressed further in the next chapter.

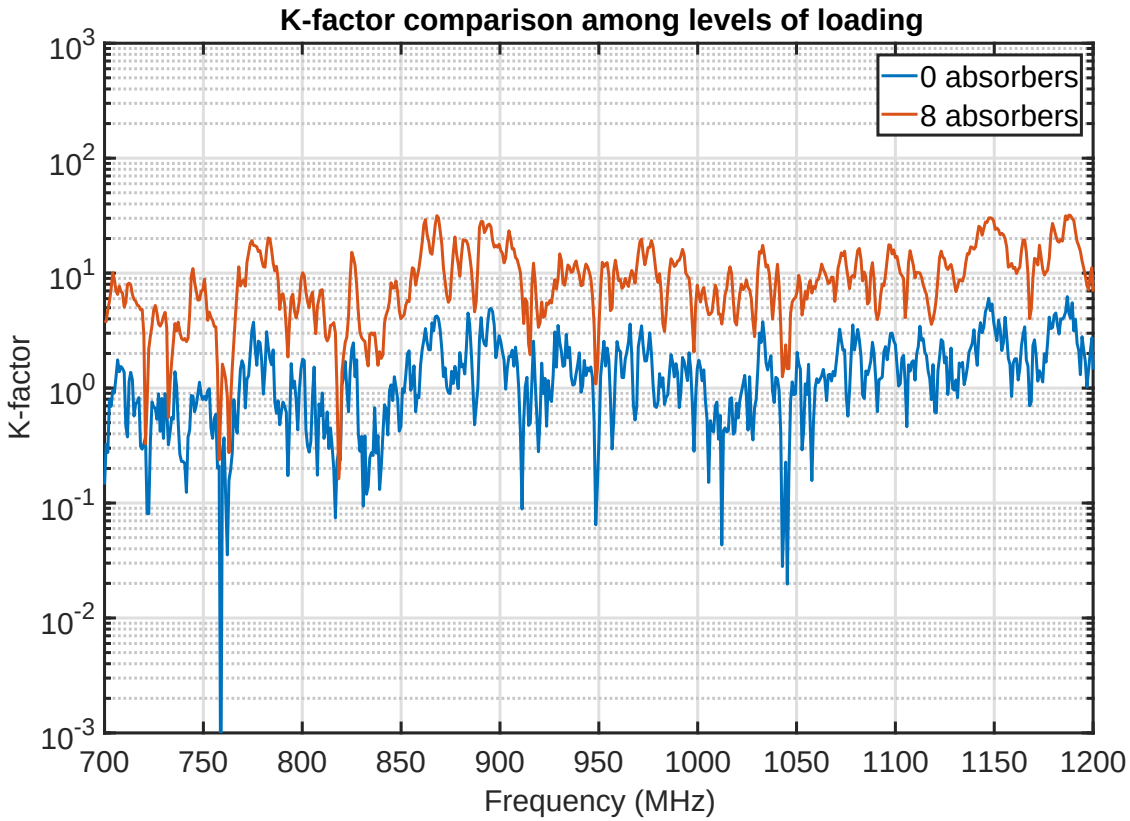


Figure 3.25: Comparison of resultant K-factor by modifying the loading levels in RC

The K factor of the Rician pdf could be altered also by the antenna polarisation. Having the same absorber configuration, a rotation of the Rx antenna is investigated to boost cross-polarisation. Giving the nature of the application to which this system is aiming, cross-polarisation of 90 degrees is unlikely to happen. However, it is useful to assess the contribution of having this scenario.

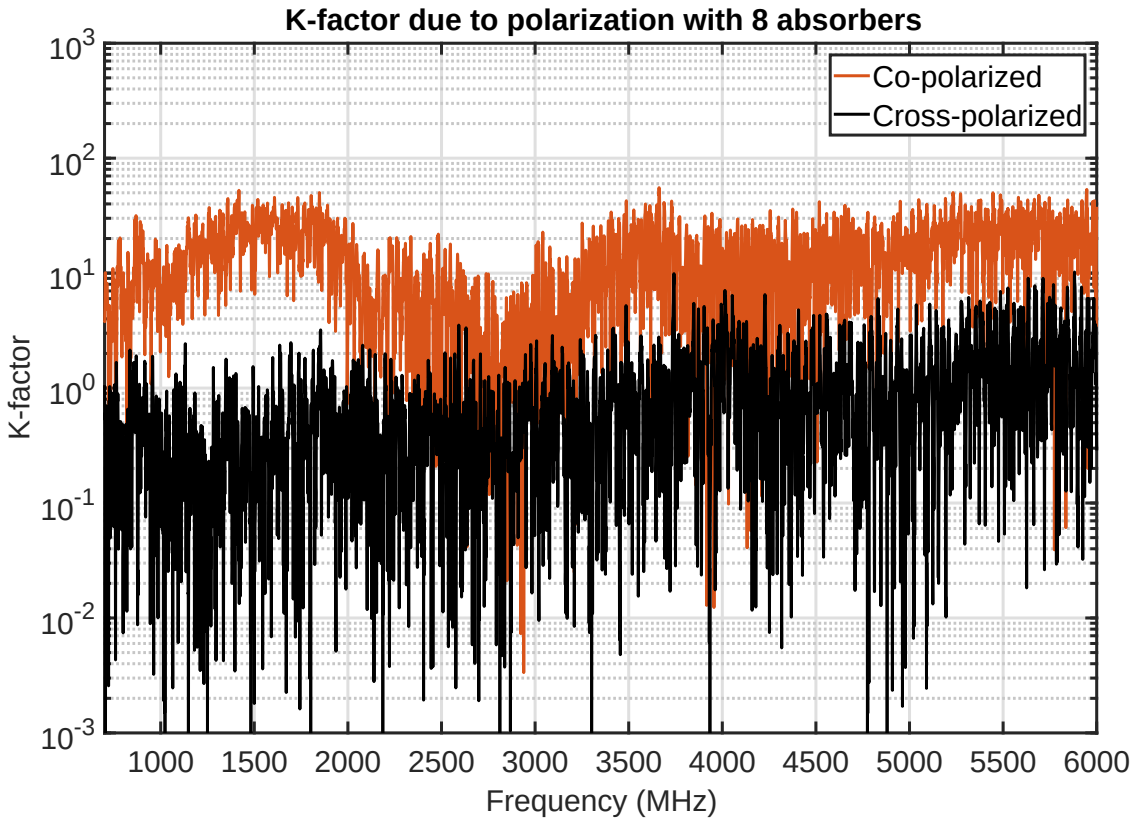


Figure 3.26: Comparison of resultant K-factor by modifying the antenna polarisation in RC with 8 absorbers

As shown in Figure 3.26, a change in the polarization produces a noticeable decrease in the k-factor for the same contidions in the RC. Focused on the 863 to 868 MHz band, the k-factor reduced approximately by 20 times compared to the co-polarized configuration.

On the other hand. regardless of the absorber's position in the RC, it is expected to obtain the same S_{21} values in a full stirrer rotation in a well-stirred RC. In order to prove this, a cubic RAM absorber was constructed and placed in multiple locations within the chamber, as shown in Figure 3.27.



Figure 3.27: Cubic absorber in the RC elevated 2m from the ground plane

For this experiment, four absorber positions were considered in the RC, and he resultant K-factor is shown in Figure 3.28, where it can be observed that the four measurements are on top of each other, demonstrating that the average of each measurement in a full rotation is independent of the absorbers position.

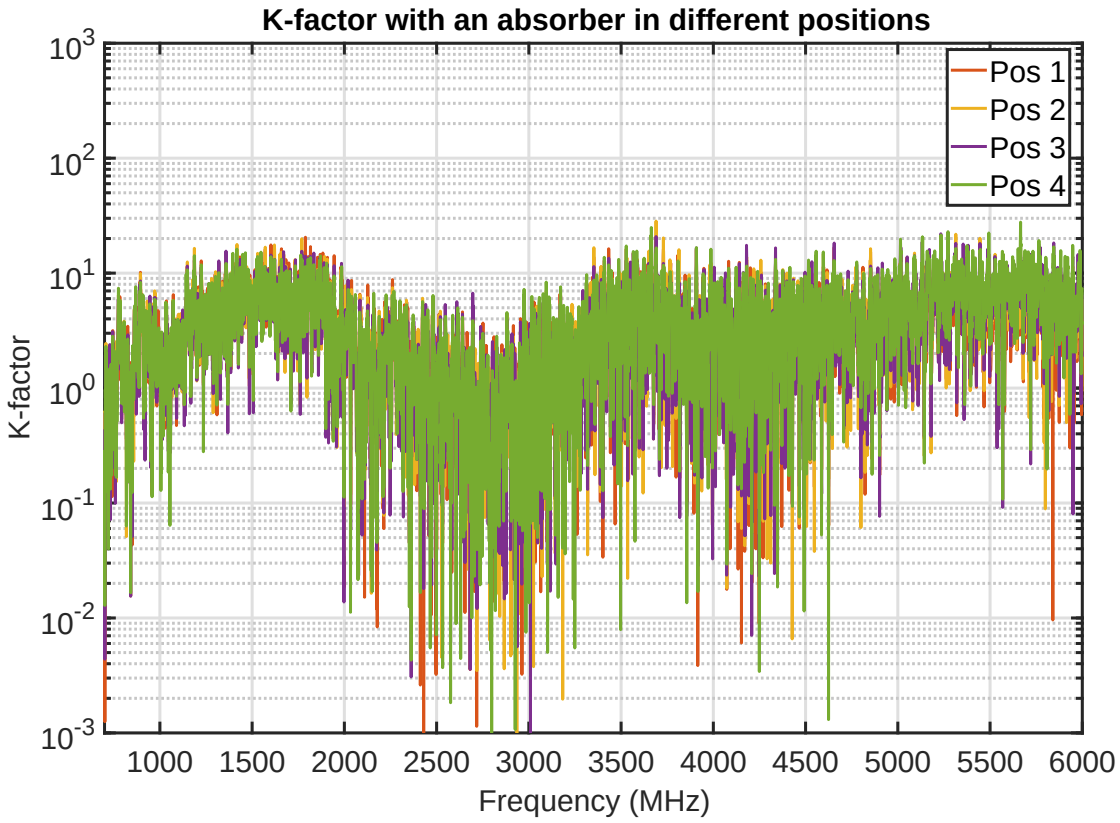


Figure 3.28: Comparison of resultant K-factor by modifying the loading levels in RC

The configurations (antenna positions and loading levels) that have been considered in this section will be utilised to asses the XBee performance. The purpose of this is to mimic possible realistic environments inside the RC for wireless communication devices evaluation.

In comparison with the Q-factor, the K factor increases when the number of absorbers increased, whilst Q-factor decreases, and vice-versa when the number of absorbers decrease, e.i. the greater the loading level, the less energy is stored within the RC, the magnitude of the multipath components is reduced and only a strong coupling component is present, allowing the K factor to increase in value.

3.3 Representation of a Overhead Line within a Reverberation Chamber

An overhead line is a way to deliver power to a train or tram, for the on-board equipment and, more importantly, to operate its motors and move. It consist in a high-voltage grid infrastructure placed over the tracks that makes contact with the train via a pantograph, which in turn is called Overhead Line Equipment (OLE). Given the current carried by these lines, an electric field is created which can be harmful for any surrounding electronic equipment or instrument.

Any communication system on-board or aside of the train is exposed to other type of potential interference caused by the OLE infrastructure. In some points throughout the grid, the contact between the pantograph and the lines is interrupted briefly because of the bouncing of the train caused by imperfections of the tracks and this interruptions cause high current drain producing a temporary electric arc or spark. This spark produces an electromagnetic disruption that may affect electronic equipment and degrades communication links in the surroundings.



Figure 3.29: Pantograph producing a spark as it moves along the power line

In order to emulate the effects caused by this phenomenon, a technique presented in [43] where the GSM-R system performance is evaluated, will be replicated and used. The process consists of a spark or electromagnetic discharge (ESD) gun that produces HV pulses, which represent transient interference. Firstly, it is necessary to investigate the intermittent emissions of the ESD gun, and this is measured inside the RC with an spectrum analyser. Figure 3.30 shows usual current waveform produced by the discharge of a ESD generator.

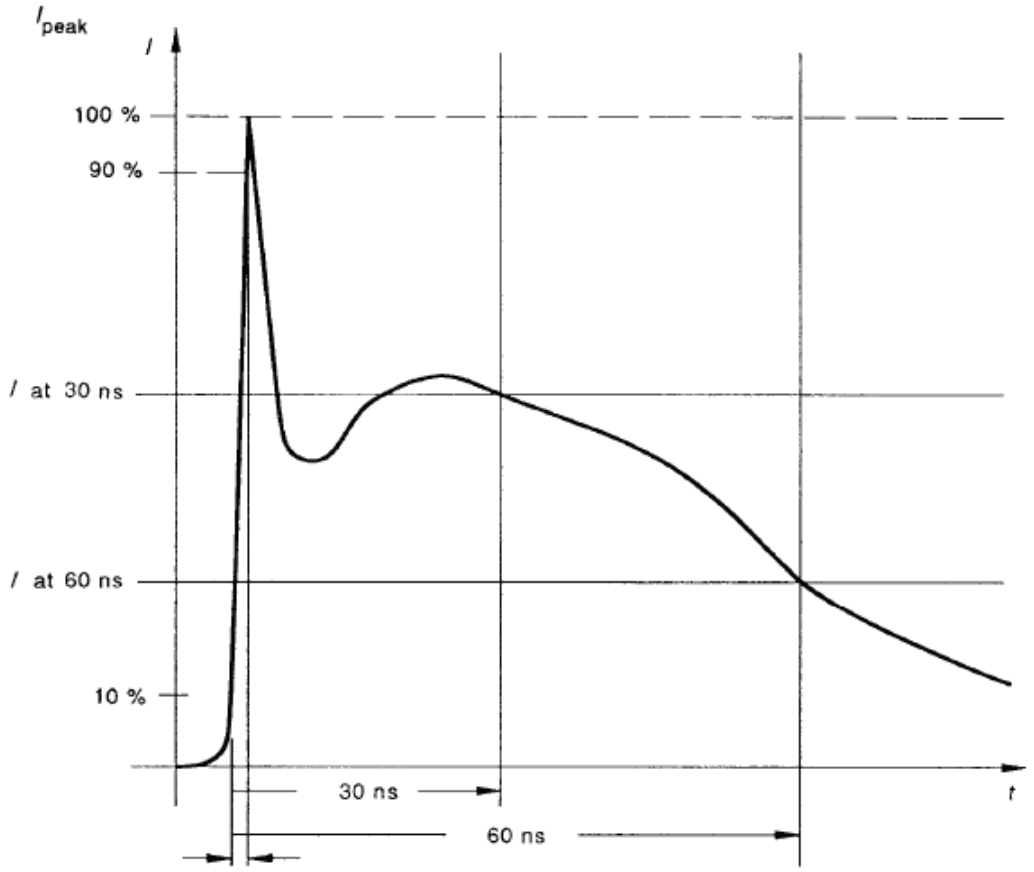


Figure 3.30: Typical and representative waveform of the output current produced by the ESD generator [44]

For this project purposes, a similar procedure will be followed, placing the ESD gun in the vicinity of the XBee Rx antenna and set it to produce a transient or intermittent spark, whilst the error rate is monitored.

Currently, the IEC 61000-4-2 is the International Electrotechnical Commission's standard on ESD for immunity testing [44]. This standard describes the adequate set-up for the instrumentation, EUT and discharge levels, shown in Table 3.4.

Table 3.4: Test voltages specified in the IEC 61000-4-2 standard

	Contact discharge	Air discharge
Level	Test voltage	Test voltage
1	±2kV	±2kV
2	±4kV	±4kV
3	±6kV	±8kV
4	±8kV	±15kV
x	special	special

The last level x is left to manufacturer's discretion, and depends on the target application. The current and discharge times seen in Table 3.5

Table 3.5: Test voltages specified in the IEC 61000-4-2 standard

Level	Indicated voltage	First Peak current of discharge ±10 %	Rise time t_r with discharge switch	Current (±30 %) at 30 ns	Current (±30 %) at 30 ns
1	2kV	7.5A	0.7 to 1 ns	4A	2A
2	4kV	15A	0.7 to 1 ns	8A	4A
3	6kV	22.5A	0.7 to 1 ns	12A	6A
4	8kV	30A	0.7 to 1 ns	16A	8A

In general, all the ESD generators allow to set the previous levels on its screen, as shown in Figure 3.31, which corresponds to the Dito ESD gun, used for this experiment.

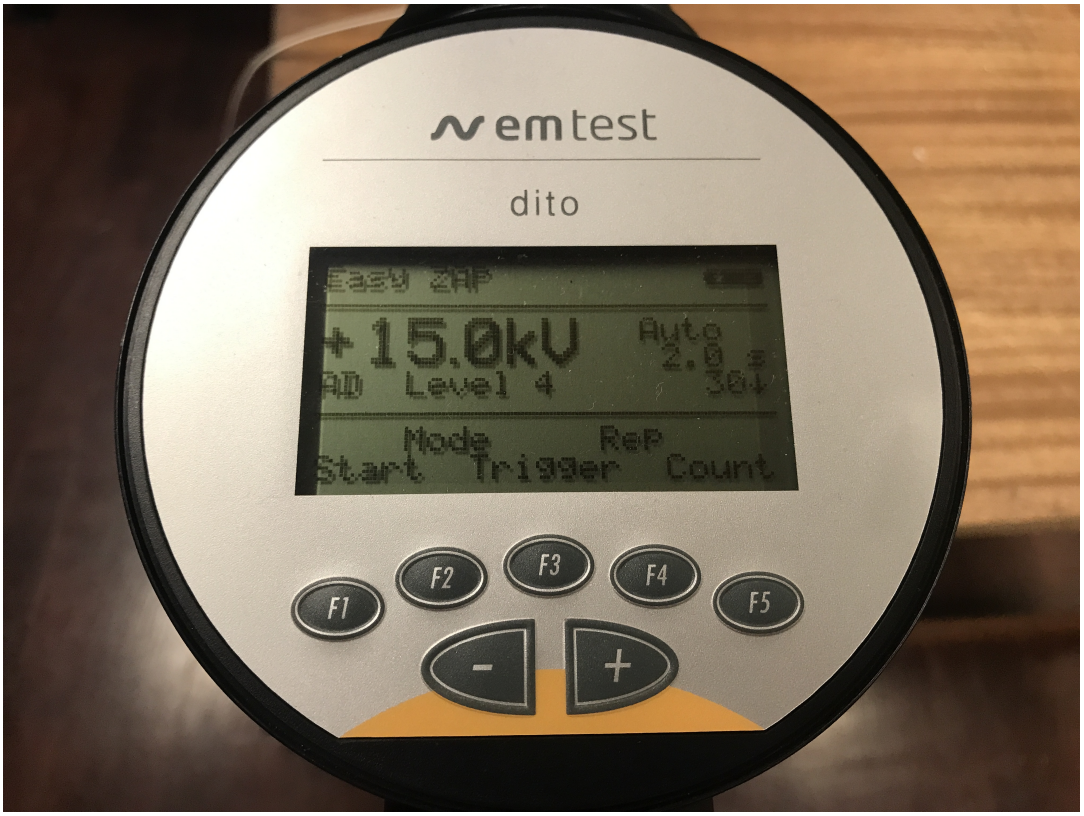


Figure 3.31: ESD gun set-up screen.

The table-top set-up for this type of experiments is displayed in Figure 3.32.

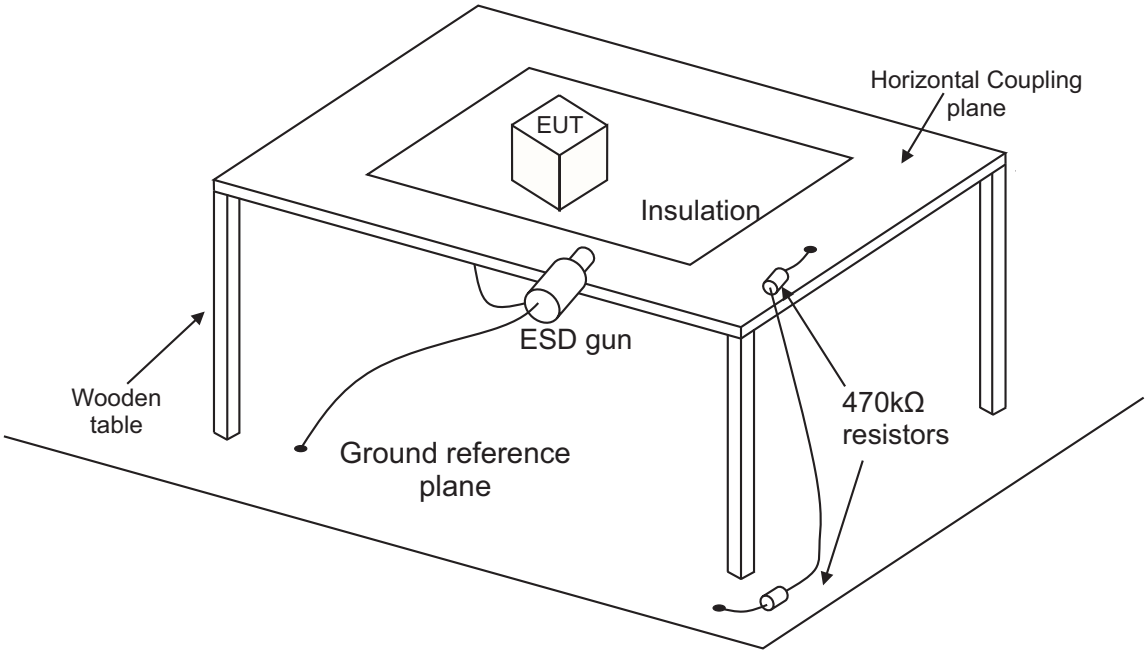


Figure 3.32: Schematic of table-top set-up for ESD laboratory test

To emulate the sparks generated by the OLE and its effects, it is necessary to generate a discharge. Hence, it is required that the ESD gun is properly connected to the ground reference with a 2m ground cable and, at the same time, the horizontal coupling plane (HCP) or the vertical coupling plane (VCP) should be connected using 2×470kΩ resistors in order to have a closed loop, as seen in Figure 3.33. Otherwise, the discharge will flow through the body of the operator.

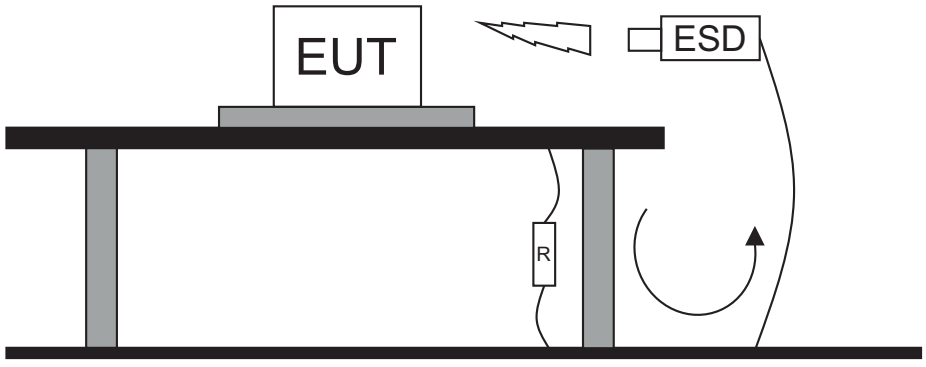


Figure 3.33: Schematic of circuit closed loop for the ESD table-top test.

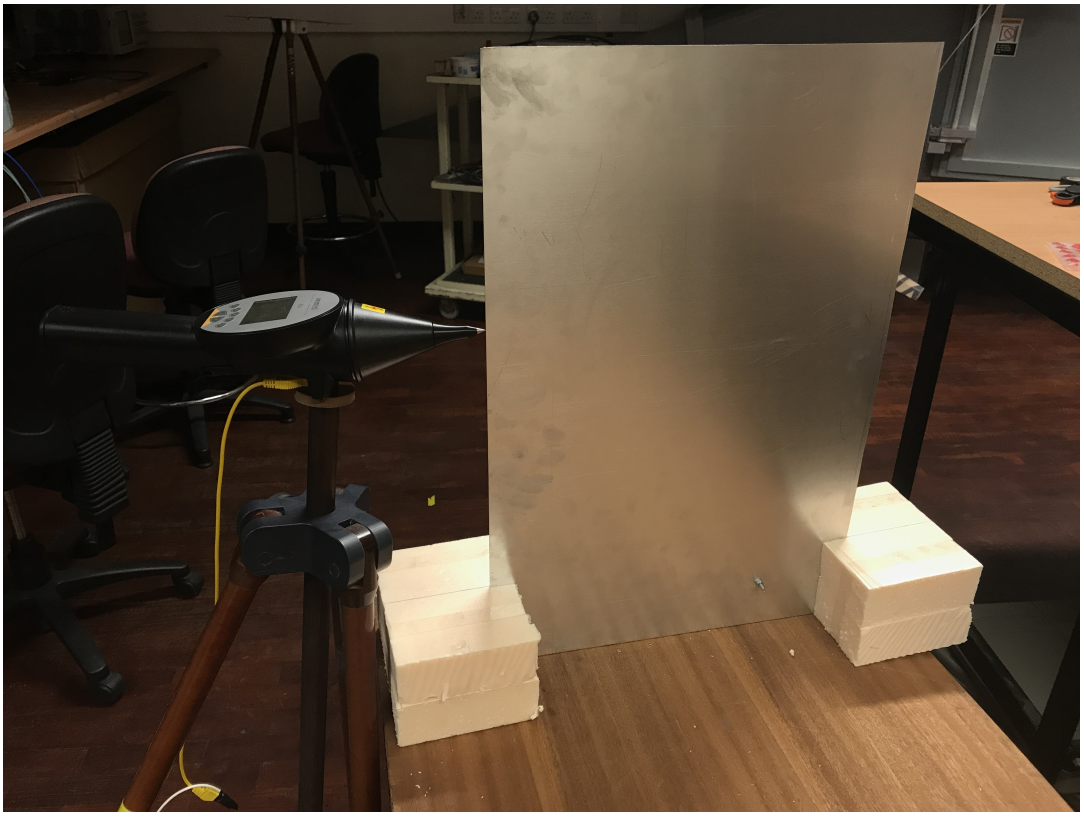


Figure 3.34: Contact discharge set-up for RF emission on the a vertical coupling plane (VCP).

Depending on the application, 4 types of discharge can be produced: Air discharge, contact discharge or indirect discharge. For the air discharge the round tip is used, as shown in Figure 3.35. Whereas the pointy tip is used for the contact discharge, as shown in Figure 3.36. Usually, the contact discharges are used when the metallic surfaces of the EUT can be easily accessed.

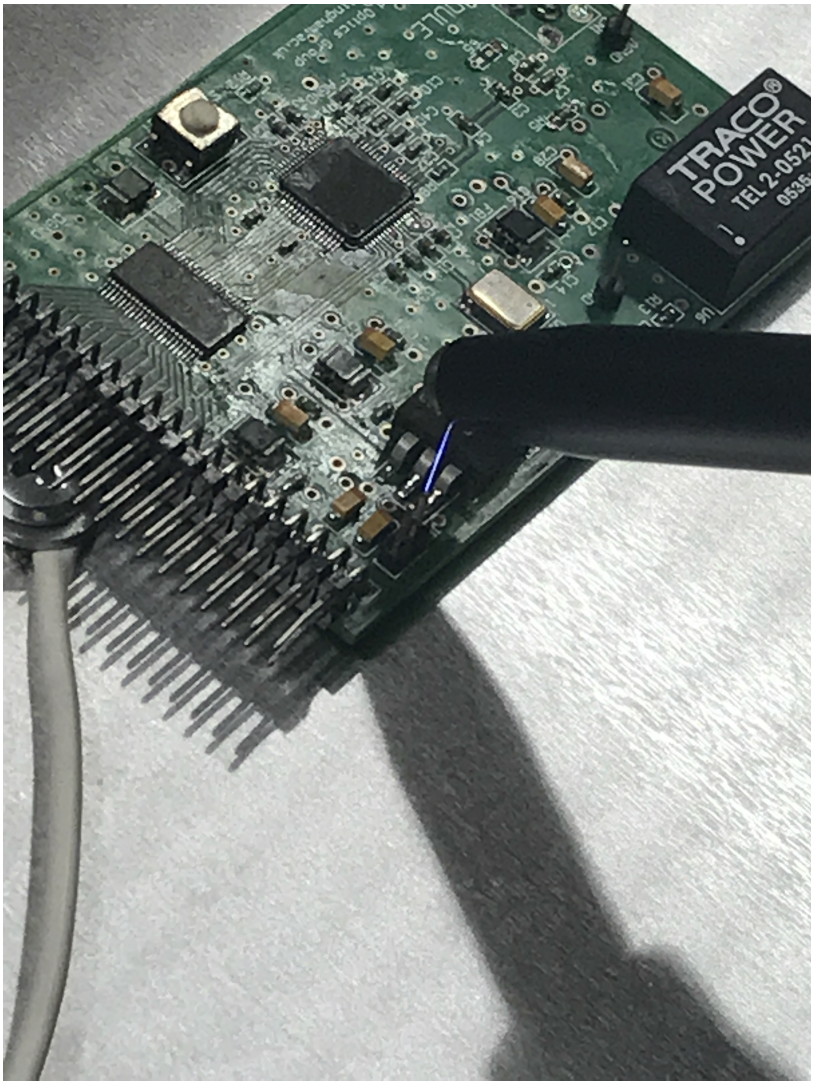


Figure 3.35: Air discharge projected onto a PCB.

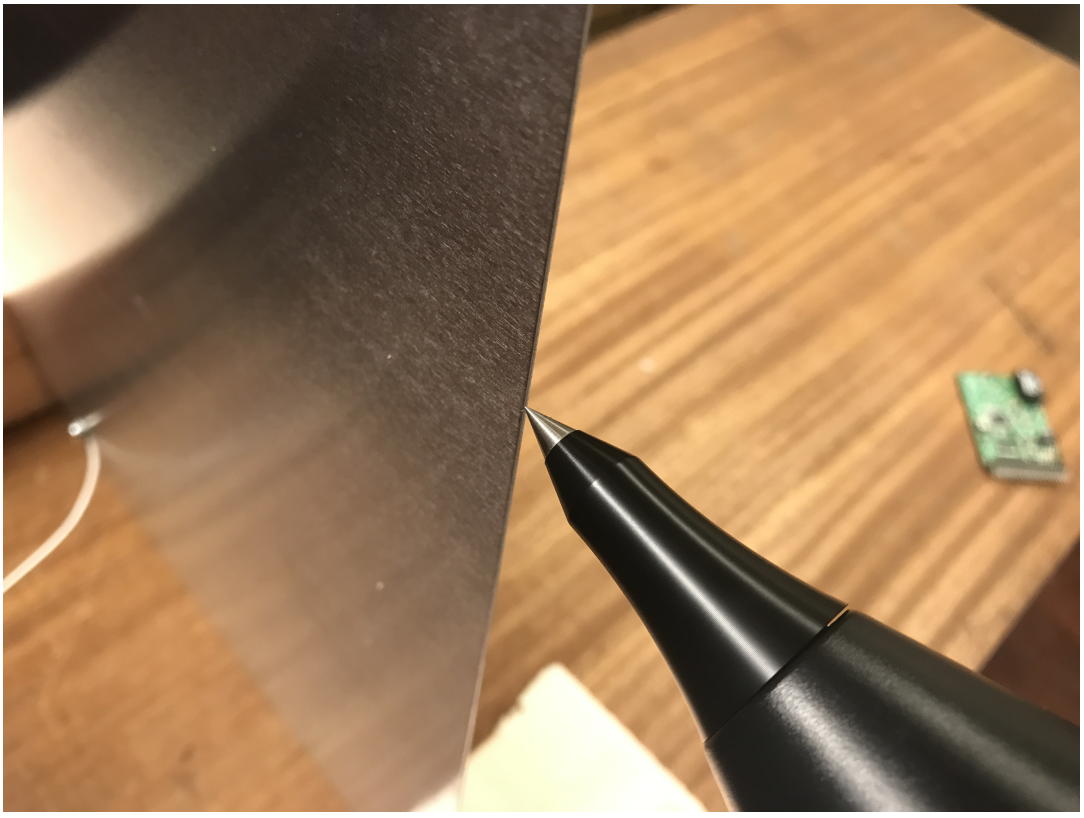


Figure 3.36: Contact discharge configuration.

The spark generated by the air discharge is easy to visualise as the current flows from the electrode to the surface throughout the air. When the contact discharge is used, it is harder to visualise the spark, as the current flows when the electrode is in contact with the surface. The discharges can be configured to be triggered manually or automatically. Additionally, the number and duration can be also configured.

The indirect discharge is achieved by using the contact discharge tip and make contact either with the HCP or VCP. For RF testing, the VCP is used. The RF field of such discharge can be simulated by making a contact discharge to this plane, being a discharge near the EUT but not directly onto the device, as it was generated by another device in its vicinity, similar to the effect of the OHE of a tram, as shown in Figure 3.37.

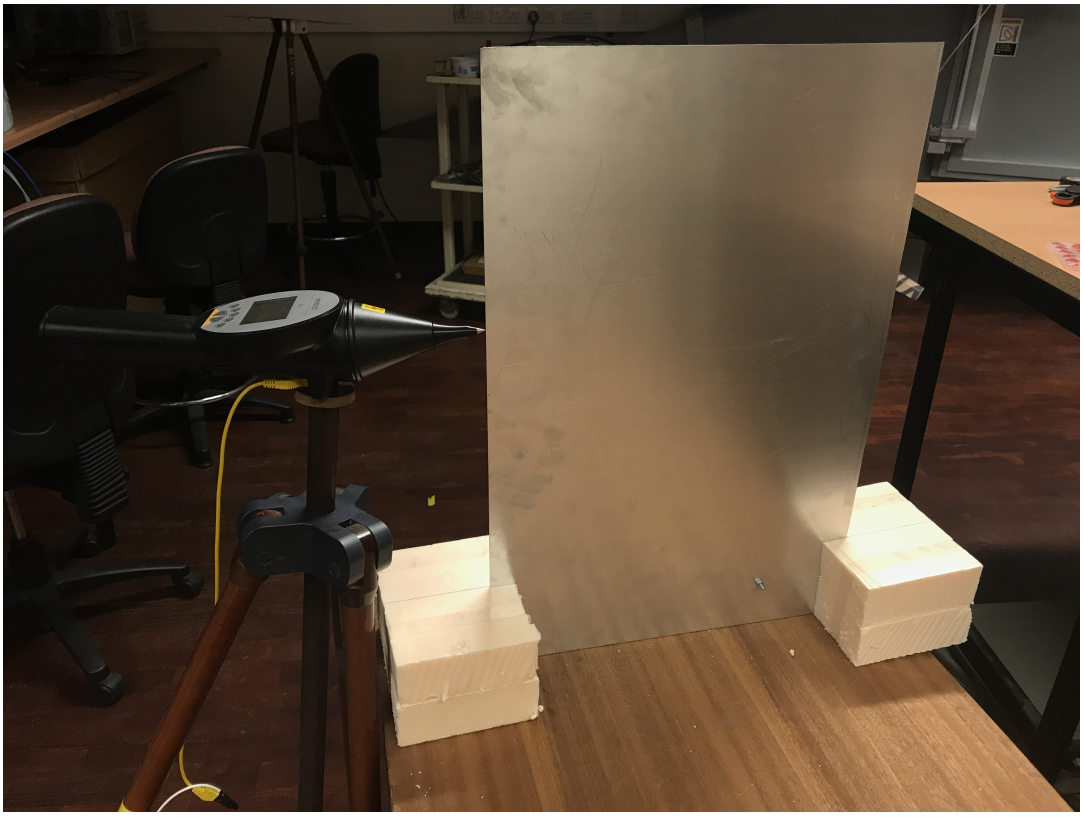


Figure 3.37: Contact discharge set-up for RF emission.

It is worth to mention that the zapping will only be tested as RF emissions to generate EM fields with the VCP in the RC, and the PCB board will not be target for arc ESD, as this is an interference test.

3.4 Conclusion

Reverberation chambers are widely used testing facilities by a diverse range of industries. The internal geometry and composition creates a statistically uniform environment when having a well-stirred mechanism. Signals with fairly low power, can be enough to excite a large amount of modes inside the chamber due to the reflection present. This allows to create a rigid testing environment in the frequency domain for any device placed inside.

On the other hand, placing absorbers inside the RC reduces the contribution of the multipath generated, allowing the possibility to mimic scenarios where only LOS is present in different intensities.

Unexpected external factors can contribute to the performance reduction of systems on-board the train and interfere with the instrumentation, as in this case is the ZigBee radios, such as sparks generated by the OHL. Hence, the ZigBee will be intentionally targeted with a ESD spark generator gun to observe its performance when exposed to such discharges in its vicinity.

The experimental set ups or environments presented in this chapter will be used to establish different environments for a ZigBee communication system, where its reliance, capabilities and ability to maintain communication will be challenged. Specially in the case of the ESD gun, the overall conditions are representative of a realistic environment unable to recreate in full in the RC due to the total operational current utilised in a OHL. Hence, the obtained environment would help to estimate and evaluate the performance of the communication system in the presence of an arc. These experimental set ups are discussed in Chapter 5.

Chapter 4

Wireless Communication Technologies and Train Infrastructure

4.1 Wireless Communication Technologies

One of the most commercially utilised portions of the electromagnetic spectrum is the ISM bands. Most mobile and radio based communications, as well as home appliances operate in these bands. ISM frequencies are located in both licensed and unlicensed bands. For this reason, the ISM frequencies allocated in the licensed bands are less likely to be used due to potential interference with communication or broadcasting paid services. The use of licensed and unlicensed varies by country or region due to their internal regulations. As an example, the European ISM band spectrum allocation is shown in Table 4.1.

Table 4.1: ISM bands in Europe

Frequency band	**Frequency centre**
13.553 MHz - 13.567 MHz	13.56 MHz
26.957 MHz - 27.283 MHz	27.12 MHz
40.660 MHz - 40.700 MHz	40.68 MHz
2.4 GHz - 2.5 GHz	2.45 GHz
5.725 GHz - 5.875 GHz	5.8 GHz
24 GHz - 24.25 GHz	24.125 GHz

Nowadays, many sensor networks including health monitoring systems are based on RF radio communication and also use these bands.

4.1.1 Modulation Techniques: Spread Spectrum

The document will only focus on the spread spectrum techniques as they are the backbone of the communication protocols of the ZigBee radios, which is the area of research of this work.

4.1.2 Frequency-Hoping Spread Spectrum

Frequency-Hoping Spread Spectrum (FHSS) is a modulation technique consisting of using a change in the carrier frequency, according to a pseudo-random sequence known at the transmitter and at the receiver, within a previously established range, as shown in Figure 4.1. Every time that the Tx changes the carrier frequency, the Rx must change as well at the same time.

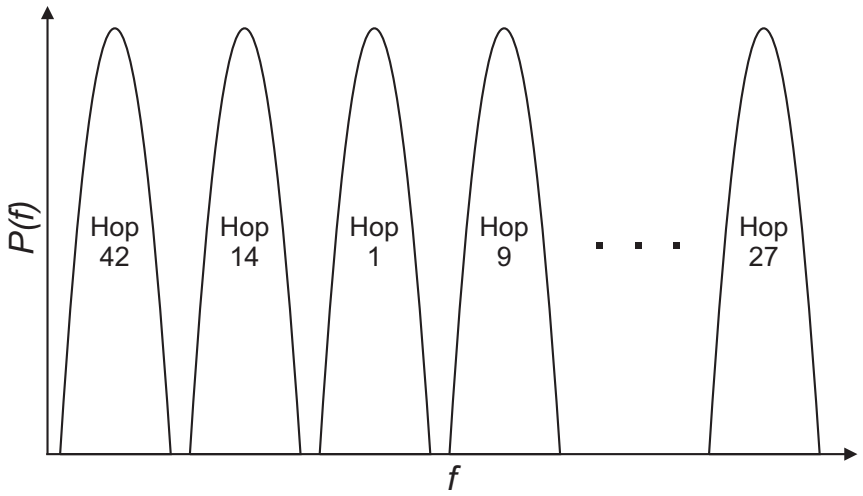


Figure 4.1: FHSS spectra occupancy

The carrier switches or hops across the frequency spectra. As seen in Figure 4.2, in a given time slot, a specific set of bits is sent. In the next slot, a hop in frequency is done, followed by another transmission. The arrows demonstrate the hopping pattern previously established by Tx and Rx. This process continues throughout the entire transmission.

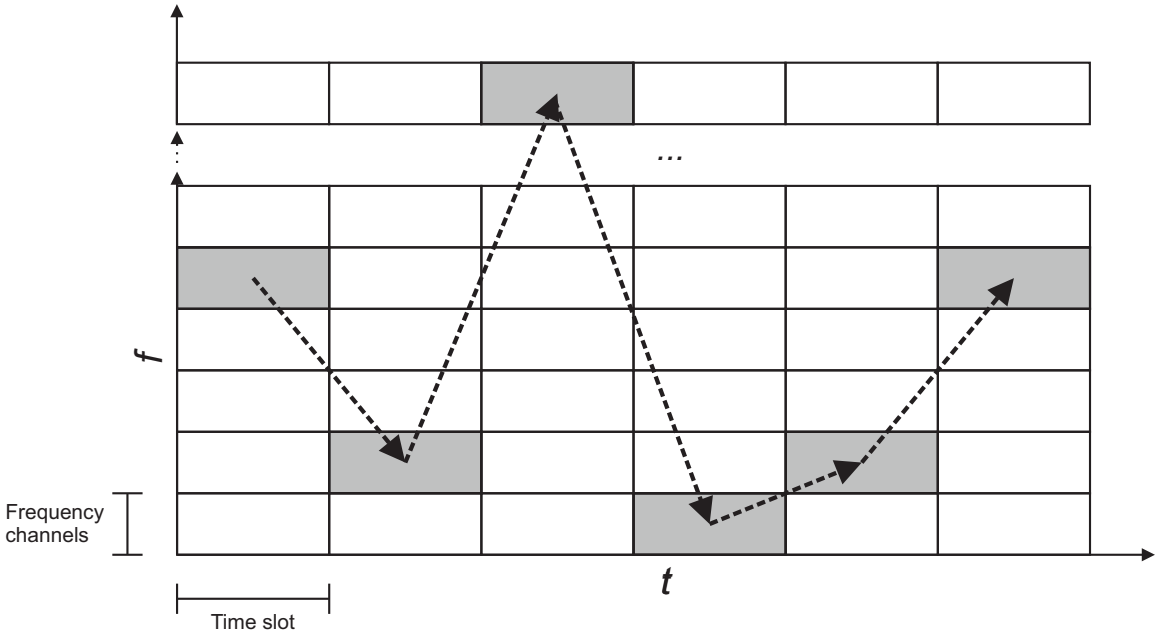


Figure 4.2: FHSS scheme

Although this method prevents narrowband interference, it does not present resilience against noise.

4.1.3 Direct-Sequence Spread Spectrum

Direct-Sequence Spread Spectrum (DSSS) modulation technique uses a pseudo-random noise (PN) code sequence of 1 and -1-s to spread the single baseband signal or data. Each code symbol is called "chip". The chip rate is much higher than the original signal bit rate. The baseband data is multiplied by the PN, which is generated randomly locally at the transmitted, converting the original signal into a wideband channel. This has the effect of increasing the resilience against noise and interference. At the Rx, the same PN code is generated to decode the modulated signal.

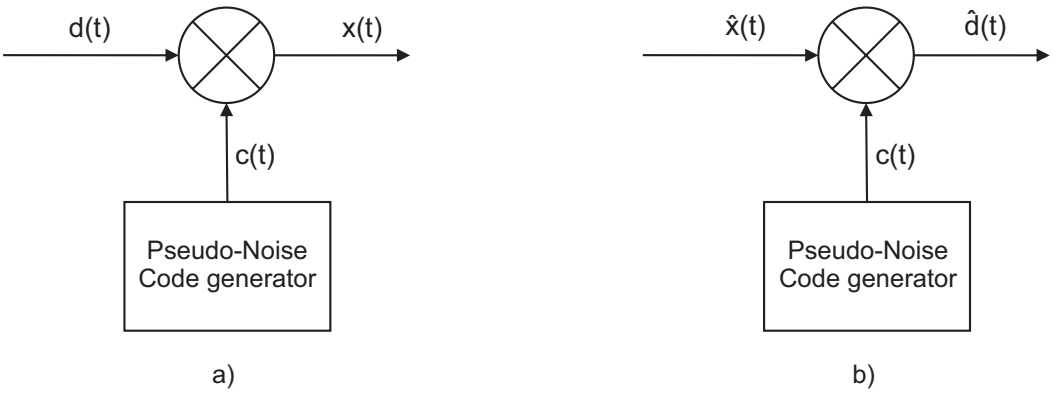


Figure 4.3: DSSS transmission scheme. a) Tx, b) Rx

An example of DSSS is shown in the figure 4.4: a narrow band single signal is spread out across the frequency space, increasing the occupancy.

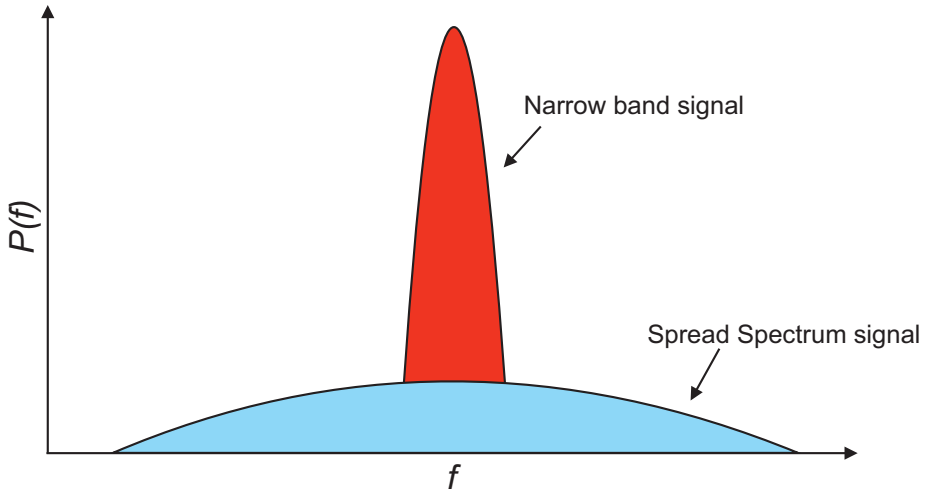


Figure 4.4: Narrow Band to a Spread Spectrum signal schematic.

The advantages of converting the original narrow band into a spread spectrum wide band signal is that, the total power of the narrow band is divided across a wide band and the resultant behaves similarly to a white noise signal, which is resilient to narrow band jamming or interference.

DSSS decoders relies on decorrelation using the same PN code. All the multipath generated received with a delay greater than the chip rate will be rejected

and the decoder or de-correlator selects the greater signal produced to demodulate and retrieve the original signal.

An example of this modulation is shown in Figure 4.5. The original signal input Figure 4.5a is modified by the pseudorandom code Figure 4.5b generated at the Tx.

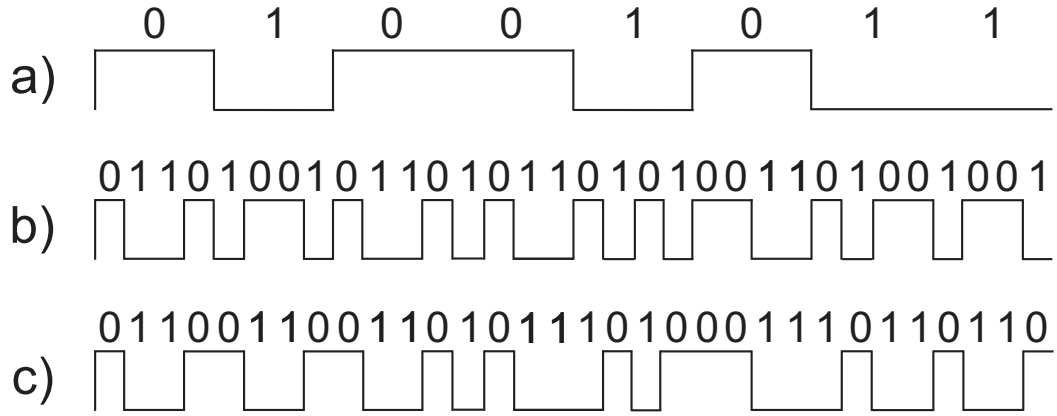


Figure 4.5: Example of DSSS modulation. a) Original signal, b) PN code, c) Resultant signal

The resultant modulated signal C (Figure 4.5c) is the outcome of the logic operation XOR ($A \oplus B$), using the alphabet from Table 4.2, which is subsequently sent thought the channel to the Rx.

Table 4.2: Logic table for DSSS modulation

A	$\oplus$	B		C
0	$\oplus$	0	=	0
0	$\oplus$	1	=	1
1	$\oplus$	0	=	1
1	$\oplus$	1	=	0

Given the speed of operation, it is considered to be slow for current modern communication link networks. However, can be used as multiple access technique by generating different spreading codes simultaneously operating across the same frequency. DSSS is used in IEEE 802.11b and ZigBee wireless technologies.

4.1.4 CDMA

Code-Division Multiple Access (CDMA) is a channel access multiplexing spread-spectrum modulation. In TDMA, for each user a time slot is defined to transmit. In FDMA, a frequency band is defined for transmission per user. On the contrary, in CDMA each user is given a specific code which is orthogonal to the others [45]. This codes are pseudo-random are spreading waveforms to create noise-like transmissions. As an example, considering two different channels for two distinct user, their two transmission signals produced can be written as:

$$\begin{aligned} s_1(t) &= \sqrt{2P_1}b_1(t)\cos(\omega_1(t)+\theta_1) \\ s_2(t) &= \sqrt{2P_2}b_2(t)\cos(\omega_2(t)+\theta_2) \end{aligned} \tag{4.1}$$

where P_i is the transmitting power, b_i is the data signal, $\omega_i(t)$ is the transmitting frequency, and θ_i is the frequency offset of the i-th user.

At the receiver, having the sequence obtained and normalised to the desired signal ($s_1(t)$ for this case), such received signal can be written as:

$$r_1 = s_1(t) + \sqrt{PL_r}s_2(t) + n(t) \tag{4.2}$$

where PL_R is the path loss between transmitter 2 and receiver 1 and n_t is de additive Gaussian noise. Aussiming for simplicity that square pulses were the signals transmitted, the output of a matching filter for any given symbol period T for the user 1 is:

$$Z = \frac{1}{T}\int_0^T r_1(t)\cos(\omega_1(t)+\theta_1)dt \tag{4.3}$$

Having $|\omega_1 - \omega_2| \gg T$, the signal s_2 will produce no response to the match filter for signal s_1. Hence, we can say that the channels are orthogonal.

As the channels in CDMA are defined by spreading codes, it can be defined

that the two signals for the two users are described as:

$$\begin{aligned} s_1(t) &= \sqrt{2P_1}a_1(t)b_1(t)\cos(\omega_1(t)+\theta_1) \\ s_2(t) &= \sqrt{2P_2}a_2(t)b_2(t)\cos(\omega_2(t)+\theta_2) \end{aligned} \tag{4.4}$$

where a_1 and a_2 are spreading codes that define a channel for each user.

Hence, by being orthogonal spread codes resulting in orthogonal signals, the cross correlation at the receiver is low with the remaining channels and high when it is performed on the one with the same spreading code.

4.1.5 CSK

The Code Shift Keying modulation technique is a DSSS signaling method which overcomes the spreading gain versus data rate limitations [46], designed to increase the transmission rate of a spread-spectrum signal [47]. It implies the use of M different coded phase shifts of a Pseudo-Random code sequence.

In this method, the transmitter gathers the input data into k-symbols of period T, and each symbol selects a signalling waveform from a M-ary alphabet, where $M = 2^k$. Each selected waveform consist in a single PN code sequence $p(t)$ of length L and chip interval or period T_c, and is modulated at carrier frequency ω. The output from the transmitter block is defined as:

$$s(t) = Ap_m(t)cos(\omega t) \tag{4.5}$$

where $p_m(t) = p(t - m_c t_c)$ is the m-th ($m = 1 \leq m \leq M$) waveform from the alphabet with phase shift $m_c = m[L/M]$.

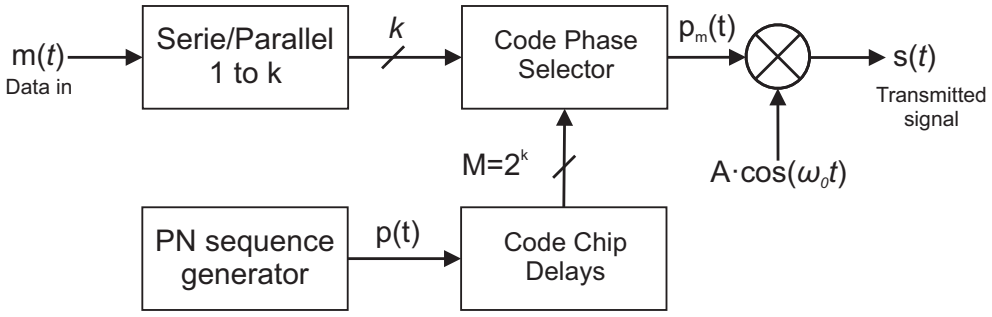


Figure 4.6: CSK transmitter block

The received signal consists of the original signal, a potentially threatening signal $j(t)$ and additive white noise $n(t)$, in the form:

$$r(t) = s(t) + j(t) + n(t) \tag{4.6}$$

The receiver consists of a bank of M correlators or matched filters, where a correlator decides the more likely phase shift of the received symbol and decodes such symbol into k-bits:

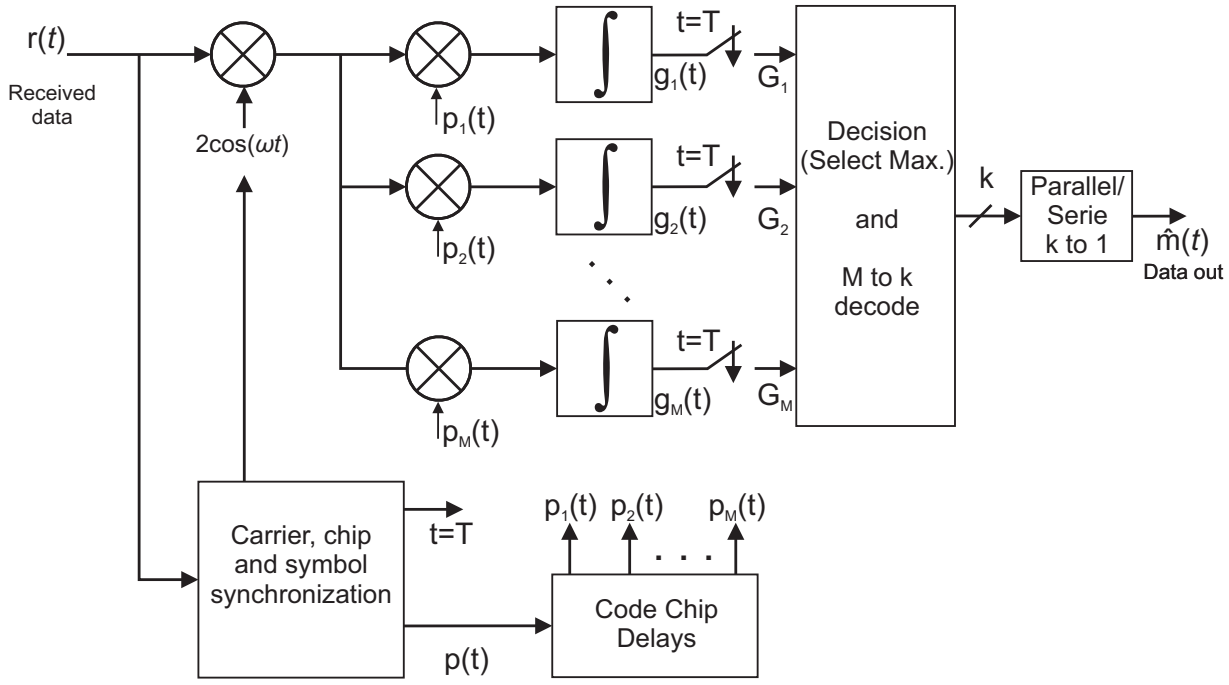


Figure 4.7: CSK receiver block

The correlator requires chip and symbol interval synchronisation to successfully demodulate. After the matched filter, the resultant output of the M-th correlator is:

$$G_m = g_m(T) = 1 + J_m(T) + N_m(T) \tag{4.7}$$

whilst the output of the other correlators are:

$$G_l = g_l(T) = 1 + J_l(T) + N_l(T) - \frac{1}{L}, \quad l \neq m \tag{4.8}$$

Subsequently, the receiver selects the largest G_m, which is greater than the other outputs G_l, $l \neq m$ and decodes k bits corresponding to the m symbol.

This is the modulation technique frequently used by ZigBee radios.

4.1.6 Low-power Consumption Communication Technologies

WLAN - 802.11b

WLAN is a wireless variant of the LAN that allows mobility to the devices sharing same network. It is based on the IEEE 802.11 standard, which at the same time is based on DSSS. IEEE 802.11b has a strong capacity for anti-interference and anti-multipath fading. It has a maximum data rate of 11Mbps and is designed for point-to-point communications. The standard defines 14 carrier channels of 22 MHz, from 2.412 to 2.484 GHz

WLAN is considered the backbone of the train-ground communication for the Communications-based Train Control (CBTC) signalling system. CBTC is mainly used in driverless trains or metros, specifically for transportation between terminals in airports, where the distances to cover are short compared to inter city distances covered by regular trains.

Bluetooth

Bluetooth is a low-power wireless technology for short-range communications which operates in the ISM band at 2.4 to 2.485 GHz, using FHSS and full-duplex signal, previously standardized as IEEE 802.15.1. It is widely used in mobile devices for file sharing, audio transmission and sensor network operations. Therefore, this technology provides levels of security between transceivers. For sharing, it follows a pairing mode in which the receiver waits for a conformation from the user in order to start pairing the devices. Once this is done, both devices recognise the authorisation for further communication. On the other side, this paring mode involves a pairing time, even when authentication has been done.

In a Bluetooth personal area network (PAN) the connection follows a master/slave scheme where all the devices are nodes and the master controls the network, as well as the behaviour of the other nodes. All the communication is done

through the master and not between nodes directly. In these networks, it is possible to have up to 7 nodes. In order to expand the network, different techniques should be used to connect masters, allowing a greater PAN.

The range of a device is defined by the specifications as follows:

Table 4.3: Bluetooth classes

Class 1	100 mW (20dBm)
Class 2	2.50 mW (4dBm)
Class 3	1 mW (0dBm)

However, these specifications could be modified by manufacturers depending on application purposes. In addition to Table 4.3, Class 3 radios have a coverage radius of 10m whilst Class 1 radios have a range up to 100 meters and a maximum experimental data throughput rate reached of 2.1 Mbps [48].

With 100m being the maximum distance from point-to-point, it will be required to have a dense device population if the application requires coverage over a wide area.

ZigBee

ZigBee is a low-power communication technology used in low-data rate applications that require long battery life and secure networking. ZigBee Standard defines only the networking, application and security layers of the protocol and adopts IEEE 802.11.4 Physical (PHY) and Medium Access Control(MAC) layers of the Open Systems Interconnection model (OSI model), as part of the networking protocol. Given its low complexity, this technology was designed mainly for sensor network purposes, where high data transfer is not required. Instead, reliability and stability are fundamental. In fact, the maximum data rate is defined as $250 kbps$.

For those devices, two operational frequency ranges are defined according to the geographical location:

- 863 - 870 MHz for Europe

- 902 - 928 MHz for the Americas and Australia
- 2.4 - 2.4835 GHz Worldwide (Unlicensed)

Among others, its main feature is the low power consumption. Compared with Bluetooth and WiFi, ZigBee can operate with batteries for a long period of time, making it easy to maintain in operation continuously when deployed in areas hard to reach.

Comparison

The multiple characteristics of the communication technologies mentioned above are summarised in the Table 4.4, showing the key common features.

Table 4.4: Comparison between Wireless PAN technologies [49]

Characteristics	**Technology**		
	IEEE 802.11b	Bluetooth	ZigBee
Frequency band (MHz)	2412-2484	2402-2485	863-868.8, 902-928 2402-2482
Channels	14	3	16
Modulation	CCK	GFSK	BPSK & QPSK
Max data rate	11 Mbps	1 Mbps	20-250 kbps
Nodes/Master	-	7	65,000
Range	100m	10m	100+ m
Power consumption	400 mA (Tx mode) 20 mA (Standby mode)	60 mA (Tx mode)	25-35 mA (Tx mode) 3 μA (Standby mode)

4.2 Communication Systems for Railway Transportation

Railway signalling systems are used to efficiently control railway traffic. Railway systems are mainly composed by three subsystems: infrastructure, rolling stock and signalling system.

Increasing the throughput of a railway network allows having a larger number of rolling stock per time slot. Hence, the occupancy of the railway is maximized, and the unused space between trains is reduced, in addition to increase the throughput of rolling stock on the railway network without compromising security and safety, allowing railway transportation operators to allocate a greater number of trains on the same track.

Modern trains are equipped with multiple sensors that continuously check the train conditions and preserve its integrity. They are also responsible for controlling the train displacement according to traffic conditions provided by the control center. When a message is received indicating speed reduction or a complete stop but is omitted by the driver, an automatic response should take over the control. Train protection systems were designed to prevent those circumstances to happen, increase security, and avoid collisions.

In this section, the two major control and signalling systems currently used are addressed, as well as their main features.

4.2.1 Communication-Based Train Control

Communication-Based Train Control (CBTC) is a continuous automatic control system for trains, that is able to determine the exact position of the rollig stock in order to manage traffic within railway network efficiently, using a moving moving-block scheme. In a fixed block scheme, the block occupancy of the railway is defined in function of the length, speed and braking distance of a train, these being constant. The braking curve is calculated with those variables and this

block division remain constant throughout the railway. The occupancy includes the total length of the train plus an additional gap, as shown in Figure 4.8. The following train is not allowed to move to the next block unless the upcoming block is cleared.



Figure 4.8: Fixed-block scheme. The train footprint and braking curve are constant.

As CBTC maintains constant communication with the train, it is possible to know the exact position, current speed and estimate the braking distance. Depending on the current speed and track configuration, the braking curve and safety distance is established.

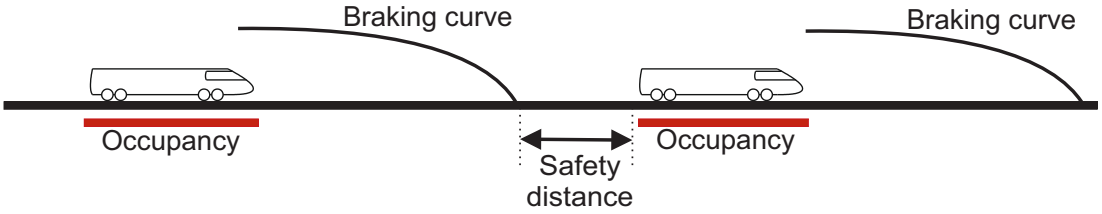


Figure 4.9: Moving-block scheme. The train footprint, safety distance and braking curve are calculated based on the track occupancy and train speed.

In this scheme, the train occupancy is reduced to the train length itself. Thus, the footprint (braking curve and safety distance) varies according to these parameters and a moving block for each train is calculated, as shown in Figure 4.9. Consequently, the distance between consecutive trains could be reduced and optimised, and the total occupancy of the railway is maximised, allowing more rolling stock population.

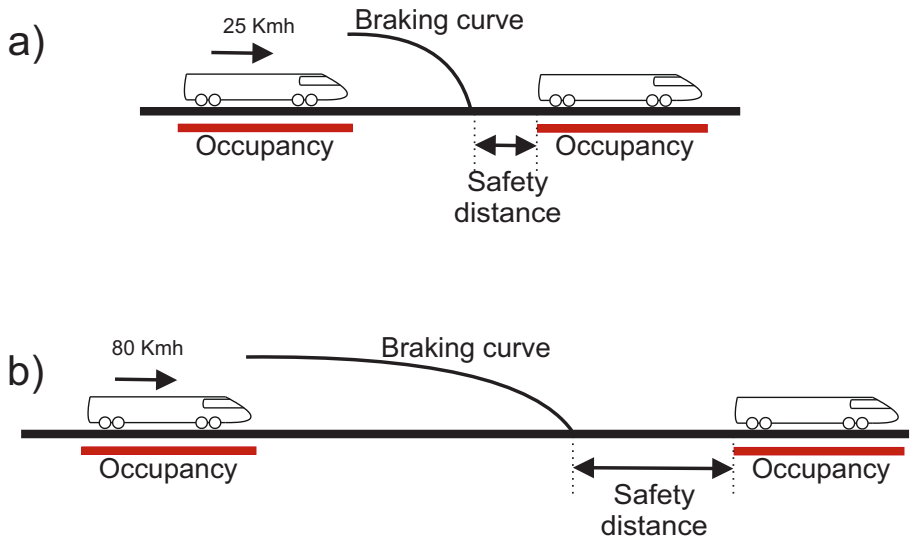


Figure 4.10: Braking curves variation at low speed a) and high speed b) in moving block scheme

Hence, if the oncoming train speed is low, its footprint is short (Figure 4.10a). On the other hand, when the travel speed is high, the footprint increases accordingly (Figure 4.10b).

Nowadays, as this is a highly automated system, it is mostly adopted in airports as driver-less transport between terminals, where the service is under demand oriented rather than following a predefined schedule.

On the other hand, it could have repercussions if CBTC is deployed as massive signalling system for railway, as it should cover long distances across the railway track infrastructure. When the train-ground distance is greater than 200m, the receiving power is very low. Therefore, more Access Points are required to minimize this distance and ensure hand off from node to node [50].

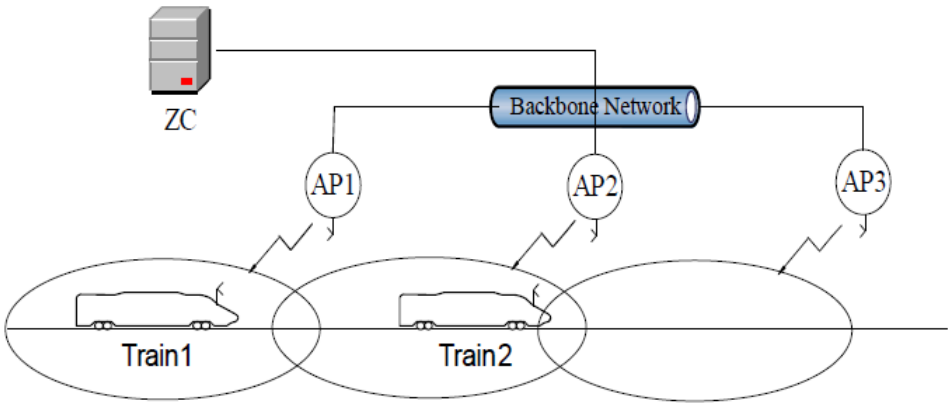


Figure 4.11: Train-ground communication in CBTC

It is capable of implementing automatic train operation (ATO), automatic train protection (ATP), and automatic train supervision (ATS) functions, which is composed of five fundamental subsystems: Central Control System (CCS), Station Control System (SCS), Onboard Control System (OCS), Block Control System (BCS) and Communication Network System (CNS) [51].

CCS Control centre of the CBTC system, where the train plans, traffic and operations are gathered.

SCS This system controls the physical actuators for interlocking, which are in charge operate track switches, and signalling for routes.

OCS Set of equipment on board to sense and control speed, acceleration, and braking.

BSC Controls train safety operations, particularly moving block conditions. Additionally, receives data from wayside sensors.

CNS Consist in the RF infrastructure installed in the wayside for communication between the train, nodes and CCS. The CNS of CBTC is based on the 802.11b WLAN Wi-Fi for Train-Ground communications.

IEEE 1474

As mentioned before, CBTC is able to implement several functions, as it is based on the IEEE 1474 protocol which defines several functions mainly for security purposes, specifically the Automatic Train Control system[52], which is in charge of perform the following:

- Automatic Train Protection. This system provides the train with a Limit of Movement Authority (LMA) based on current speed and track occupation of the upcoming block, given the constant train monitoring and based on the moving-block scheme mentioned previously.
- Automatic Train Operation. Performs the automated operations related to the train movement, except the doors closing, reducing the risks caused by human factor errors.
- Automatic Train Supervision. This system compares the actual train movements and compare that to the established timetable. It alerts ATP if the train is restricted to move at certain speed if the track is being occupied at the time.

CBTS is fully based on levels or Grades of Automation system (GoA).GoA defines the degree of automation depending on the level of responsibility assigned to the train control system [53]. This could be either human control (driver) or computational control. Each grade is classified according to the driver contribution in their operation, as given in Table 4.5.

Table 4.5: Grades of Automation [54]

Grade of Automation	**Type of Operation**	**Setting train in motion**	**Stopping train**	**Door closure**	**Operation in even of disruption**
GoA 1	ATP with driver	Driver	Driver	Drive	Driver
GoA 2	ATP and ATO with driver	Automatic	Automatic	Drive	Driver
GoA 3	ATP with driver	Automatic	Automatic	Train attendant	Train attendant
GoA 4	ATP with driver	Automatic	Automatic	Automatic	Automatic

All of these functions mentioned above depend of GoA.

4.2.2 European Rail Traffic Management System

In the early 90's, the European Commission started a project with two working groups to reduce the cost of the signalling and the communication systems. The first working group investigated a new suitable communication system and introduced Global System for Mobile Communications – Railway (GSM-R) for internal voice and data communication in the railway environment. The other group worked on establishing a new signalling standard defined as European Train Control System (ETCS) as the new control-command system. The combination of both created the European Rail Traffic Management System (ERTMS).

European Train Control Systems

The European Train Control Systems (ETCS) monitors and transmits movement authority that conveys both speed and distance limits to a driver. An on-board computer compares the train's location and speed with authorised speed limits, automatically applying the train's brakes when necessary [55]. This system comprises three levels as follows.

Level 1 facilitates the communication between the moving train and the track-side equipment, with the use of balises, usually known as "eurobalises". Balises are installed to the track, as shown in Figure 4.12 and linked to the control centre. The train detection equipment sends the train position to the control centre which determines the new movement authority (permission to proceed). Afterwards, it is received by the train and the on-board unit calculates the maximum speed allowed and the next braking point. Finally, the information is displayed to the train driver[56], as shown in Figure 4.13.



Figure 4.12: Eurobalise installed on the track

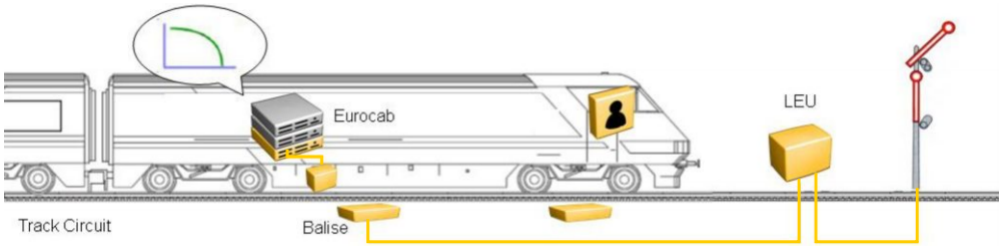


Figure 4.13: ETCS Level 1 [56]

Unlike Level 1, in Level 2 balises are only used as position markers. The train detection sends the train's position to the control centre which determines the new movement authority. The on-board unit calculates the maximum speed for next braking point and the information is displayed to the train driver [56]. It provides complete supervision through "continuous transmission", which allows higher line throughput (more trains per hour) and enables a reduction in the number of track balises and therefore a reduction in maintenance costs throughout the life of the equipment [55]. Furthermore, lineside signals are not required, as shown in Figure 4.14.

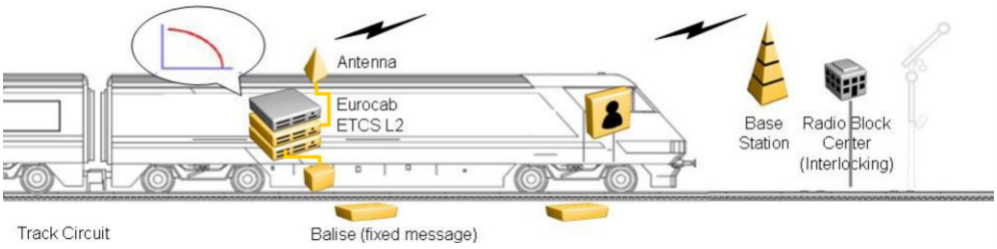


Figure 4.14: ETCS Level 2 [56]

In Level 3, the on-board unit calculates the train's positon using balises as position reference and pre-programmed track characteristics. The train sends its position via radio signals to the control centre, which receives all train positions, determines the new movement authorities and sends it via radio to the train.

The on-board unit calculates the maximum speed for next braking point and the information is displayed to the train driver [56], as shown in Figure 4.15. The intention is to further reduce trackside equipment and to allow trains to operate in individual moving block mode as is the case in advanced mass transit systems [55].

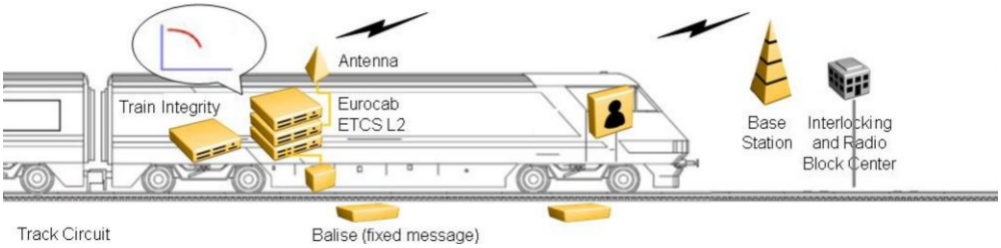


Figure 4.15: ETCS Level 3 [56]

Global System for Mobile Communications – Railway

GSM-R is the radio system used by the ERTMS for train/driver-control centre communications, based on GSM technology, providing security and reliability to the communication scheme. Currently based on the 876.2 to 960 MHz band, 876.2-915 MHz for uplink and 921.2-960 MHz for downlink.

4.2.3 Driver Assistance Systems

In railways, the train displacement is restrained to the Movements of Authority (MA) and the train is only allowed to move on to the next section when then the control centre gives the instruction. The control centre makes the appropriate predictions or calculations according to the track occupancy, weather conditions and train speed to grant this MA. Throughout the history of rail transportation, this has caused countless incidents and, in many cases, fatalities. Hence, driver assistance systems have been implemented to alert the driver upon risk or to act automatically without driver's intervention.

When the signalling is displaying a stop light and the train continues its trajectory ignoring it, a Signal Passed At Danger (SPAD) alert is triggered. SPAD is a emergency signal sent to the control centre indicating that the train is moving in an irregular way (related to displacement, acceleration, or speed) or has failed to obey an order to stop. This could be caused by driver's fault or a braking system malfunction.

Hence, various protection systems are currently implemented, which some of them require additional hardware to be included in the infrastructure. Since its implementation, SPAD risks and accidents have been reduced [57].

Train Protection & Warning System

Train Protection & Warning System (TPWS) is a train protection system used in the UK. Its purpose is to stop the train by automatically initiating a brake demand when the train passed a signal at danger without authority (SPAD), approached a signal at danger too fast, approached a reduction in permissible speed too fast or approached buffer stops too fast [58].

The system uses two transmitters: an arming and a trigger loop. Firstly, when a train passes over an arming loop a timer is starts. Then, when passed over the trigger loop within, as shown in Figure 4.17, a set period of time indicating excess of speed, a brake demand is initiated.

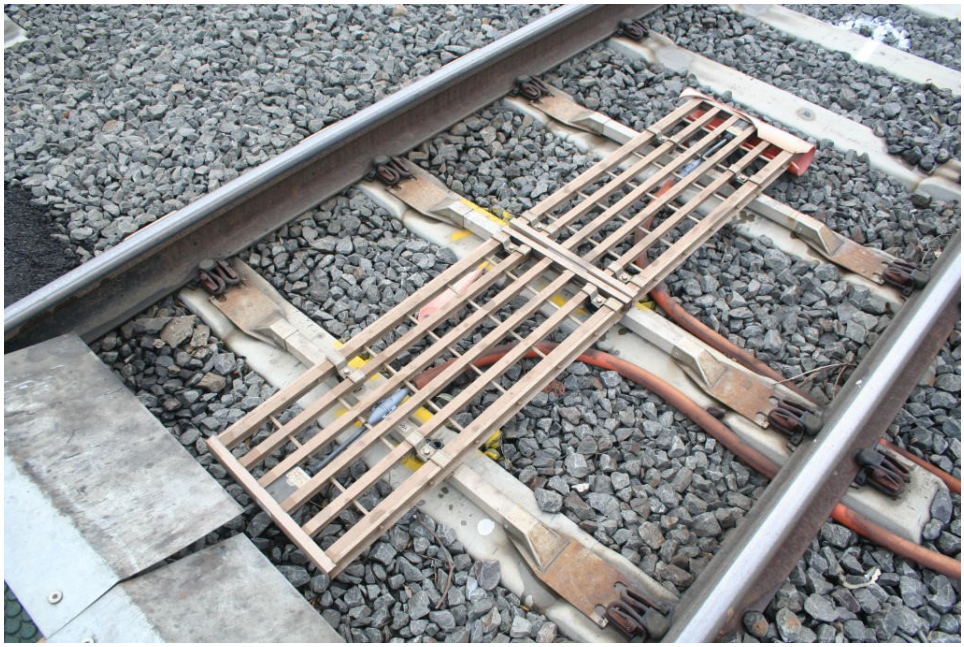


Figure 4.16: TWPS Loop Sensor

If a train is approaching a stop signal at high speed, it will be forced to stop, regardless of any action by the driver [52].

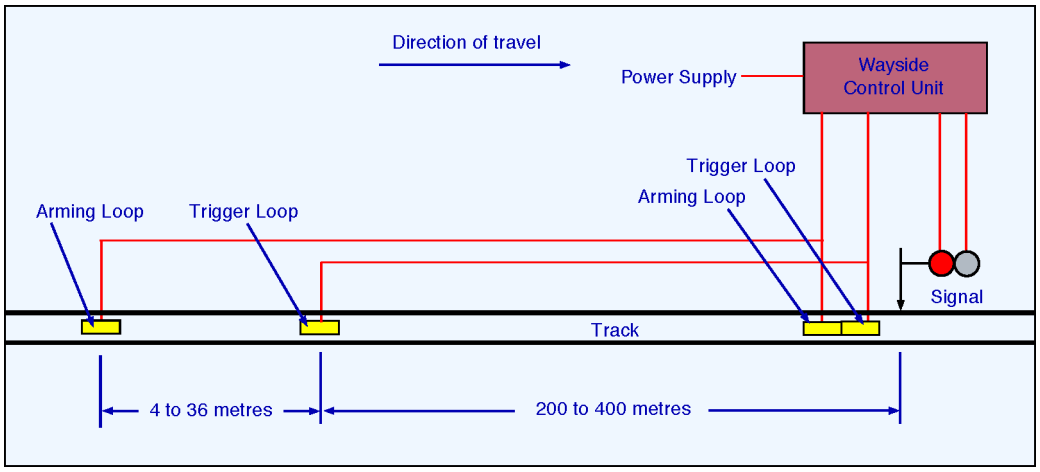


Figure 4.17: TWPS Schematic [52, 58]

Automatic Warning System

Automatic Warning System (AWS) is an on-board signalling that assist the driver by informing the status or aspect of the oncoming signal, via visual and audible indications. Additional to the previous, a series track equipment consisting in a set of permanent magnet and a electromagnet installed between the rails at least 200 yards before the approaching signal [58], as shown in Figure 4.18. This distance may vary in high-speed sections.

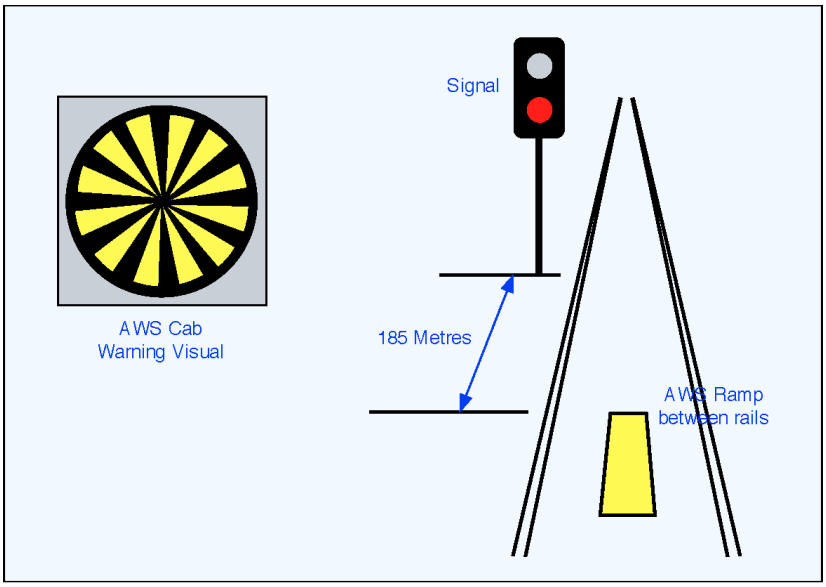


Figure 4.18: On-board and track elements of AWS [52]

The ramp (set of permanent and electromagnet) functions as an aspect indicator of the approaching signal. When the train moves over the ramp, the permanent magnet triggers a braking set up in the on-board visual. Then, when passing over the electromagnet, this could be energised or de-energised, depending on the approaching signal. If it is "clear" the electromagnet is energised and the brakes are deactivated. If the signal is "warning" or "stop", then the electromagnet is de-energised and the brakes are activated, preventing further displacement.

4.3 Conclusion

During this chapter a fundamental background of modulation techniques was mentioned and revised, making emphasis in the spread-spectrum techniques used nowadays by wireless devices due to its high resilience against noise. It was primarily important to make a comparison in order to find a balance between complexity and power consumption. Less-complex systems in terms of processing capabilities, are usually low-power consuming, as their processors are limited and have basic input/output compatibility. DSSS was designed to be a modulation scheme to be implemented in low-complex communication devices. Therefore, this devices tend to be also low-cost and straightforward to implement. However, it has many limitations which will be addressed in further chapters. In particular, ZigBee RF radios have caught attention due to its low-complexity and low costs of implementation, being non-invasive scalable sensor network and will be the base of this research.

Since the aim of this project is to present an alternative for current wired signalling systems, the current systems utilised have been explored. Both systems mentioned are based on sophisticated wireless technologies, which makes a robust system less likely to fail, delivery data safely from point to point, i.e. train-ground link. In summary, both CBTC and ERTMS are signalling and control systems that share the same structure including track-side infrastructure for train-ground communication, which are in constant communication to a big central station where traffic management is done.

Based on the operational structure for traffic management of the these mentioned signalling systems, a wireless alternative will be proposed and will be address in the following chapters. In order to study and validate its features, and make an actual statement about the potential use of this technology, a few experimental tools were studied, such as RC, which is a crucial testing environment where a device or system electromagnetic characteristics can be investigated, as discussed previously in this work.

Chapter 5

Towards an Alternative Solution for Railway Signalling Systems Applications

Current U.K. signalling systems rely on a physical interconnection grid for power supplying and data transferring of over 40,000 signals across the whole network [59]. Hence, a very high cost is related to infrastructure implementation, maintenance and repairs. The infrastructure and implementation costs of signalling systems (especially network and wayside systems) are high due to the physical data and power interconnects required between systems along the railway. Hence, a cost reduction is paramount for the transportation industry. Developing alternatives such as wireless signalling systems leads to cost reduction in infrastructure, whilst having the same reliability provided by the wired systems.

With current signalling systems relying on a physical grid for power and data delivery, the installation and maintenance costs are considerably high, as the installations include high number of miles of substantial electrical cabling. Additionally, they are also subject to metal theft. National Rail has estimated that every year £16 million worth of metal and cable theft occurs, due to the reselling of materials in the illegal market, causing costly repair costs and disruptions to service [60]. In

fact, aside for faulty components and heat failures, one of the most common causes of signalling failures aside is power failure, due to cable ageing or cable/metal theft [59].

Thus, there is a need for a low cost, and low power modular wireless system, able to be easily deployed and incorporated within existing signalling networks which can be replaced in a short period of time without compromising connectivity.

The main goal of this research project is to provide with a low power and non-invasive alternative for current UK signalling systems, led by the need of reducing cost of implementation, maintenance and power consumption.

5.1 ZigBee Implementation

ZigBee is a low-power and low-data rate wireless communication technology standard, widely used in applications that required long battery life and secure networking. It operates in the ISM and is licence-free. The ZigBee Standard only defines the networking, application and security layers of the protocol, whilst the PHY and MAC layers rely on the IEEE 802.15.4 standard.

5.1.1 IEEE 802.15 protocol

The IEEE 802.15 is the IEEE 802 (Local and Metropolitan Area Networks: Overview and Architecture) standards committee for Wireless Personal Area Networks (PANs), which consists in seven tasks groups (parts):

- IEEE 802.15.1: Wireless Medium Access Control (MAC) and Physical Layer (PHY) Specifications for Wireless Personal Area Networks (WPANs).
- IEEE 802.15.2: Coexistence of Wireless Personal Area Networks with Other Wireless Devices Operating in Unlicensed Frequency Band.
- IEEE 802.15.3: Wireless Medium Access Control (MAC) and Physical Layer (PHY) Specifications for High Rate Wireless Personal Area Networks (WPAN).

- IEEE 802.15.4: Low-Rate Wireless Personal Area Networks (LR-WPANs).
- IEEE 802.15.5: Mesh Topology Capability in Wireless Personal Area Networks (WPANs).
- IEEE 802.15.6: Wireless Body Area Networks (WBAN).
- IEEE 802.15.7: Short-Range Wireless Optical Communication Using Visible Light.

IEEE 802.15.4

The IEEE 802.15.4 (Task Group 4) was created to investigate a low data rate solution with multi-month to multi-year battery life and very low complexity. Main features:

- Data rates of 250 kbps, 40 kbps, and 20 kbps
- Allows a maximum 127 bytes per packet
- Low latency [43]
- Carrier-sense multiple access with collision avoidance channel access (CSMA/CA) [44]
- Automatic network establishment by the coordinator
- Fully handshaked protocol for transfer reliability
- Power management to ensure low power consumption

Furthermore, the physical layers defined in the standard are:

- O-QPSK PHY: direct sequence spread spectrum (DSSS) PHY employing offset quadrature phase-shift keying (O-QPSK) modulation, operating in the 780 MHz, 868 MHz, 915 MHz, and 2450 MHz bands.
- BPSK PHY: DSSS PHY employing binary phase-shift keying (BPSK) modulation, operating in the 868 MHz, 915 MHz, and 950 MHz bands.

- ASK PHY: parallel sequence spread spectrum (PSSS) PHY employing amplitude shift keying (ASK) and BPSK modulation, operating in the 868 MHz and 915 MHz bands.
- CSS PHY: chirp spread spectrum (CSS) employing differential quadrature phase-shift keying (DQPSK) modulation, operating in the 2450 MHz band.
- UWB PHY: combined burst position modulation (BPM) and BPSK modulation, operating in the sub-gigahertz and 3–10 GHz bands.
- MPSK PHY: M-ary phase-shift keying (MPSK) modulation, operating in the 780 MHz band.
- GFSK PHY: Gaussian frequency-shift keying (GFSK), operating in the 950 MHz band.

Table 5.1: Frequency bands and data rates for the 802.15.4 standard

Frequency band (MHz)	**Modulation**	**Bit rate (kb/s)**	**Symbol rate (ksymbol/s)**	**Symbols**
779-787	O-QPSK	250	62.5	16-ary orthogonal
779-787	MPSK	250	62.5	16-ary orthogonal
868-868.6	BPSK	20	20	Binary
902-928	BPSK	40	40	Binary
868-868.6	ASK	250	12.5	20-bit PSSS
902-928	ASK	250	50	5-bit PSSS
868-868.6	O-QPSK	100	25	16-ary orthogonal
902-928	O-QPSK	250	62.5	16-ary orthogonal
950–956	GFSK	100	100	Binary
950–956	BPSK	20	20	Binary
2400–2483.5	O-QPSK	250	62.5	16-ary orthogonal

The above Table 5.1 shows and compares the different frequency bands in which ZigBee standard can operate on, as well as its modulation techniques. In Europe, ZigBee standard is commonly used in the 868-868.6 MHz and 2400-2483.5 MHz bands.

5.1.2 XBee Modules

XBee is a variant of the ZigBee technology manufactured by Digi International. Usually, ZigBee modules operate in the 2.4GHz frequency and have a range of a few meters. The XBee 865/868 LP operates in the 863-870 MHz band and has a range up to 4km when using a 2.1 dBi antenna with a maximum radiated power of 14dBm (25mW) and a maximum data rate of 80 kbps. Each of the channels has a bandwidth of 200Hz and are distributed equally across the 863-870 MHz band. Such distribution can be seen in Table 5.2

Table 5.2: Channel frequencies available for the XBee module

Channel number	**Frequency**	**Band**
0	863.15 MHz	g
1	863.35 MHz	g
2	863.55 MHz	g
3	863.75 MHz	g
4	863.95 MHz	g
5	864.15 MHz	g
6	864.35 MHz	g
7	864.55 MHz	g
8	864.75 MHz	g
9	864.95 MHz	g
10	865.15 MHz	g
11	865.35 MHz	g
12	865.55 MHz	g
13	865.75 MHz	g
14	865.95 MHz	g
15	866.15 MHz	g
16	866.35 MHz	g
17	866.55 MHz	g
18	866.75 MHz	g
19	866.95 MHz	g
20	867.15 MHz	g
21	867.35 MHz	g
22	867.55 MHz	g
23	867.75 MHz	g
24	867.95 MHz	g
25	868.15 MHz	g, g1
26	868.35 MHz	g, g1
27	868.55 MHz	g, g2
28	868.75 MHz	g, g2
29	868.95 MHz	g, g4

By default, all the channels are available for transmission, with possibility of changing the Tx power level, up to 25mW depending on the application requirements. The frequency operation for the XBee module, is shown in Figure 5.1 as an example to provide a visual example of the channel distribution. The image

has been divided into three sub images to have an easily readable image. Hence, Figure 5.1 a) contains the channels 0 to 9, Figure 5.1 b) the channels 10 to 19 and Figure 5.1 c) the channels 20 to 19. The blue rectangles is the current transmission power, the red lines are the minimum power and the green correspond to the maximum transmitted power. The continuous purple line is the average power through the measurement.

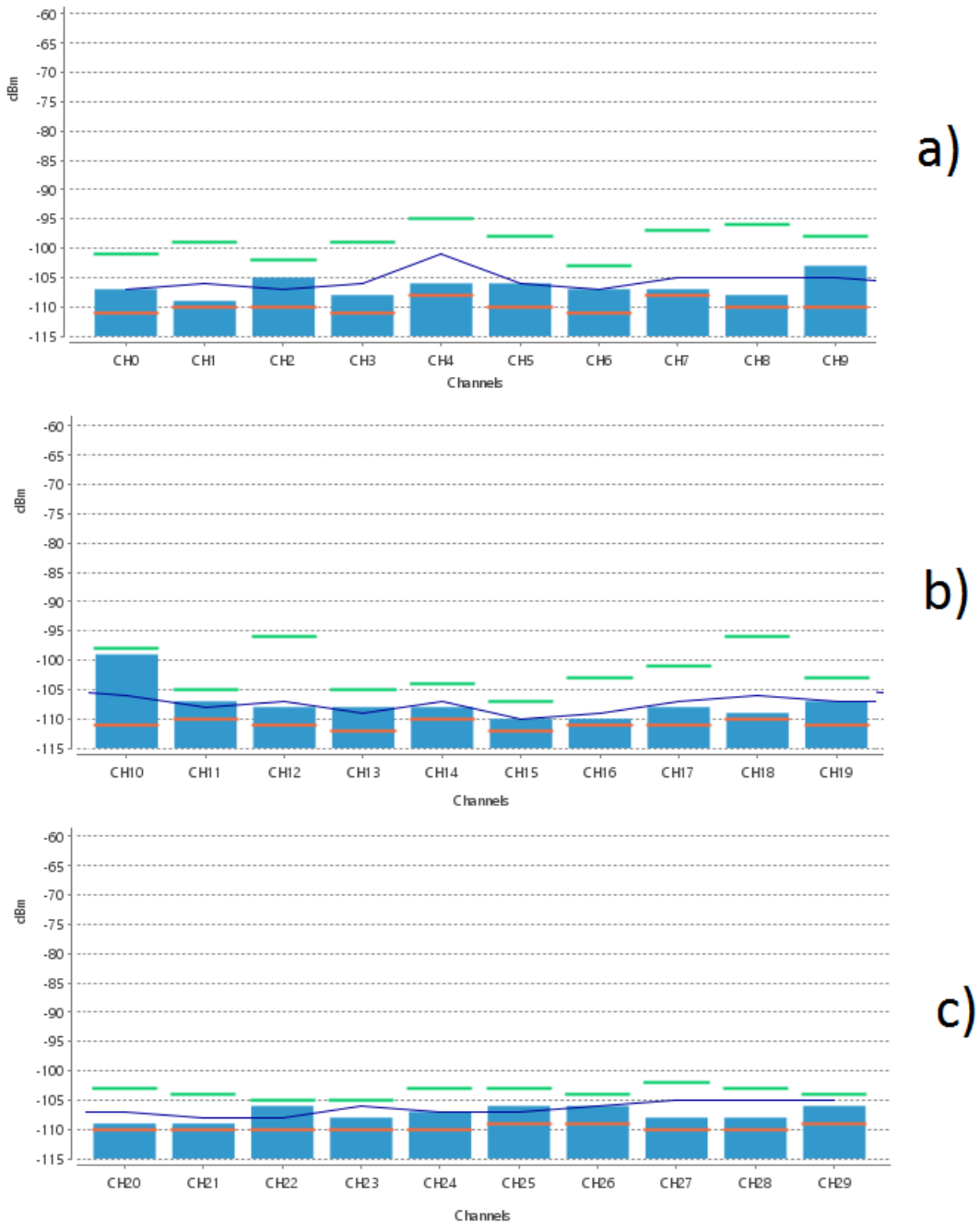


Figure 5.1: Example of channels available for XBee use, and its current, maximum and average transmitting powers during a test.

As mentioned before, ZigBee modules can transmit using different power levels.

The total occupancy when active or transmitting is show in Figure 5.2, where the orange line corresponds to the maximum transmitting power of 25mW, whilst the red and blue correspond to 16 mW and 5mW respectively.

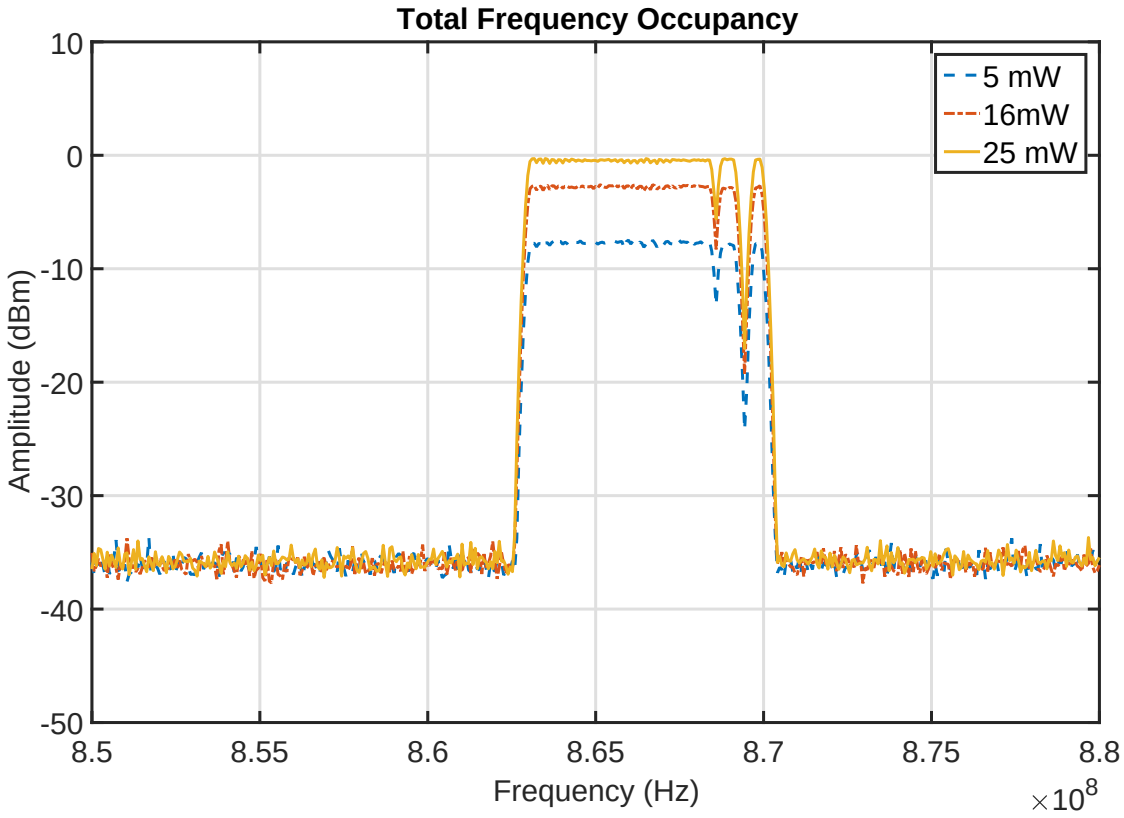


Figure 5.2: Default and total frequency occupancy of XBee: all channels active

Transmission requires at least 2 channels: one for sending data and one for acknowledgement of successful packet reception, and said channels are randomly selected by each radio.

Frequency selection follows a method known as Listen Before Talk + Automatic Frequency Agility (LBT+AFA) [61], where the transmitter measures the received signal strength indicator (RSSI) of each channel for 5ms. If the first selected channel is being used, then another channel is selected. At least two are required for transmission. On the other hand, it is possible to limit the channel switching within a certain band, as defined in the below Table 5.3:

Table 5.3: Channel Mask bands

Band number	Frequency
1	863-865 MHz
2	864-865 MHz
3	863-865/868-868.6 MHz

Furthermore, a specific pair of channels could be selected, in order to avoid disruption from another service using the a frequency band within the total ZigBee operational occupancy. The frequency of the multiple bands able to use from ZigBee listed in Table 5.3 are show in figures 5.3, 5.4 and 5.5, showing Band number 1, 2 and 3 respectively.

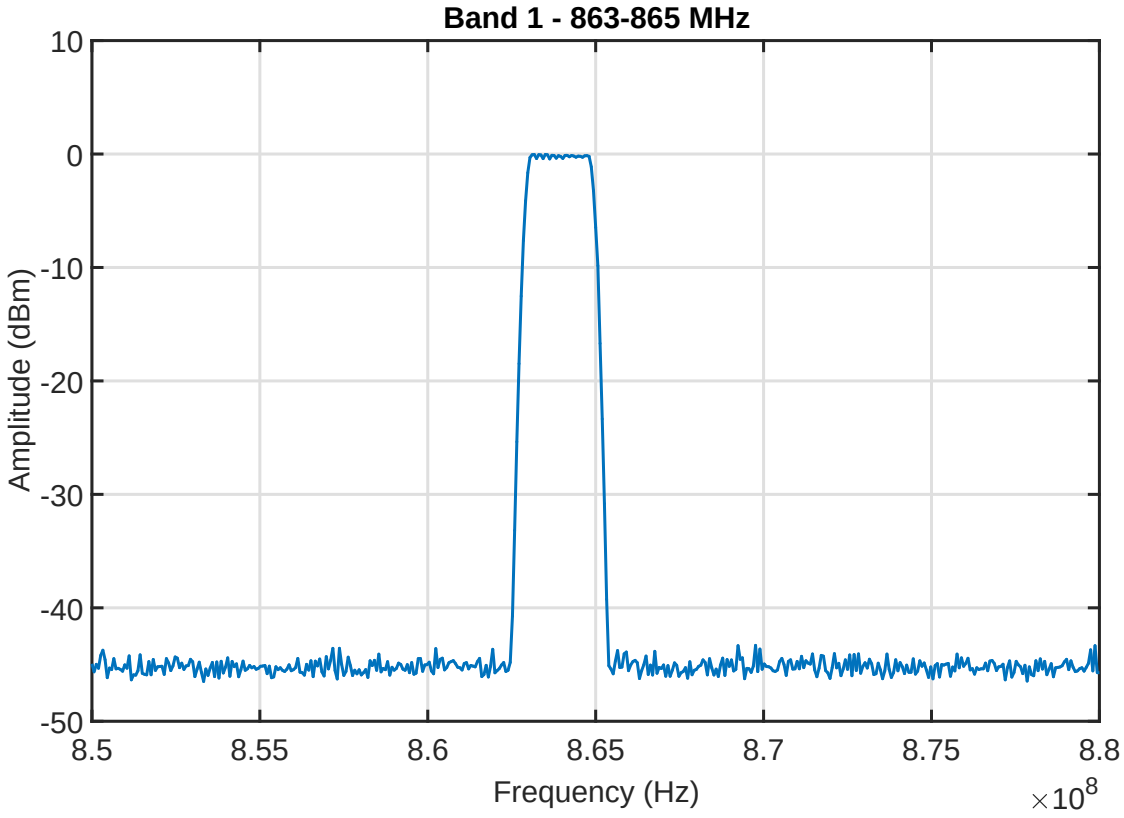


Figure 5.3: Channel Mask Band 1 occupancy

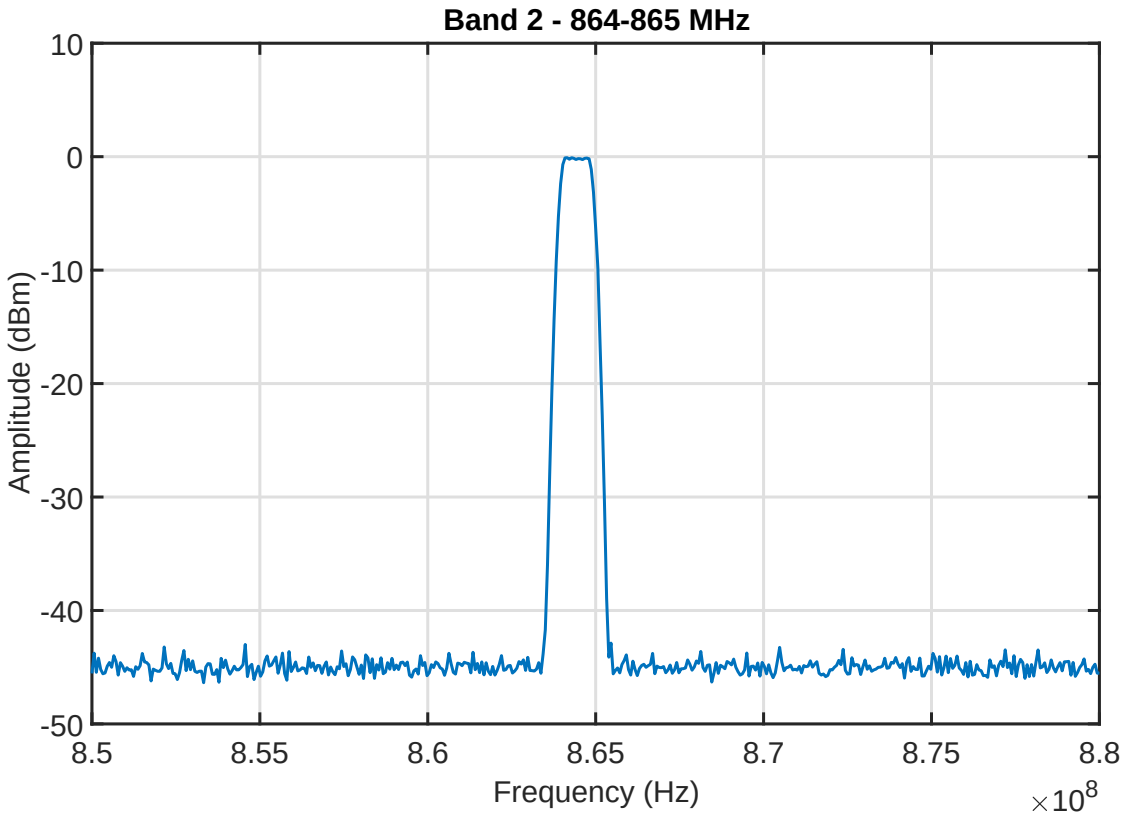


Figure 5.4: Channel Mask Band 2 occupancy

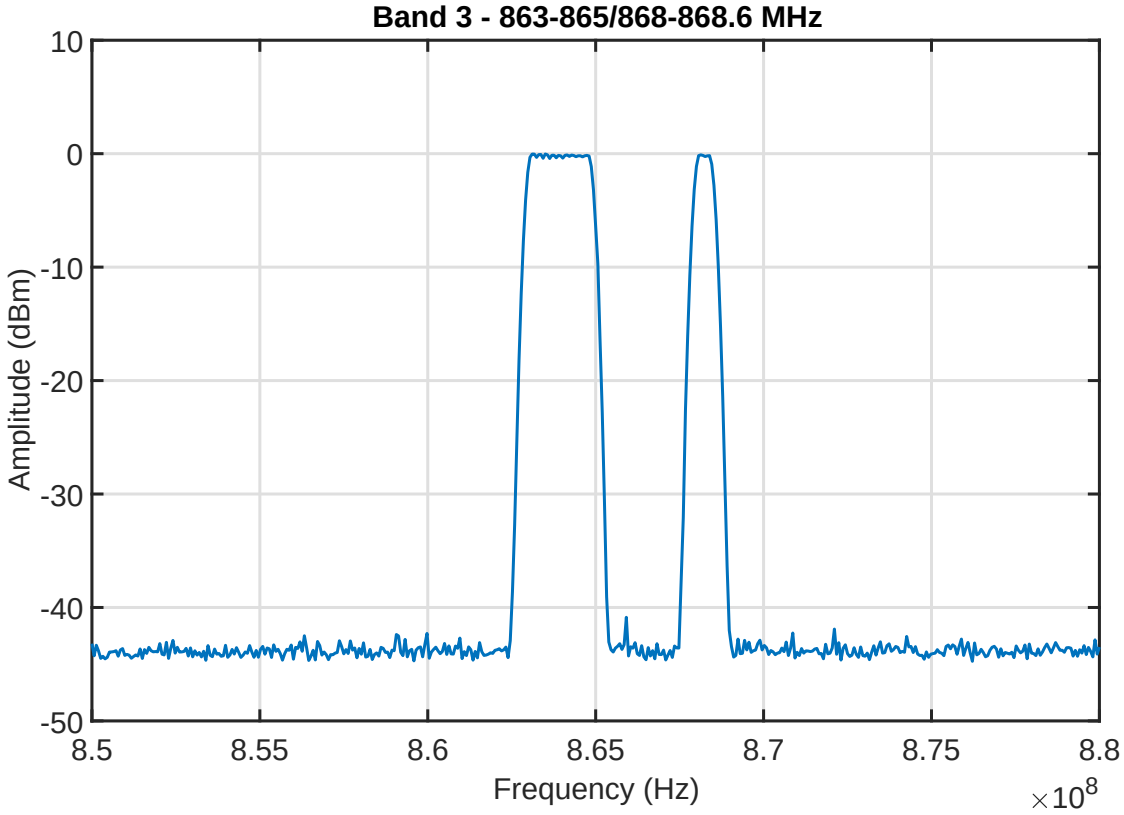


Figure 5.5: Channel Mask Band 3 occupancy

Furthermore, it is possible to switch off the LBT+AFA mode, forcing the communication to the 29th channel from Table 5.2 (868.95 MHz), regardless the condition of the channel. For these two modes, the mode selection must be established equally in both Tx and Rx. Otherwise, the switching will take place in the whole XBee operation band using LBT+AFA. This strategy results in the frequency occupancy shown in Figure 5.6.

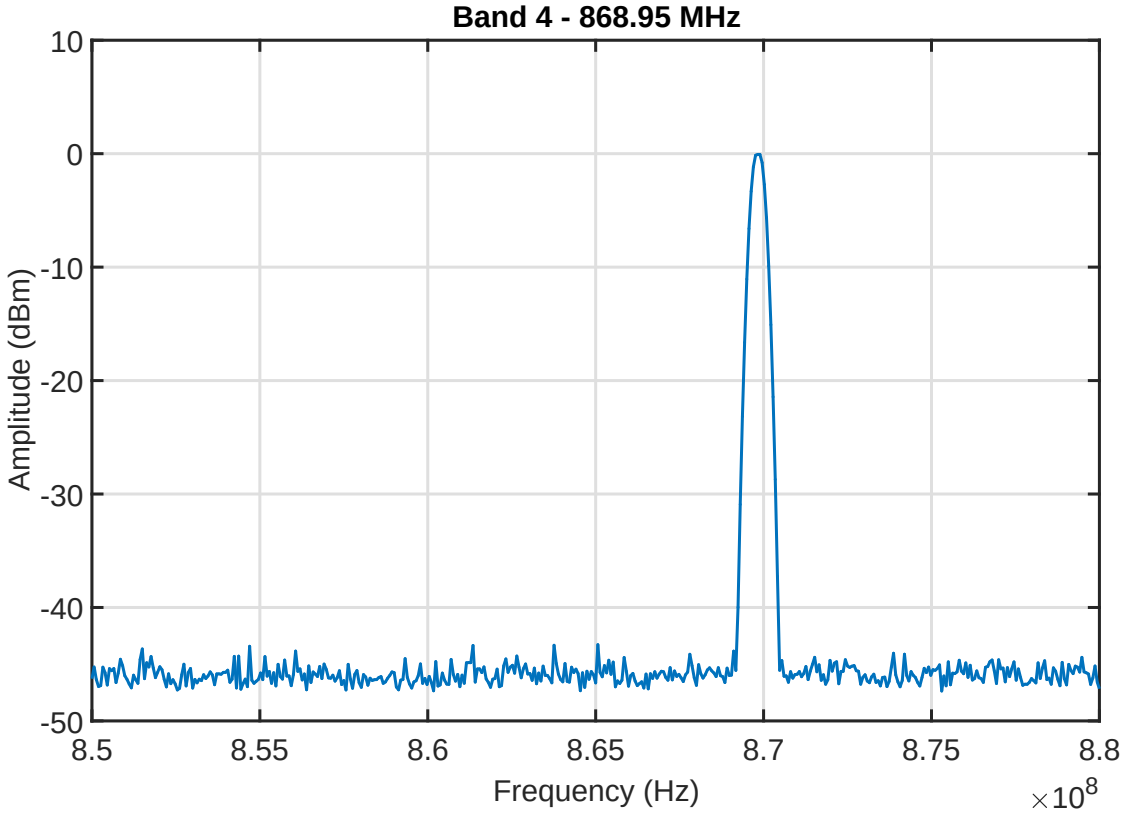


Figure 5.6: LBT+AFA deactivated: only 868.95 MHz band available

The purpose of the band selection mentioned above is to allow interference avoidance in case it is known that one or more channels are being used by other devices or are being affected by noise pollution in an specific geographical location. For example: suppose radios A, B, C and D are covering a specific region, set to default settings and in a $A \rightarrow B \rightarrow C \rightarrow D$ link. But before deploying, high noise levels are found between B and C that potentially would interfere with certain channels. Using channel mask, B and C could transmit in a defined band whilst A to B uses the full channel list, as well as C to D.

5.1.3 Frame format

The frame transmitted and received by an Xbee module (under given configuration), is divided into 22 bytes in an HEX description seen in Figure 5.7,

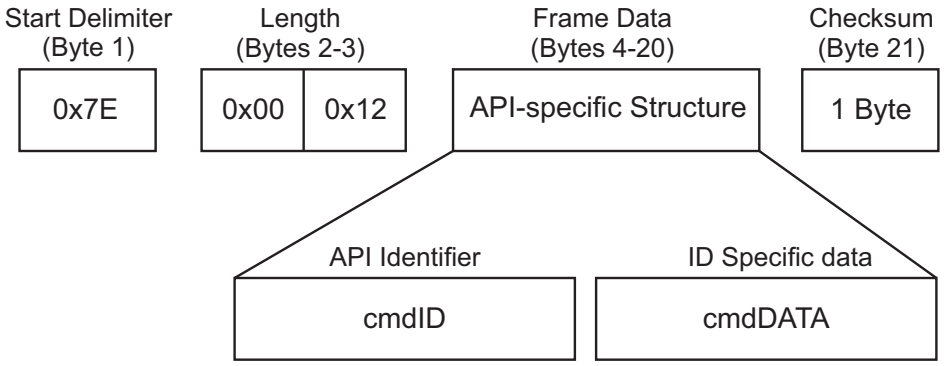


Figure 5.7: Frame division

- **Start Delimiter:** Determines the beginning of the whole frame.
- **Segment length:** describes the number of bytes between the byte 3 and 20, to define the data structure.
- **Frame Data:** Is divided into two segments as follows:

  cmdID frame. It contains the 64-bit address of sender or source.

  cmdData frame. It is defined from the byte 14 to 20, where byte 14 specifies the receive Options (network topology configuration) and the data transmitted is contained from byte 15 to 20.

- **Checksum:** Verifies data integrity. It is used to request retransmission when data is corrupted.

5.1.4 Network Topologies

The standard is able to operate in two topologies: Star or Peer-to-peer topology. In the start topology, the communication is established between devices and a single central controller (PAN Coordinator). If required, the communication

between devices is possible only through the coordinator. Its application is oriented to schemes where the information should be allocated in a central system. The peer-to-peer topology also has a PAN coordinator, but the communication between devices (avoiding the coordinator) is possible. It allows more complex network formations to be implemented useful for applications such as wireless sensor networks. An example of the previous is shown in Figure 5.8. In both cases, the communication could be configured as bidirectional.

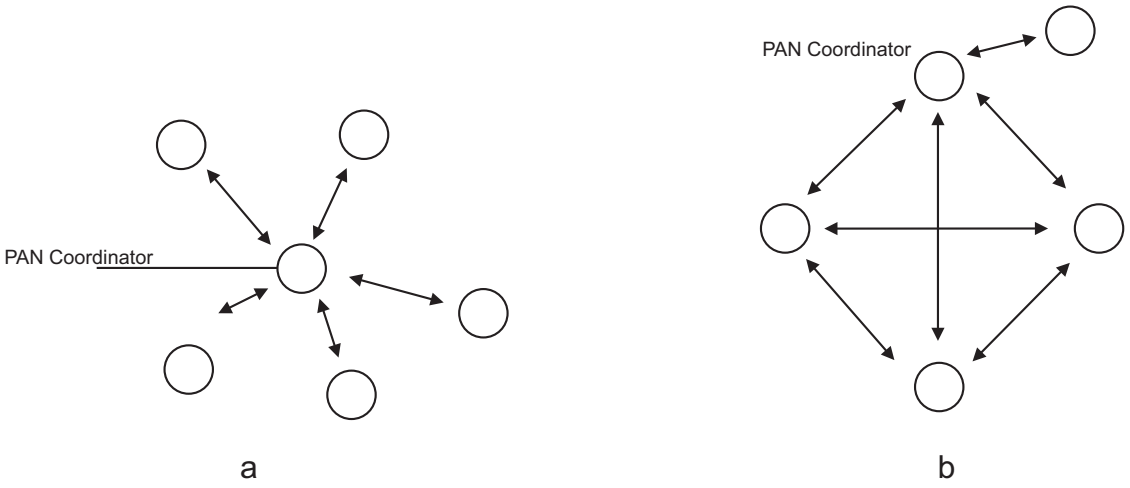


Figure 5.8: Network topologies. a) Star b)Peer-to-peer

Nevertheless, the main difference between these two topologies is that, in 5.8 a), if one of the nodes is unable to communicate to the coordinator, then there is no possible route to deliver the message, whereas in 5.8 b), rerouting is possible. Therefore, Star is more recommended for fixed sensor networks and peer-to-peer is better for mobile applications.

Within the peer-to-peer topology, three communication schemes are available: point-to-point, repeater and mesh grid. In the point-to-point, the coordinator is required to send a packet to an specific receiver node without hoping or being repeated by another.

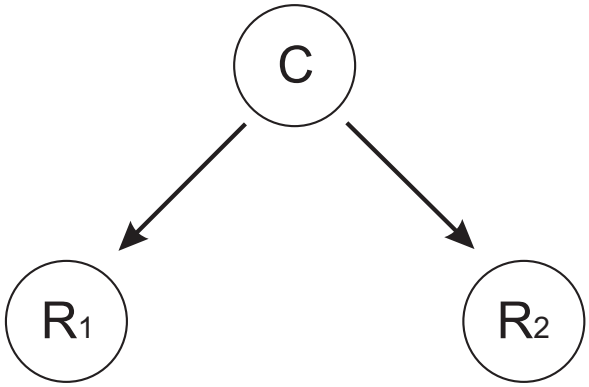


Figure 5.9: Point-to-point topology

In the repeater scheme, any node is allowed to retransmit any packet until it reaches its destination and is possible to define the path to follow, so the way to reach R_2 is only via R_1.

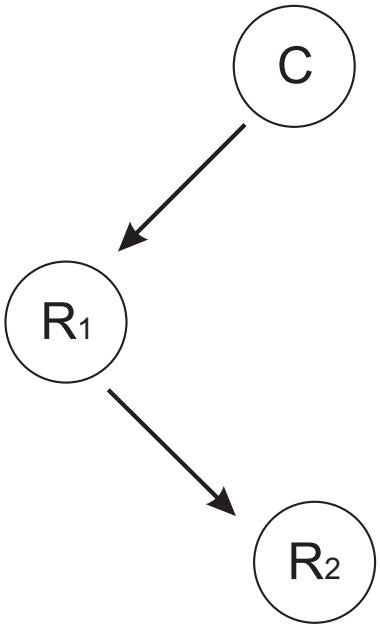


Figure 5.10: Repeater topology

The third scheme is the mesh grid, where the network autoconfigures itself and has more freedom to choose the best way to delivery packets, based on RSSI or channel occupancy, similar to broadcast. Moreover, new nodes could be added

quick and be part of the infrastructure seamlessly. Mesh grid is useful when both mobile and fixed nodes are present.

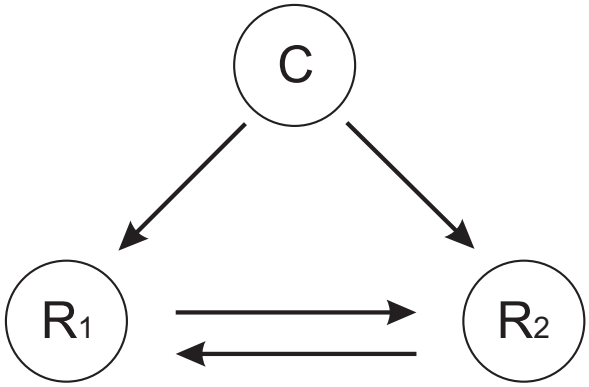


Figure 5.11: Mesh topology

5.2 Radio-Frequency Identification

RFID is a mean of electronic wireless identification system consisting in at least a combination of a reader and one tag. Depending in the source of energy, tags could be passive or active, being the passive version the most common due to the possibility of mass production. Internally, the basic system contains an antenna and a electronic circuit where the ID number is stored. When the tag is in the reader's proximity (less than a centimetre), the reader induces voltage to the antenna and energises the circuit. Afterwards, the circuit responds by sending the ID number as a pulse train, being interpreted as sequence of numbers corresponding to the ID (Figure 5.12). This response and reading should be completed in less than 400ms [62], allowing low-latency data sharing.

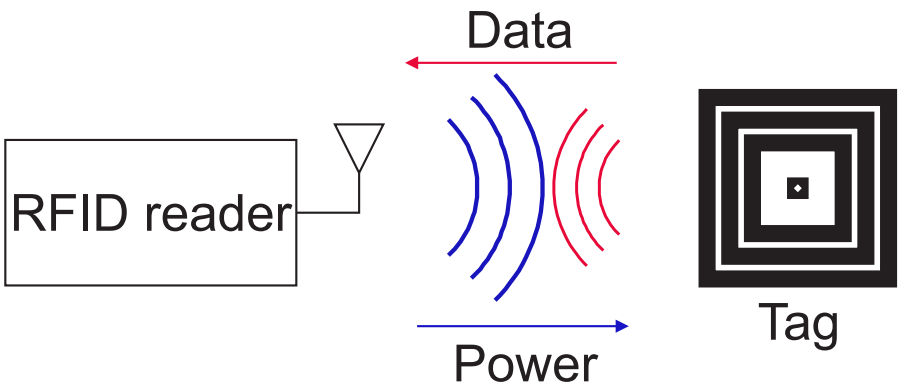


Figure 5.12: RFID schematic

RFID can operate in different frequencies depending on the application and licensing [63], as described in the table below:

Table 5.4: RFID Channel frequencies

Frequency	**Range**	**Regulation**	**Application**
125-148 kHz	up to 10cm	Unlicensed	Animal ID and factory data collection
13.56 MHz	up to 1m	ISM	Smart Cards
433 MHz	up to 100m	Non-specific	Defence applications
865-868 MHz (Europe)	up to 2m	ISM	Rail stock tracking
902-928 MHz (America)	up to 2m	ISM	Rail stock tracking
2450-5800 MHz	up to 2m	ISM	802.11b, Bluetooth

This technology is widely used in retail stores, security systems and banking. On the latter, the complexity of the circuit and modulation is higher due to security and encryption concerns. However, the time response is in the range of milliseconds as well. Nowadays, the size of this passive devices has been miniaturised to the range of a few millimetres.

5.3 System Design and Description

The communication scheme is in charge of data delivery within the network. It consists of four fundamental elements: Control Centre (CC), On-board Unit (OU), Signal Nodes (LN) and Slave Nodes (VN). The coordination of the network relies on the CC, which has de function of sending information to a specific destination. LN has the function of retransmit the information within the network. Besides retransmitting information as the LN, VN operate the traffic lights, according to the instruction received. Finally, the end-device is the OU, which collects and displays relevant information to the driver i.e. movement authority information.

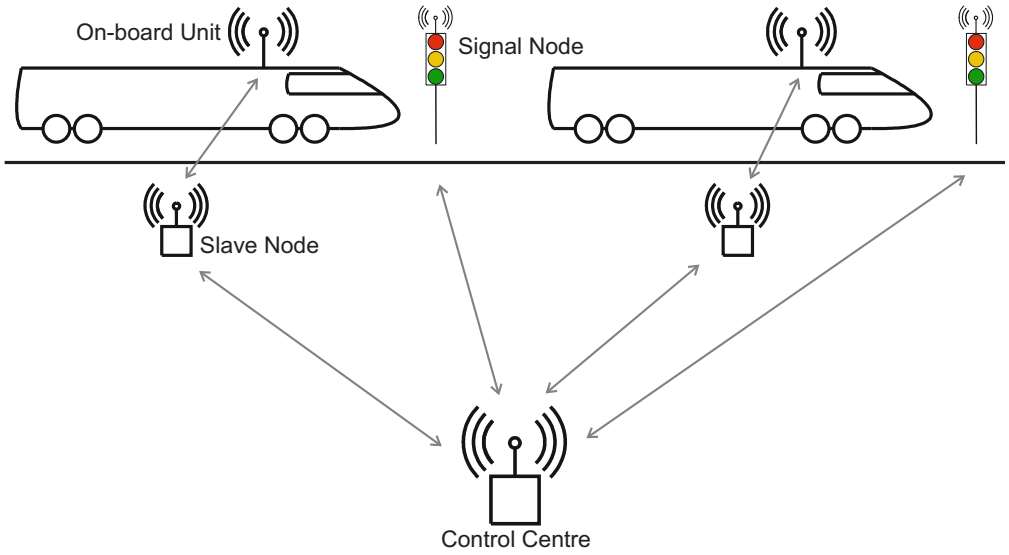


Figure 5.13: Network elements

As seen in the figure above, CC is located in a far end, operated by the operations centre where factors as traffic conditions, train positioning, speed limits and scheduling are know. Additionally, it is where movement authorities are calculated in function of the moving block scheme. It follows a semi centralised network scheme, as various CC units can control a certain section of the rail network whilst connected to the main traffic management centre.

5.4 Performance Metric Parameters

In order to asses the performance and reliability of this system, throughput, error rate and time delay properties have been addressed and studied as metrics.

Throughput

Throughput is defined as the rate of successful message delivery throughout a communication network and can be expressed in symbols per second, bits per second or packets per second, depending on the application or the vendor's definition. It is possible to measure the throughput between two transceivers in a unidirectional and bidirectional way.

Error Rate

Error rate is the percentage of correctly received bits or packets received per second, known as Bit Error Rate (BER) or Packet Error Rate (PER), respectively [64]. Usually, when bit is corrupted, the packet would be corrupted as well. Depending on the frame structure or the transmission scheme, this errors could be fixed with checksum, redundancy o retransmission. Moreover, retransmission compromises throughput and increases time delay. BER is defined as the number of bits corrupted from the total of the packet or message length, and its presented as percentage:

$$BER = \frac{error\ bits}{packet\ length} \tag{5.1}$$

Usually, PER is more adopted as a metric in the XBee protocol, as it does not perform error correction and retransmission is the only technique to transmit a correct packet. Then the probability of PER P_{PER} is defined as:

$$P_{PER} = 1 - (1 - P_{BER})^N \tag{5.2}$$

where N is the number of bits that compose the packet.

The manufacturer includes in the software provided a feature to measure packet error rate, which is useful to log data for both error rate and throughput.

Time Delay

Having retransmission from node A to node C implies a time in which the data is received by node B, processed and forwarded to C. As it could be expected, the minimum delay happens when LOS exists and noise and interference levels are low. Therefore, the channel sensing takes up to 2 ms and transmits instantaneously. The time delay is the time difference between the time when the message was sent t_{Tx} and when it was received t_{Rx} and an acknowledgement is raised. If the difference is greater than the R_x time out (usually 1000 ms), the packet is considered as lost and a retransmission is required.

It is worth to note that each hop that the packet needs to perform will add an extra time to the overall delay. Thus, the number of hops should be selected according to the total area to cover with the same section of infrastructure to guarantee a short message delivery time.

In [65], a study of a similar device was conducted in a laboratory. Using a XBee 2.4 GHz Series 2: 2mW output, QPSK, 250 kbps (max) and 120m range, and an approximation of the time delay per node was observed and presented as:

$$\frac{1}{n_{hops}} \tag{5.3}$$

where n_{hops} is the number of hops done until the destination is reached. Since the device is different, the results obtained with the proposed system may defer, but it provides an insight of its possible behaviour.

Received Signal Strength Indicator

As its name states, this value indicates the strength of the signal received, usually in dB. This indicator is broadly used as it does not require added hardware to calculate. In fact, the value is provided automatically by the device. However, the certainty of it could be affected by elements blocking the LOS, harmful emissions near the receiver, reflection or any other external components.

There is not a standard defining the calculation of this indicator. Thus, each individual manufacturer has a different calculation method, but provides a impression of the link power level and, in this case, useful to establish a node-to-node distance ratio.

Power Consumption

The current drained by the XBee modules was observed in three different modes:

1. **Idle**. The modules is in idle or sleep mode, waiting to be found by another module within the same network. This is the lowest power mode encountered.
2. **Discovery**. When a different module is monitoring the medium to find another module to include in the network, the new found modules switch from an idle mode to a discovery mode, with the purpose of pairing and to create a network connection. Once both devices are connected, each of them return to idle mode and wait for instructions.
3. **Active**. The active state is when the communication is constant within two or mode modules.

The average values found in the current consumption or a Rx XBee module is shown in Table 5.5. The values are only observed from the Rx point of view as it is assumed that the Tx is in the far end connected to a power outlet in the central station.

Table 5.5: Current consumed by XBee with a power source of 12V DC

Mode	Average Current drain
Idle	26.5 mA
Discovery	32.53mA
Active	33.9mA

The peak current is found in the active mode. In this case, the peak value was 46.2 mA. Having this value, the instantaneous power is given by:

$$P_{(W)} = I \times V = .0462A \times 12V = .5544W \tag{5.4}$$

Then, considering a continuous use with full load, the energy consumption per consecutive 24 hours is:

$$E_{(kWh/day)} = \frac{P_{(W)} \times t_{(h/day)}}{1000_{(W/kW)}} = \frac{.5544W \times 24h/day}{1000W/kW} = 0.0133056kWh/day \tag{5.5}$$

The approximately annual consumption is 4.85654 kWh/year. The energy produced by a solar panel varies from geographical location and the actual size. Theoretically, a $1m^2$ photovoltaic panel can produce up to 80kWh annually [66]. Since the aim of this system is to be self-contained and low-power consuming, the XBee technology is a suitable alternative for a modular signalling in terms of autonomy.

5.5 Performance assessment

Test Scenarios

As mentioned in Chapter 2, access to a functioning test track was granted to operate the network and test its features. Various test scenarios were planned to

be conducted using this facilities and an operating locomotive, in accordance with Thales Ground Transportation Systems:

1. **No train on track.** The network operates normally. However, the absence of the train is reported back to the CC.

2. **On-board Unit on the train.** The operation of the system is tested with on-board unit installed on the train. Train is to run at high speed. Observers are to remain on a remote location away from track to observe the changing signal aspects.

3. **Failure Mode.** The operation of the system is to be tested with simulated LN failure, achieved with the use of the "Localised Jammer". Observers are to remain on a remote location away from track to observe the changing signal aspects.

4. **Low Energy mode.** When the battery charge is low, the system enters a low energy mode, where the signalling lights are switched off. However, the radios are still active and data delivery is available to the driver.

5. **Simulation of Signal Passed At Danger (SPAD).** When SPAD signal is disregarded, which means the driver did not reduce the train's speed or did not apply the brakes, an emergency state is triggered, sending an alert to the CC.

6. **RFID train detection.** Detect train relative position and direction according to the node's location.

For these scenarios, Thales-GTS staff was on-board the train to corroborate the correct operation of the system according to the previously established sequence.

Time Delay observed

It was possible to evaluate the time delay and throughput in a multi-hop scenario. The time delay caused by multiple packet lengths is shown in Figure 5.14.

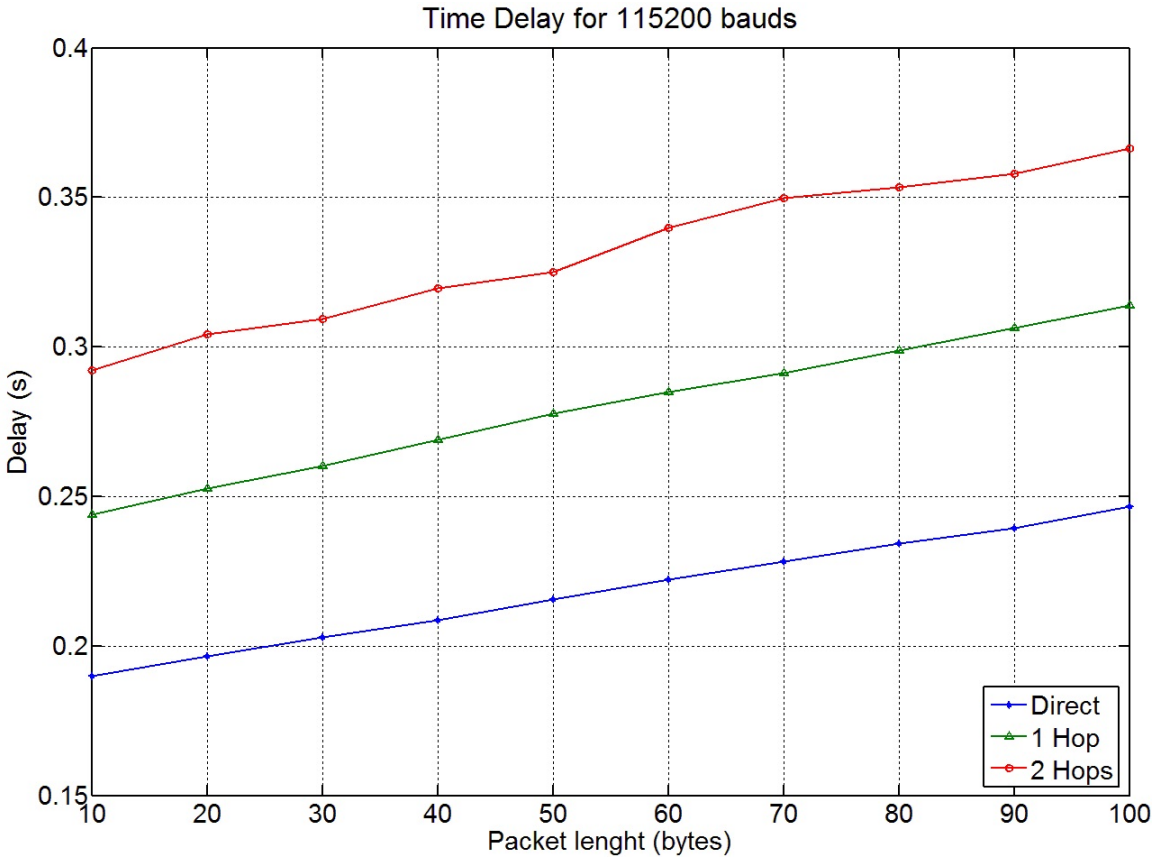


Figure 5.14: Time delay measured with multiple packet sizes.

During the test, the distance in a direct link was 420m, in a one-hop was 720m and two-hops was 1180m. Based on the RSSI results, where the connection was stable, and the theoretical coverage range of 4km for each module, we can deduce that considering a 2-hops retransmission and a separation of 1km between modules, a 100-length packet could be successfully delivered in a range of 3km in 0.366s.

This results slightly differ from [65] using Eq. 5.3, where the Author set up the experiment with a node-to-node separation of 3m within a lab facility; the direct transmission had a delay of .11s, .27s for two hops and .37s for three hops with for a maximum payload of 80 bytes, whilst during the experiment conducted in this work with the same payload, for a node-to-node communication the delay was .23s, .3s for two hops and .36s for three hops. It is worth noting that the modules

used in [65] work have a different modulation technique and operational frequency (2.4GHz),which has a greater throughput.

However, this deduction has to be proven in a larger test track, since the one available was limited to a loop and the linear distance was not greater than 2km. Additionally, as the train was transiting across coverage areas, an effective throughput was also measured, resulting in approximately 12kbps average, in contrast to [65], since the throughput in their experiment with the same package length is around 60kbps.

Railway Spectrum Occupancy

After inspecting the surrounding spectrum in the test track, no unwanted signals located at the XBee operation frequency were identified that could potentially interrupt partially or totally its operation. The spectrum in the test track environment was monitored during the test preparations for a period of 8 hours during the day and the results are shown in Figure 5.15. Both the maximum and minimum power levels are shown in blue and red respectively. The reason of holding the maximum values is to identify possible occupancy of the spectrum and locate them in the frequency domain.

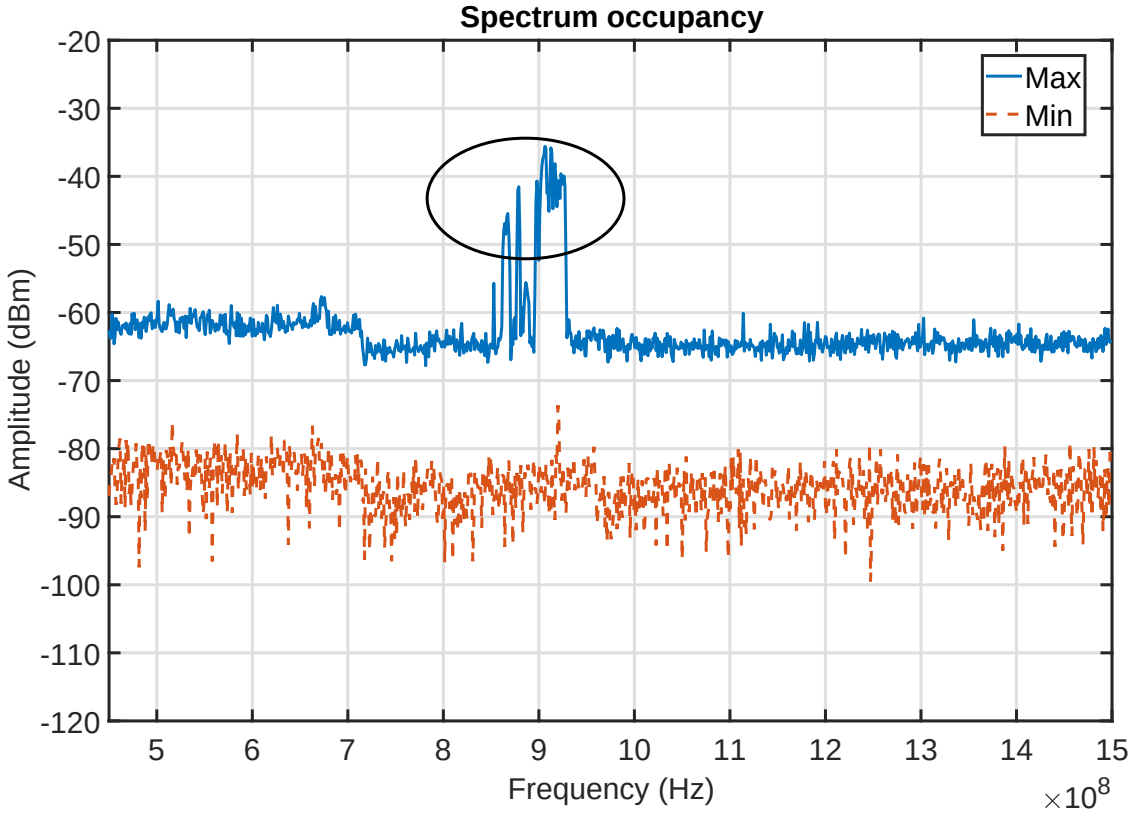


Figure 5.15: Spectrum occupancy at the test track. The ellipse in the graph contains the frequency occupancy of GSM mobile services

Some of the identified signals are placed in the typical GSM Mobile Communication allocation. Therefore, this should not be harmful to the system. It is worth to mention that, in the moment of the test, the OHE was not in in operation, since the locomotive used was diesel operated. Hence, this is not visible in the data gathered on site.

5.5.1 Evaluation in Environments Simulated in a RC

In Chapter 3, the emulation of Rayleigh and Rician channels with the user of multiple loading factors and antenna configuration has been mentioned. Hence, the same configuration is used for the system performance analysis. The set up

is similar: antenna position, orientation and loading levels. The VNA has been removed and substituted by the XBee modules. The payload of the Xbee was set to the maximum per packet, which is 256 bytes. This amount does not limit the size of the message. However, it should be considered that two or more packets are used to represent such message.

Firstly, the throughput was assessed in a unloaded RC with two antennas pointing towards each other.

Table 5.6: Average throughput achieved in a unloaded RC.

Transmission power	Frequency (MHz)	k-factor	Throughput
2mW	863.15 to 868.95	≈ 3.26	14.35 kbps
2mW	868.95	4	19.76 kbps
25mW	863.15 to 868.95	≈ 3.26	14.20 kbps
25mW	868.95	4	19.52 kbps

Having the same K-factor produced by the 10 absorbers previously mentioned, a XBee link was tested in two modes: the frequency channel switching on and a selected frequency to transmit on. The higher number of absorbers, will reduce the contribution of the multipath generated by the stirrer. The throughput achieved is shown in Table 5.7.

Table 5.7: Average throughput achieved in a loaded RC with different k-factor

Transmission power	Frequency (MHz)	k-factor	Throughput
2mW	863.15 to 868.95	≈ 22.24	15.27 kbps
2mW	868.95	30.19	17.94 kbps
25mW	863.15 to 868.95	≈ 22.24	16.42 kbps
25mW	868.95	30.19	17.87 kbps

The results show that a slightly greater throughput value was reached using only one frequency channel rather than the 30 available channels for transmission, even with a lower value of K-factor. This is due to the communication overhead. Having the ability to switch channels implies a trade off in time. This means that every switch done implies a synchronization and paring time. On the other hand, setting only one channel to communicate, reduces every synchronization time to

just one. However, limiting the link to only one frequency, i.e. turning off the rest of the channels, makes the network susceptible to be easily corrupted, disregarding the advantage of using other channels to maintain communication. According to measurements collected in [67] K-factor values similar to the obtained and shown in Figure 5.6 correspond to a indoor office, and the values shown in 5.7 correspond to a urban indoor-to-outdoor environment for values close to $K = 22$ and a rural area with low building density for values close to $K = 30$.

5.5.2 Co-existence with other signals

One of the possible failures of any communication system is due to deliberate interference generated with the purpose of interrupting a given service. Following this, the RC mentioned before was used to investigate the XBee module's performance when a certain number of channels are interfered by a signal generated and fed into the RC. The stirrer was set for 50 positions per rotation, i.e. 7.2° per step.

Based on the data provided in 5.2, a FM signal was produced in order to interfere with a part of the channels available for transmission. Initially, the first 15 channels (50% of the total) were selected as target. The FM signal produced was centred in 864.65 MHz with a span of 1 MHz and 20dBm amplitude to ensure that any connection attempt in this range is blocked. The signal produced is monitored by a spectrum analyser, where the occupancy was from 863 to 866.17 MHz as shown in Figure 5.16, slightly more than 50% of the available communication channels. This would limit the XBee module range of freedom to switch frequency.

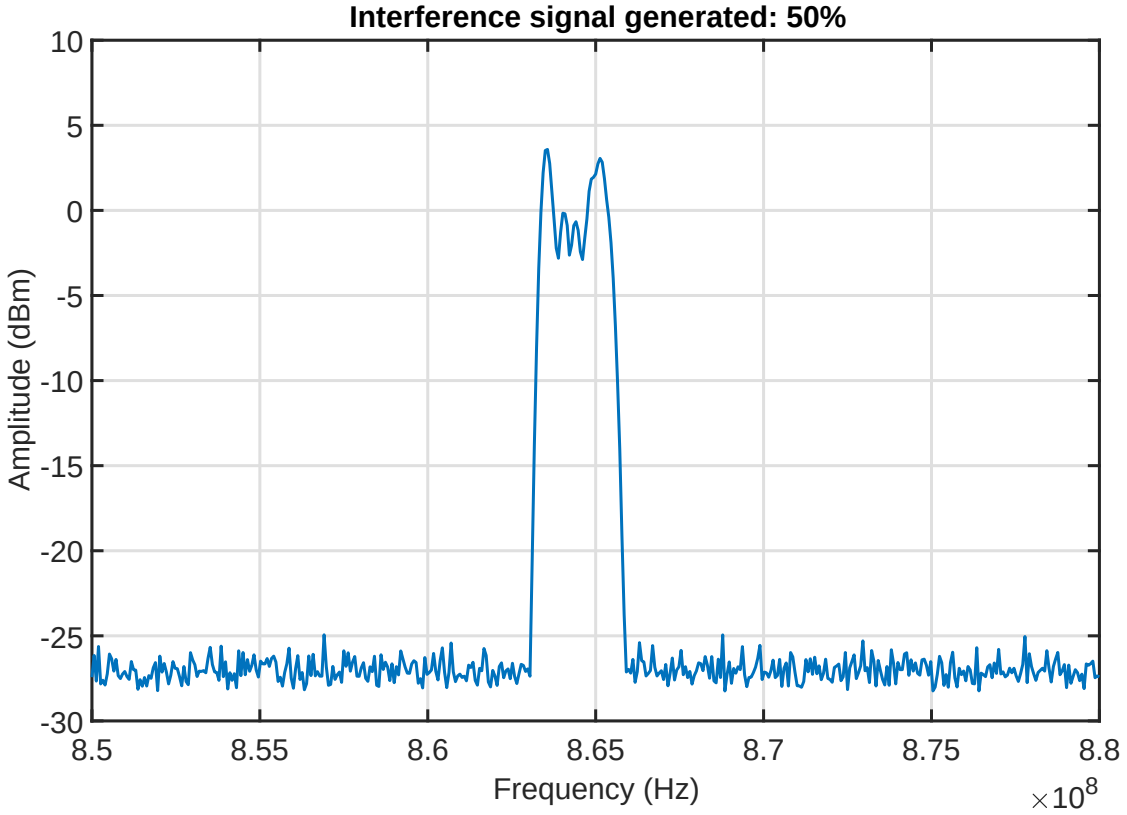


Figure 5.16: Interference generated. Half of XBee bandwidth, equivalent to 50% of the XBee channels dedicated to transmit on.

Subsequently, the occupancy was increased to interfere with more than 75% of the channels, achieved by setting the signal generator in a FM modulation centred in 865.95 MHz with a span of 2MHz and 20dBm, covering approximately from 863 to 867.55 MHz, as shown in Figure 5.17.

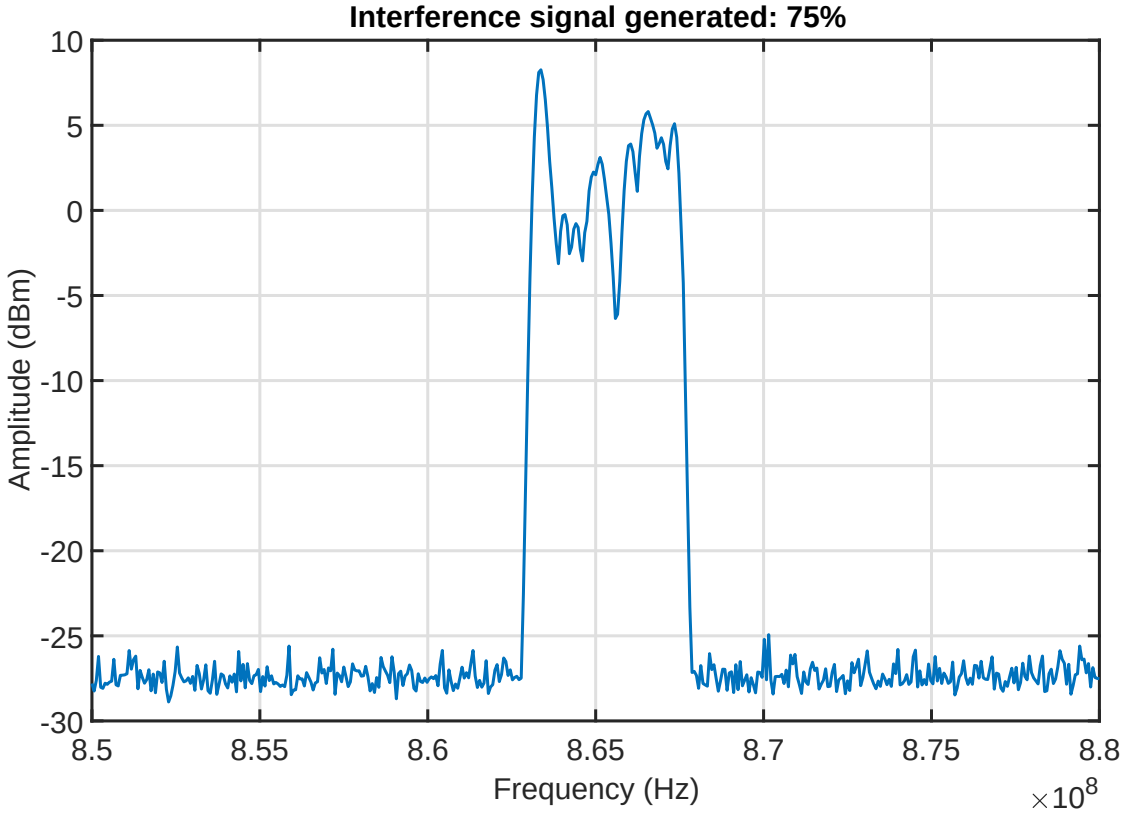


Figure 5.17: Interference generated. Three quarters of XBee bandwidth, equivalent to 75% of the XBee channels dedicated to transmit on.

LBT+AFA mode

As mentioned before, XBee modules have the ability of sensing and therefore switching channels in function of its availability. If the monitored channel is occupied, another will be selected according to a predefined sequence.

When the produced interference signal ins in operation, the XBee modules is sensing the channels until at least two are available for transmission. As it was foreseen, only a fraction of the channels are being used by the generated signal. Hence, the remaining ones are used for transmission if still meet the RSSI levels required.

Figure 5.18 illustrates some of the frequency changes the Tx perform to transmit and the channel occupancy by the jamming signal.

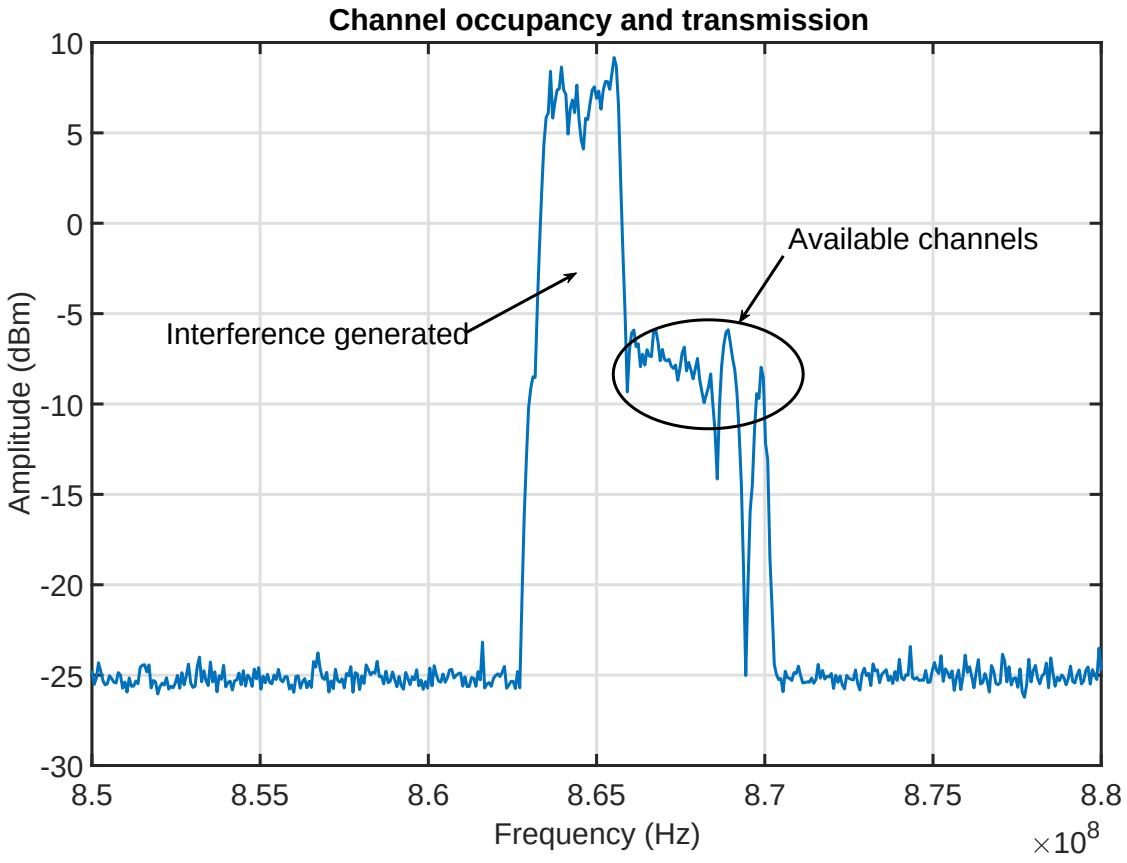


Figure 5.18: Spectrum occupancy by the inference signal generated, aiming to block 50% of the available XBee channels to transmit

The addition of a jamming signal caused a decrease in channel capacity. Nevertheless, the decrease was not substantial and the the total of the transmitted packets were successfully received without errors. This demonstrates the ability of the modules to take advantage of the AFA.

On the other hand, when increasing the interference occupancy, the level of freedom for the AFA is reduced, and it has access to fewer channels. Therefore, the XBee is sensing all the channels according to its protocol, but during this period, a reduced portion is unused and ready for transmission.

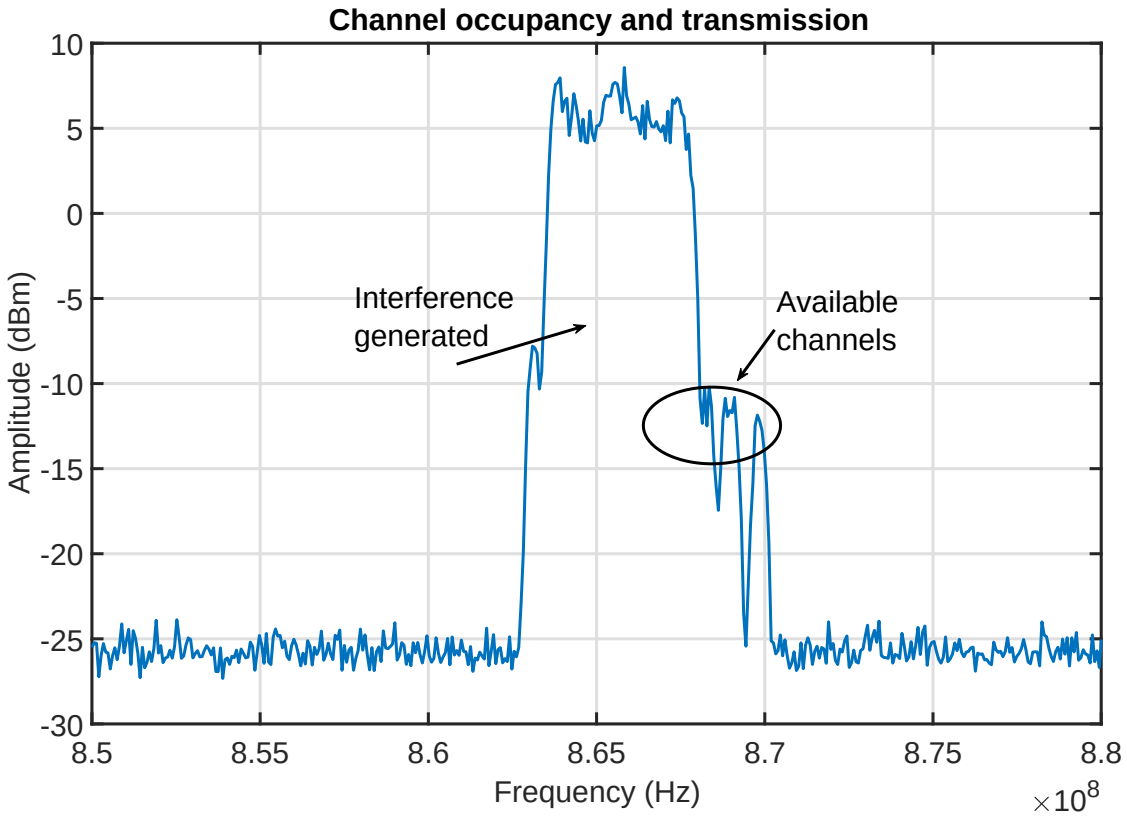


Figure 5.19: Spectrum occupancy by the inference signal generated, aiming to block 75% of the available XBee channels to transmit

On this occasion and under these conditions, the capacity decreased drastically and the transmission errors increased. However, this behaviour was expected to happen. Mainly, because of the interference power. XBee modules are designed to transmit at an specific power and has no power management to deal with stronger signals. Additionally, the modulation scheme is fixed, given the trade off due to the low complexity of the RF radios.

Finally, independent readings were taken throughout the total rotation of the stirrer and averaged. The different stirrer positions modify the internal geometry of the chamber. Hence, the mode distribution changes as well.

Interestingly, even when certain channels are selected with the channel mask mode activated, the devices still requires some other outside the selected band-

width for synchronisation and message acknowledgement.

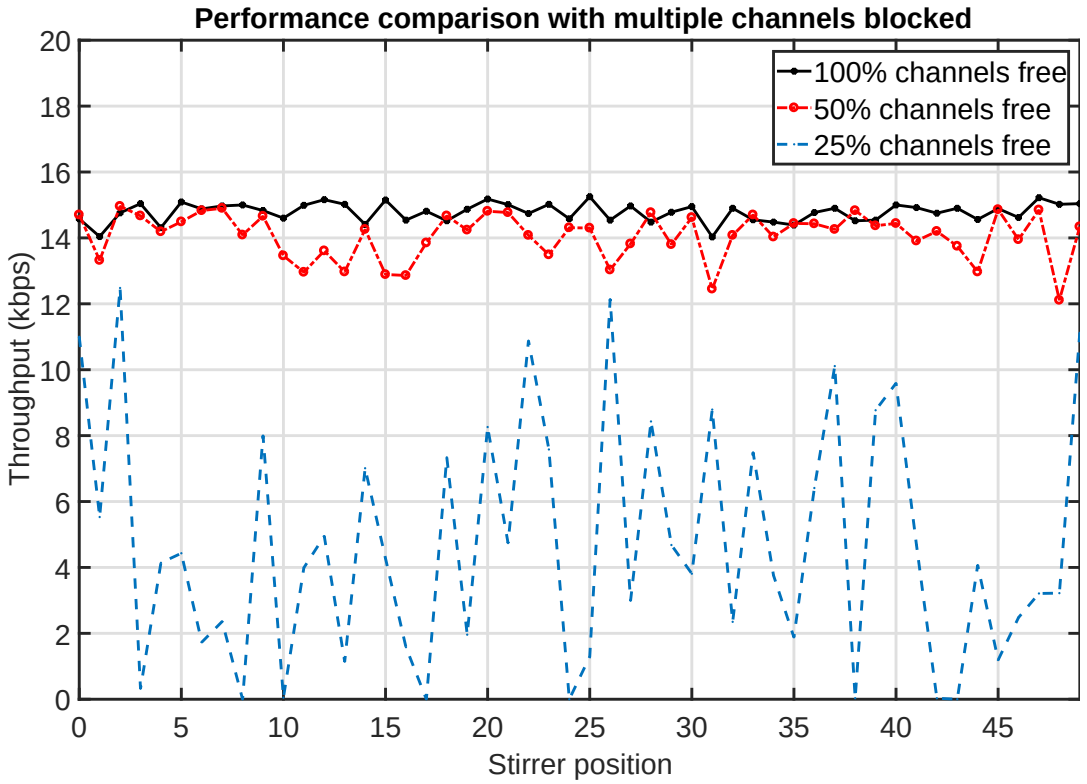


Figure 5.20: Throughput reached by XBee at specific stirrer positions in one rotation with 30 channels (black line), 15 channels (red line) and 8 channels (blue line) available for communication

The experiment consisted in 50 stirrer positions per rotation and in 1000 messages.

Due to the wave propagation change in the RC caused by internal geometry modification when the stirrer is in operation, different modes are excited depending on its current position. When there is not intentional blocking or jamming, the total 30 channels for the XBee operation are available, denoted with the black line in Figure 5.20. Thus, the system uses all the channels and switch among them to transmit freely and under this conditions, the maximum throughput could be reached. When 50% of the channels are jammed, the same selection strategy is sensing the medium to find the available frequency slots to transmit, resulting in a slight decrease in throughput noticeable, as seen in the red line in Figure 5.20. On

the other hand, limiting this freedom to only a fraction of the channels, it begins to cause throughput decay across the rotations. This behaviour is presented in the Figure 5.20 by the blue dotted line. The justification of this is that the XBee follows a random channel selection to perform transmission, but firstly it has to sense the medium to verify availability. Randomly selecting a channel to monitor it, can lead selecting a jammed one. Consequently, it has to select a different one until it finds one free. Hence, this consumes times and compromises transmission overall.

Table 5.8: Throughput and success rate measured in the RC

Channels targeted	Average Throughput	Success rate
0	14.7814 kbps	100%
15	14.0670 kbps	98%
24	4.7254 kbps	56%

5.5.3 Spark Generator

As mentioned before, a spark generator has been used to asses the system performance when a ESD occurs. Moreover, it is used to simulate the effects of a spark generated when the train OHL separates momentary from the power lines. Thus, two aspects of configurations have been considered. The use of the vertical conductive plane (VCP) facilitates the recreation of the RF or emission effects of a ESD to a piece of equipment, which in this case is a communication system. Firstly, to analyse the emissions caused by the spark, a Rx antenna was situated close to the VHP to measure its emissions. The resultant occupancy is shown in Figure 5.21. As it can be seen, the spark generates narrow band signal peaks across the frequency monitored. The ESD gun was set to trigger 10 10kV sparks per second (10Hz).

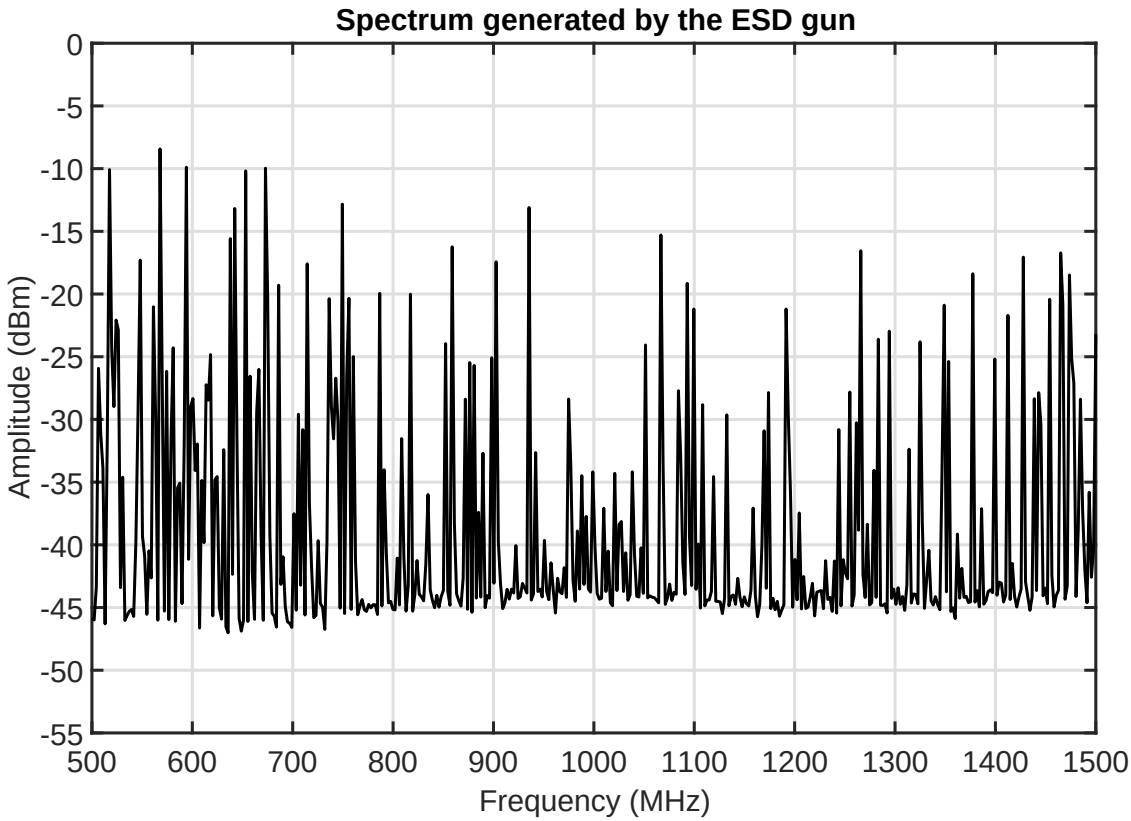


Figure 5.21: Emissions generated by the ESD gun in the RC.

Observing the 863-870 MHz range, the occupancy is still considerably high, as shown in Figure 5.22. The run time for this test was 20 minutes with the stirrer in operation.

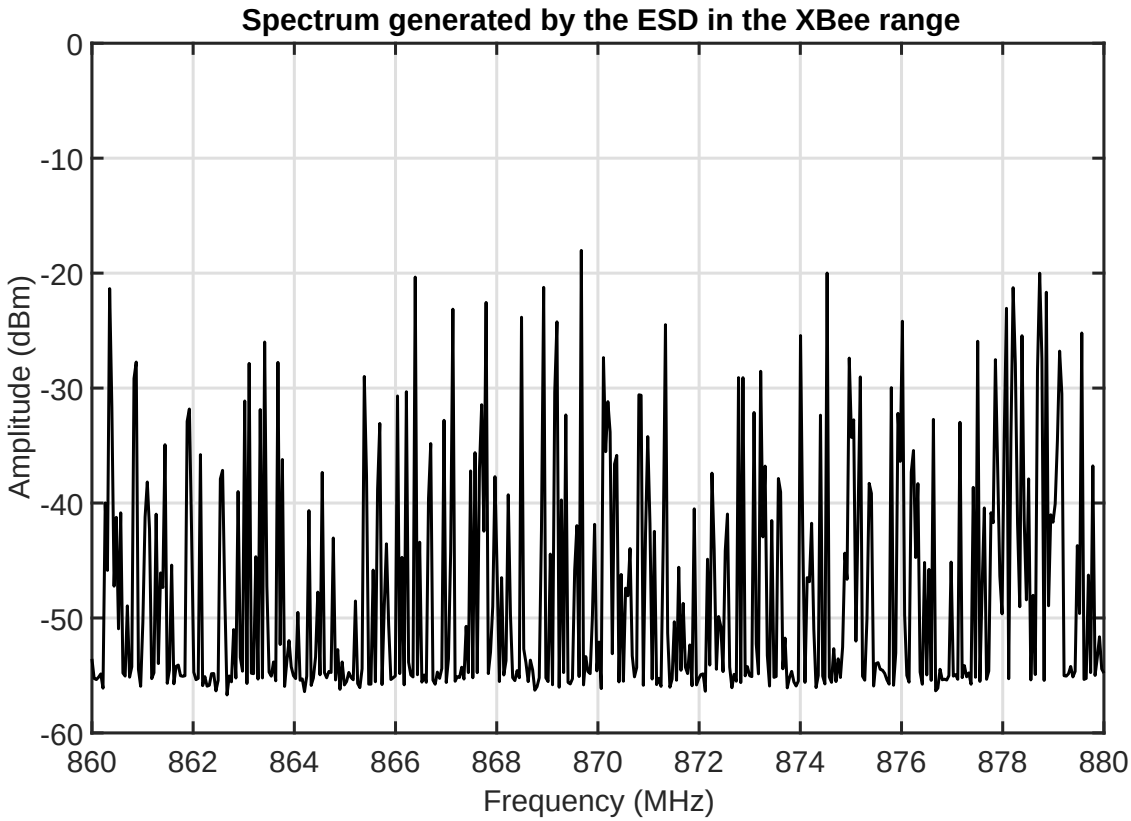


Figure 5.22: Emissions caused by the ESD gun in the RC centred in the XBee bands.

Subsequently, both Tx and Rx were placed in the vicinity of the VCP, and verify if the field generated alters or has a negative impact on the throughput.

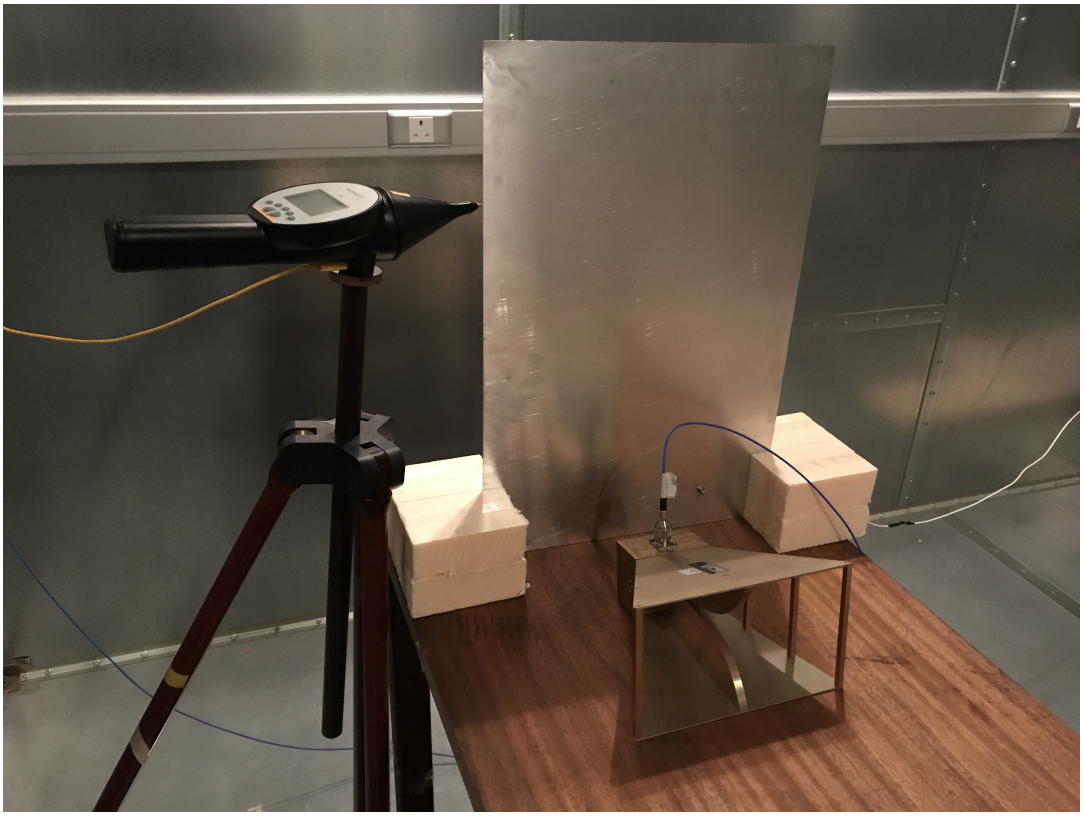


Figure 5.23: ESD test set-up in RC for immunity testing

The XBee transmission power levels are greater and exceeds the produced by the spark generator, even using its lower transmission power, as shown in 5.24. This make it more resilient. The generated spark's duration is no longer than 60ns. Hence, each channel is free for a longer period of time. Then, the LBT strategy registers the channel to be available and then transmit.

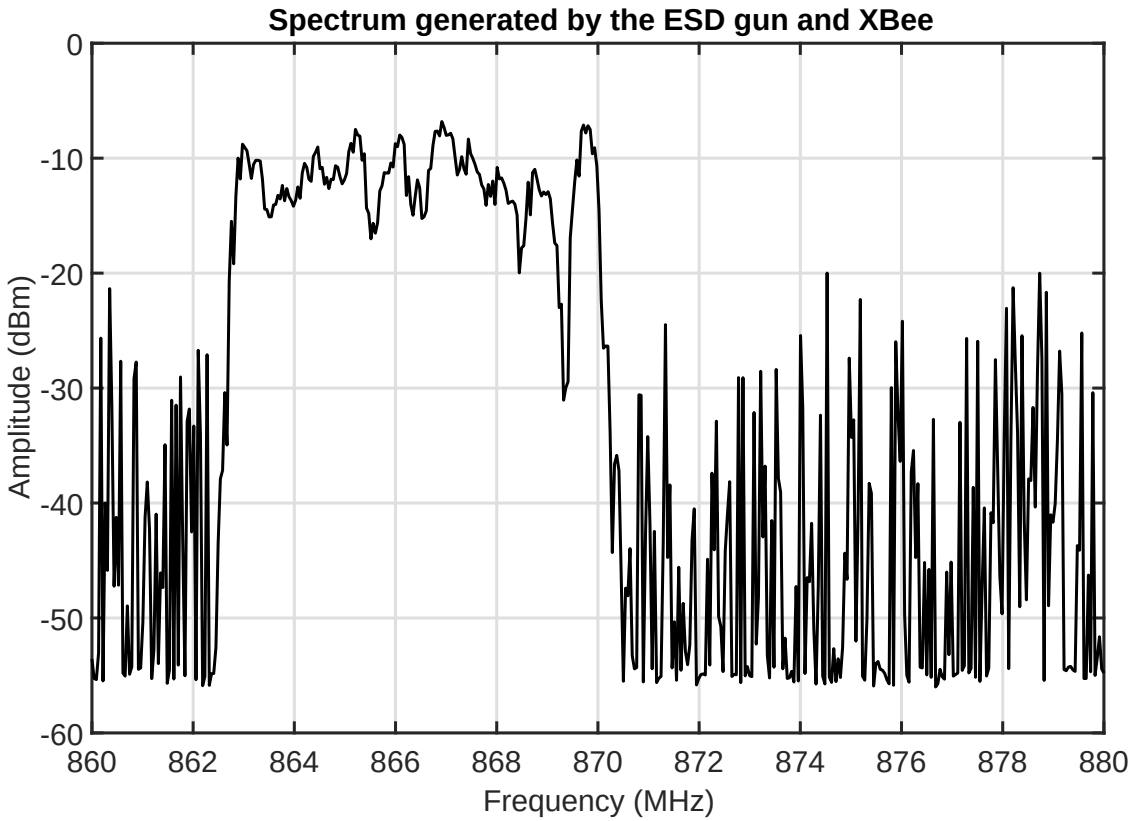


Figure 5.24: Spectrum occupancy by the ESD and the XBee radio

It was observed that the sparks do not affect the overall system performance. However, the ESD caused temporary disruptions, e.i. the communication failed temporary, as shown in Figure 5.25. This causes a decrease in throughput, to which the system recovers. The recovery time is around 5s in average. This recovery time could be considered as high and potentially dangerous for high-speed trains in the UK, as at their 201 km/h top speed, in 5s their displacement is 279m. However, these high speed trains does not rely on by power lines to function, as their engines are diesel-powered. For transports such as trams, as they can go as fast as 70 km/h [68] and the displacement in 5s will be less than 10m.

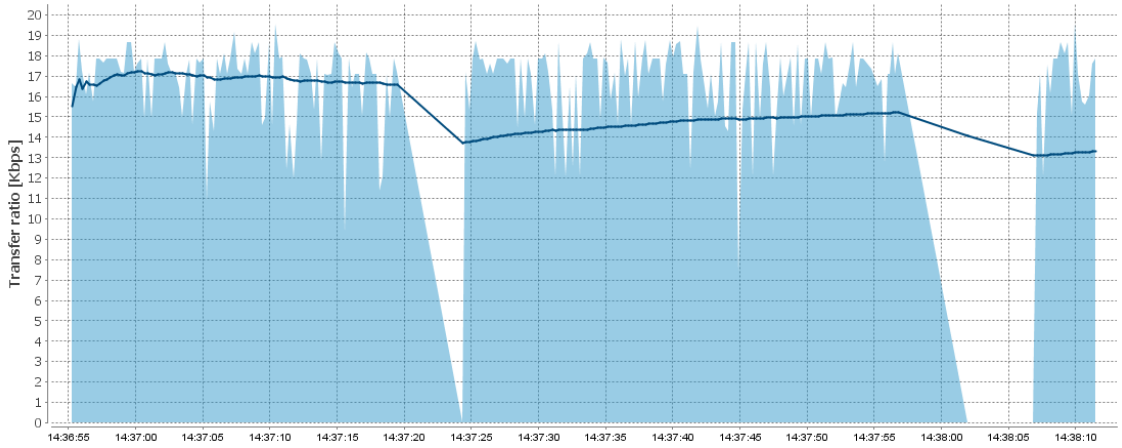


Figure 5.25: Throughput obtained whilst the spark generator is in operation.

On the other hand, the ESD also causes disruptions in the power received, as shown in Figure 5.26.

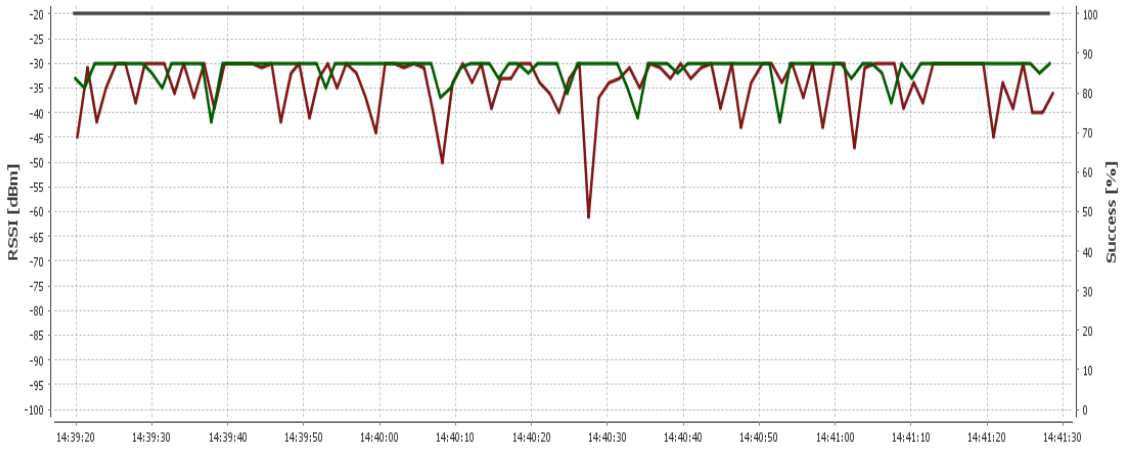


Figure 5.26: RSSI measured whilst the spark generator is in operation. Red line is the Tx and green line is Rx

The same procedure was followed to investigate the performance when the LBT+AFA is disabled. In this case, the channels are not monitored and regardless of the occupancy, the XBee will transmit on the 868.95 MHz band.

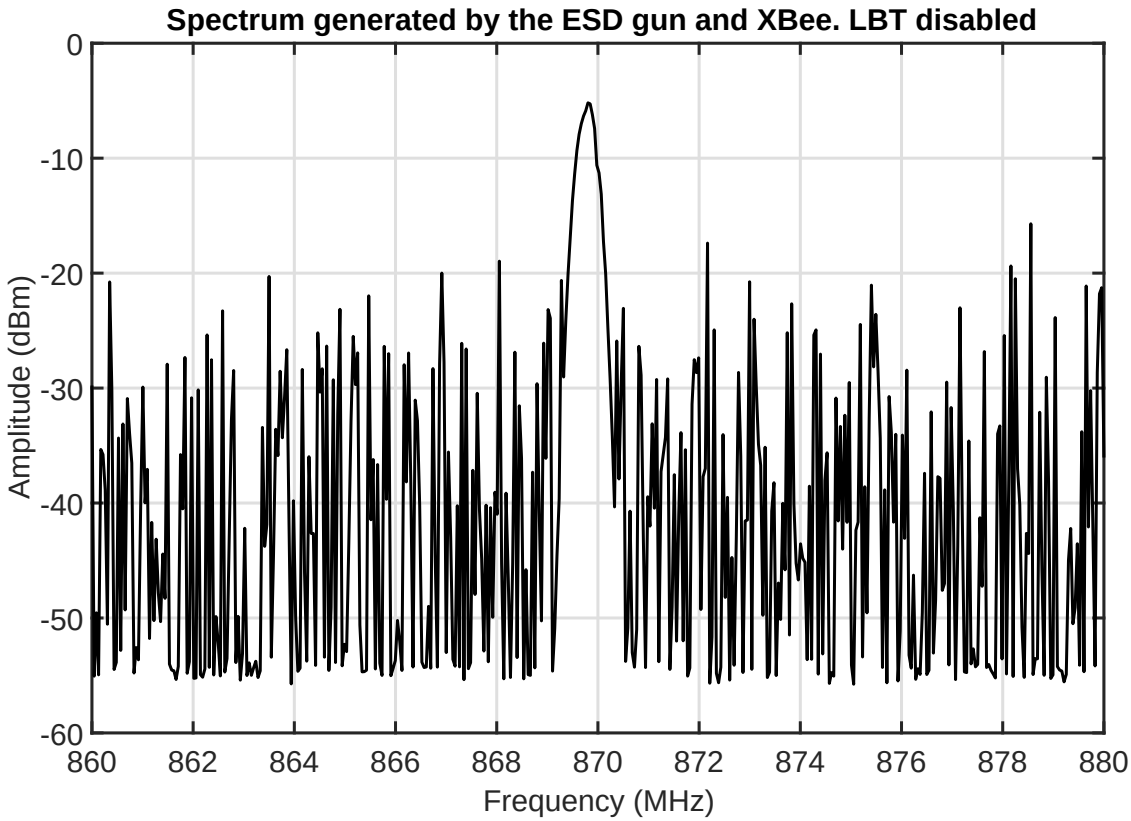


Figure 5.27: Spectrum occupancy by the ESD and the XBee radio with LBT+AFA disabled.

Stopping the LBT+AFA feature, the throughput is more stable than switching channels. As shown in Figure 5.28, the average throughput converges quicker using only one band to transmit. However, the sparks still cause disruptions. During the test a noticeable decrease in the transfer rate was identified, as low as 6 kbps. This could lead eventually to disconnection, but in this case the recovery time is shorter, around 2s.

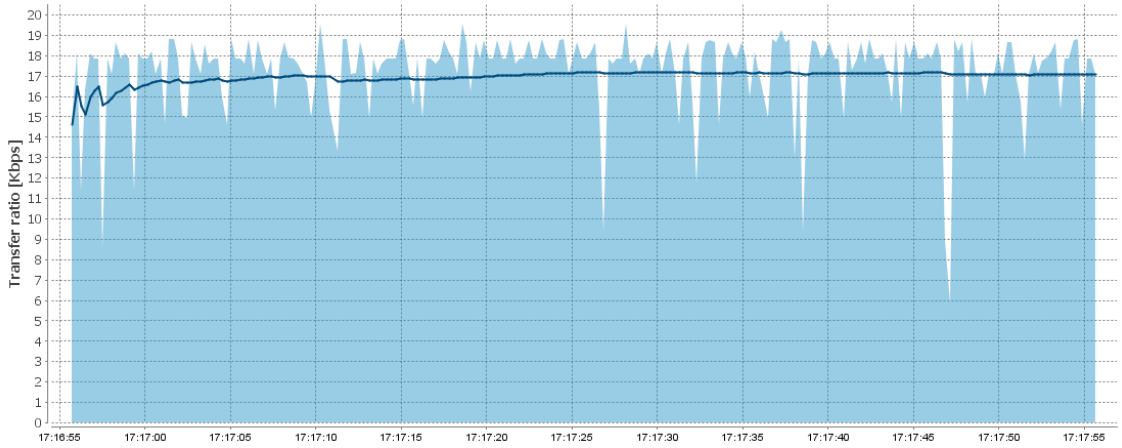


Figure 5.28: Throughput obtained whilst the spark generator is in operation.

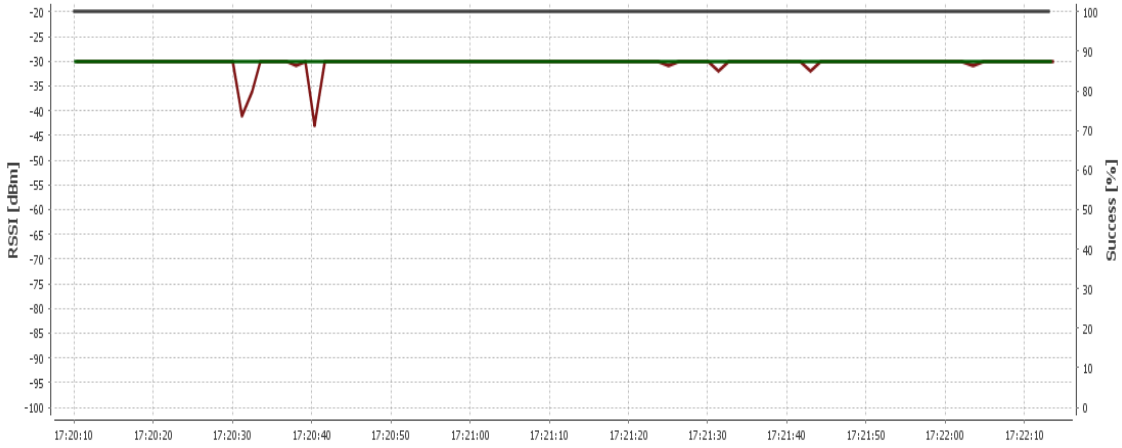


Figure 5.29: RSSI measured whilst the spark generator is in operation. Red line is the Tx and green line is Rx

Table 5.9: Throughput and success rate measured in the RC in presence of the ESD

Transmission power	Peak Throughput	Average Throughput	Success rate
2mW	19.45 kbps	13.31 kbps	100%
10mW	18.97 kbps	16.76 kbps	100%
16mW	18.77 kbps	15.19 kbps	100%
25mW	19.53 kbps	16.67 kbps	100%
25mW - LBT Off	20.48 kbps	17.08 kbps	100%

Observing Table 5.9, it can be concluded that the success rate is not compromised. Nevertheless, spontaneous disconnection exists, making the link unstable under certain occasions, produced by transient sparks. This disconnection period and recovery time should be considered in high speed trains, as it could have a considerable displacement in that period. On the other side, current high-speed trains do not rely on OHL or equipment. Usually trains or trams using OHL are low speed compared with diesel trains.

5.5.4 Additive Gaussian White Noise

The Tx and Rx were placed in the RC, which at the same time was fed with AWGN signal produced by Agilent E4438C Vector Signal Generator. The XBee modules were first set to transmit using the frequency switching strategy operating in presence of the noise signal, covering from 861 to 871 MHz. The amplitude of this signal was increased in order to observe the performance alteration of the XBee. The results are shown in Table 5.10, where the peak and average throughput values are presented.

Table 5.10: Throughput and success rate measured in the RC in presence of noise.

AWGN power	Peak Throughput	Average Throughput	Success rate
-25 dBm	0 kbps	0 kbps	0%
-30 dBm	5.5 kbps	1.01 kbps	1%
-35 dBm	10 kbps	2.82 kbps	30.1%
-40 dBm	18.5 kbps	10.37 kbps	100%

The results show that fairly small amplitude values of noise, specifically above -30 dBm inclusive, are enough to block the communication and decrease its performance. In reality, the reason for this is that the XBee is sensing every channel before transmit as part of its listen before talk strategy (LBT+AFA). As the AWGN is located in every frequency, the XBee implies that the channel is busy and in consequence it will not transmit unless, given the nature of the randomness of the noise produced, one of the channels are unoccupied and the messages are able to go through, as shown in Figure 5.30.

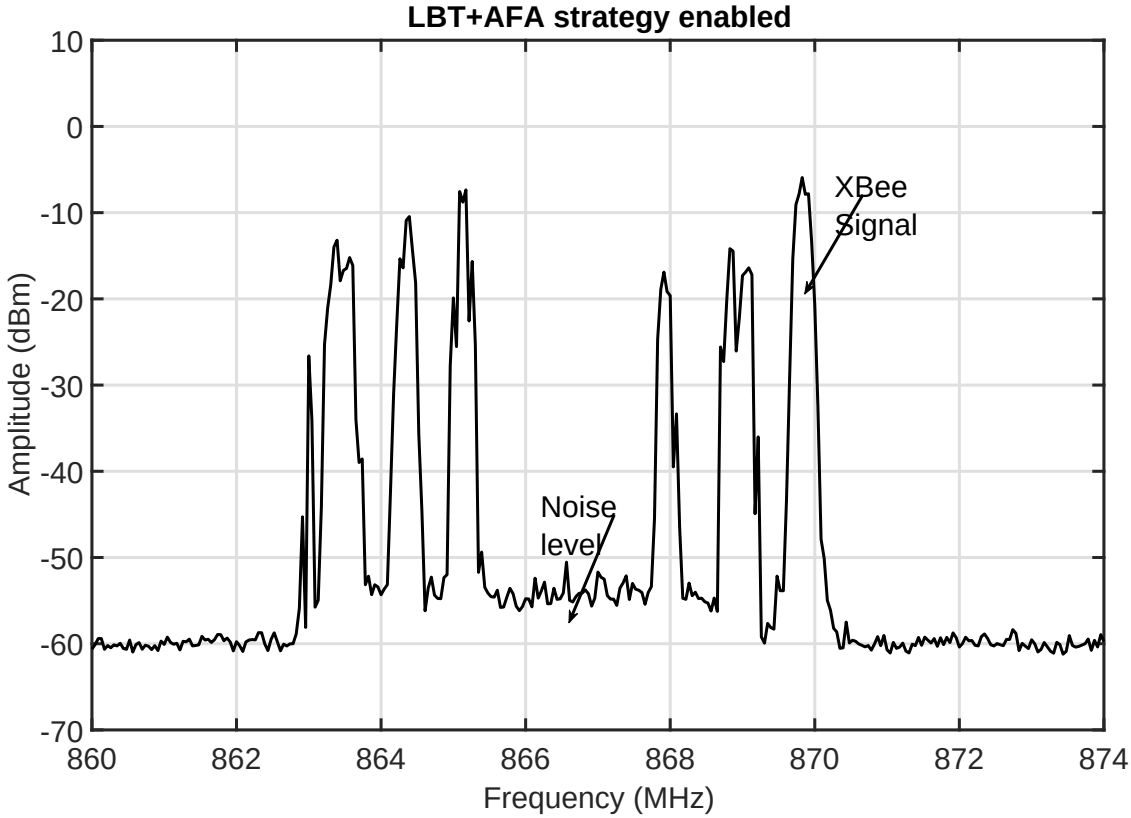


Figure 5.30: XBee signal with LBT+AFA enabled and -30dBm noise signal.

The peaks shown are the message sent when a channel was briefly available and detected by the sensing method, allowing the communication.

On the other hand, it is possible to disable the LBT+AFA method and, regarding the channel state, the message is sent. Once deactivated, it was proven that high levels of noise did not interfere with the communication link, and the messages were not disturbed, as shown in Figure 5.31. In this case, the noise level was increased to 0dBm. Even with high levels of noise, the throughput reached was above 20kbps and 100% of success rate.

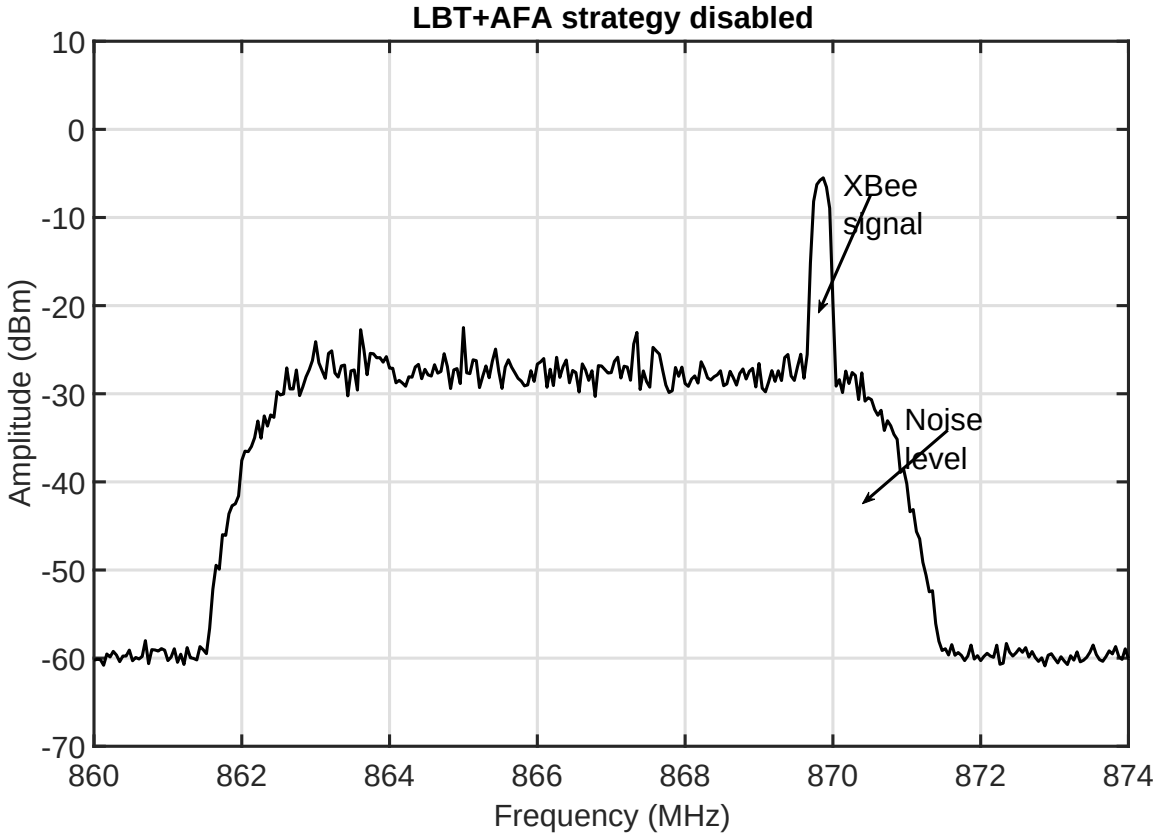


Figure 5.31: XBee signal with LBT+AFA disabled and 0 dBm noise signal

Subsequently, in order to corroborate its resilience, the noise signal power was increased to the limit produced by the signal generator, which is 20dBm, shown in Figure 5.32. The 20 kbps throughput was still persistent and stable. This demonstrates the high resilience to noise with the LBT+AFA strategy disabled.

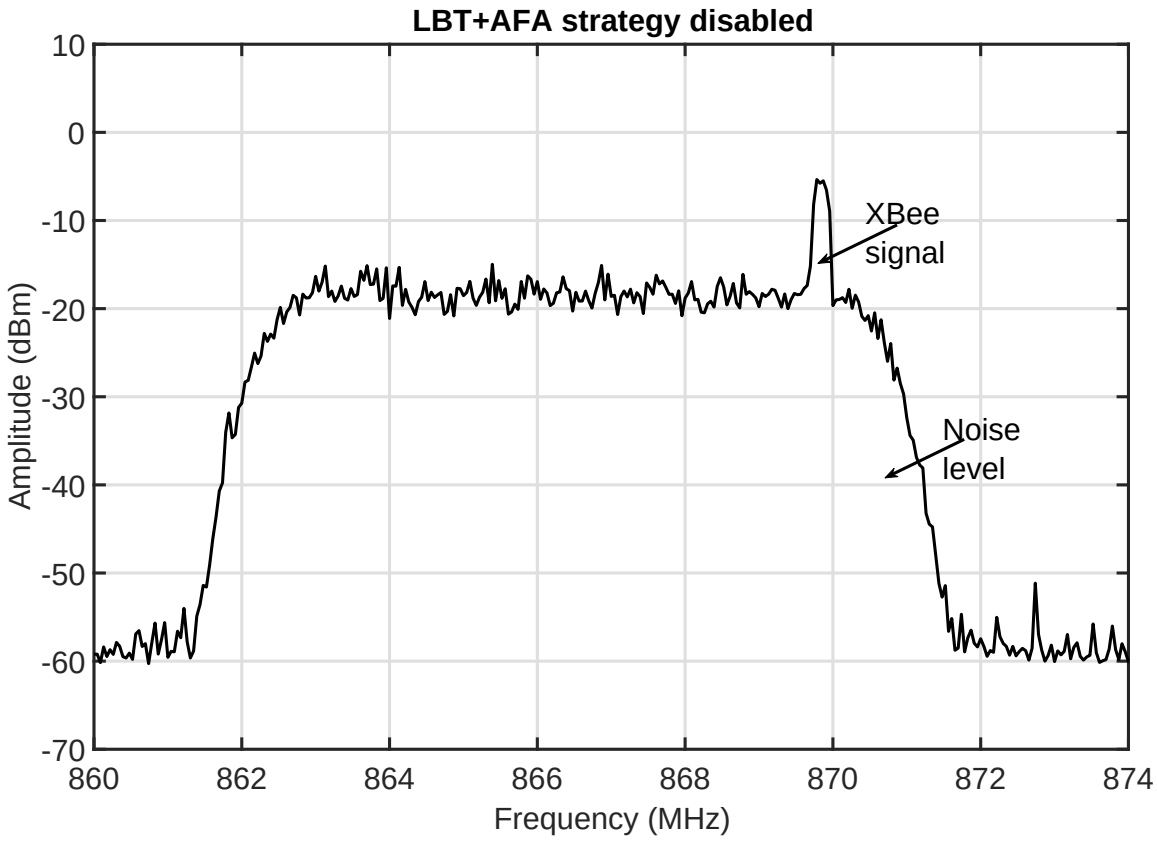


Figure 5.32: XBee signal with LBT+AFA disabled and 20 dBm noise signal

5.6 Proposed prototype

Based in all the previous assessment and along with the requirements from the industrial partner (which consisted on a commercial modular off-the-shelf, non-invasive, battery-powered and easy-to-deploy system), a final modular prototype was designed and constructed. The signalling system has three major challenges: distribute information and preserve a decent communication link able to distribute such information with minimum delay and provide estimated train position.

5.6.1 Signalling system

The final proposed and deployed prototype consist in the XBee RF radios previously mentioned connected via serial port to a Arduino processing unit, as shown in Figure 5.33. This serves the purpose of input from the user interface to the system. Additionally, it increases the processing capabilities for further applications.

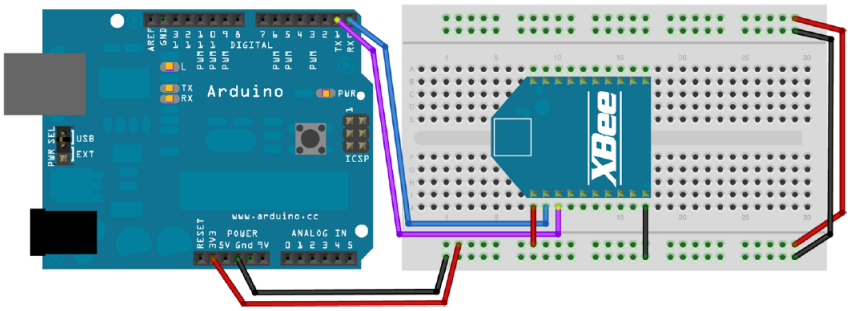


Figure 5.33: XBee and arduino interconnection.

The final prototype presented to the industrial parter is shown in Figure 5.34, where the traffic lights and a box in the back houses both Arduino, XBee and batteries are displayed.



Figure 5.34: Signalling system prototype with traffic lights.

On board the train, a screen is placed which displays the following, current and previous signal status from the signalling system. Additionally, it shows traffic conditions to assist the driver. The system is designed to be non-invasive to the already installed instruments. In general, any message can be sent throughout the network until it reaches the cabin and is read by the driver. A set of photographs captured during the test will help to visualise this on-board unit in further in this document, more specifically in Figure 5.11b.

The aim of major train system operators is to eventually remove the track-side signalling lights and leave only the on-board unit screen, moving towards a high populated sensor network where high amount of data is gathered, such as train location, speed, direction, carriage status, nowadays known as Rail Internet-of-Things. With all this information, traffic models can be designed to have a smart, more efficient and reliable transport system.

Table 5.11: Photographs taken during the rail test



(a) Thales crew on-board



(b) OU and display



(c) Metallic structures



(d) Platform and OHL



(e) Control centre



(f) Control centre set-up



(g) Train-RFID distance



(h) System powered by generator

During the test, crew from Thale-GTS was present to supervise the test and corroborate the expected outcome of a fully operational system as shown in Figure 5.11a. Furthermore, they could observe the node activity on the display of the OU, as shown in Figure 5.11b.

Part of the challenges encountered were the metallic shielding structure, represented by the stationary locomotives, as shown in Figure 5.11c. Additionally, a section with an OHL was present, as shown in Figure 5.11d.

The control centre was on a table-top configuration, where the system could be controlled and monitored remotely, as shwon in Figures 5.11e and 5.11f. On the same set-up, the RFID reader was fixed to identify the RFID tags adhered to the train and make possible the train detection, as shown in Figure 5.11g.



Figure 5.35: On-Board unit and Light Node in the background.

A more detailed view from the OU, is shown in Figure 5.35, where the node status is presented to the driver. For this test, it was necessary to use petrol power generators in order to have quick access to energy, as shown in Figure

5.11h. However, as mentioned before, the system's power requirement is low and is planned to use energy harvesting derived from solar panels.

5.6.2 Detection and Location System

Current signalling systems use GPS for train location thanks to its high accuracy. Since is a licensed technology, signalling manufacturers are exploring other methods to estimate train position with licence-free and low-power options. Led by this, two alternatives are presented as part of a self contained system.

RSSI

As mentioned before, this indicator provides a quantitative measurement of the signal at the receiver. This magnitude can be associated directly to the Tx-Rx distance. In order to find a distance-RSSI correlation, a measuring was conducted at the University of Nottingham, increasing the distance between both devices devices. A message was sent continuously to maintain communication and RSSI was monitored.

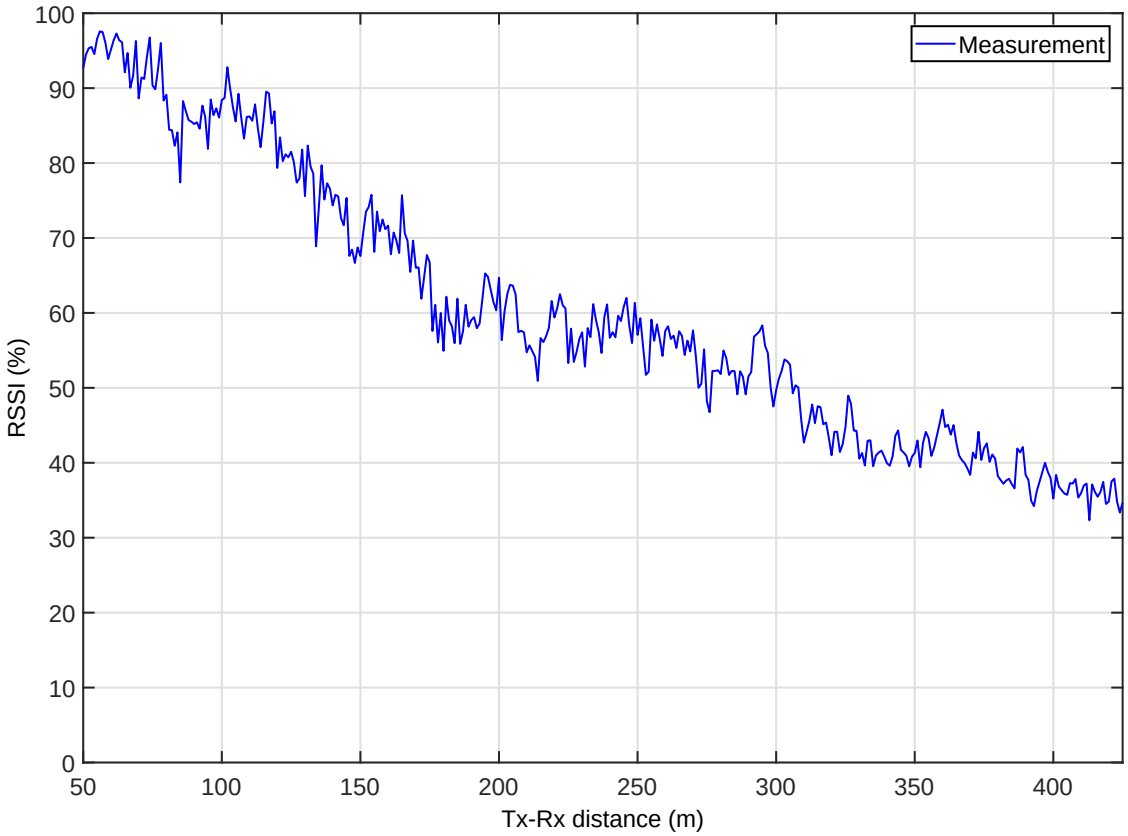


Figure 5.36: Tx-Rx RSSI measurements

The readings recorded show a loss related to the distance, as seen in Figure 5.36. Although there is a evident distance-RSSI ratio, this value could be easily affected as this is a highly changing environment, where people and moving objects were present as well as reflection from buildings. Nevertheless, this system is considered to be placed in an open-field environment, where the geometry hardly changes.

The intensity decrease follows the behaviour of a second degree equation and using Matlab, was possible to fit an approximation, as shown in Figure 5.37. With this, and the implementation of a second degree filter, the Tx-Rx distance estimation can be more accurate.

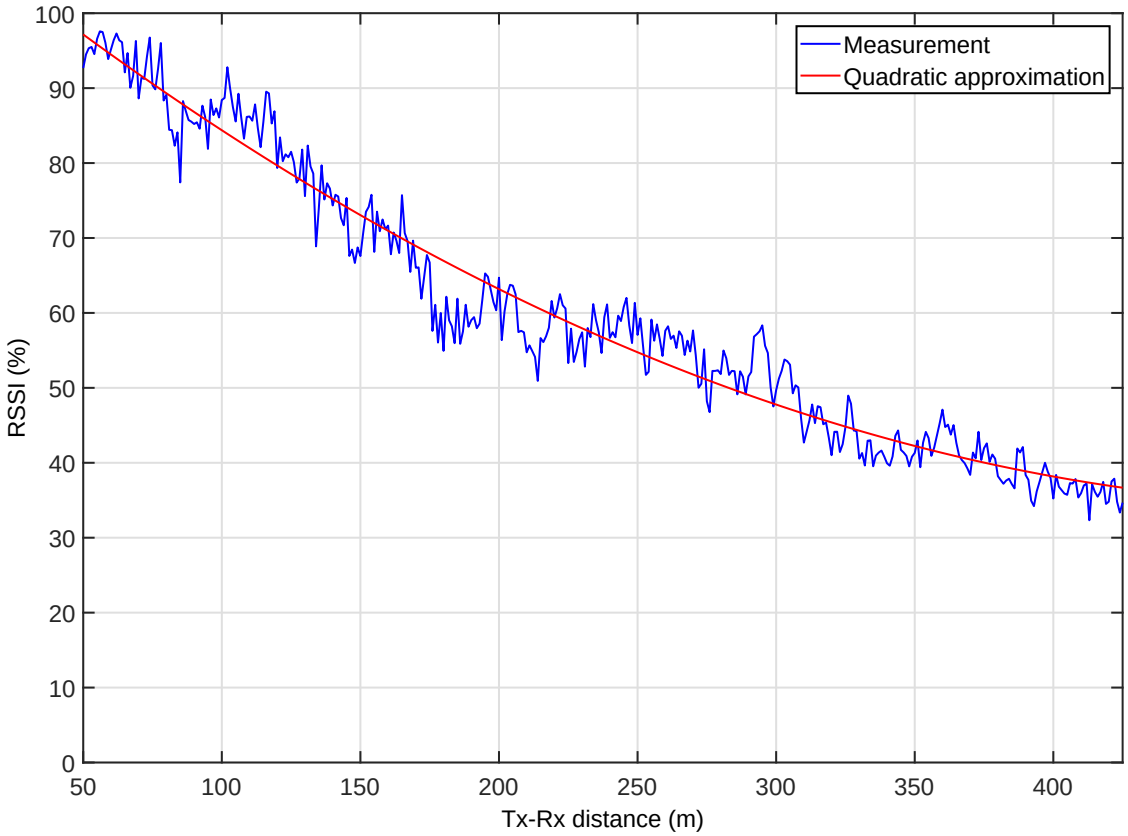


Figure 5.37: Quadratic approximation

Based on this indicator, two threshold related to RSSI are established which define detection areas. Having a previous characterisation where each threshold is associated to a linear d_1 and d_2 distances to the VN, it would be possible to identify the train's direction and position.

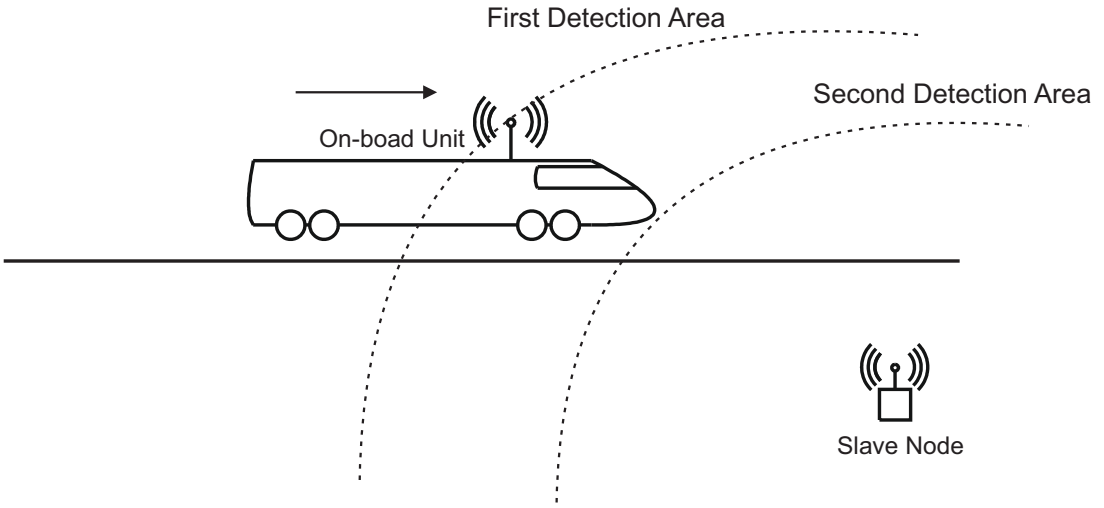


Figure 5.38: RSSI detection areas

As the train moves towards a VN, the RSSI at the VN increases as mentioned before. When the first threshold is exceeded the time t_1 is recorded. Subsequently, when the second threshold is reached, a second time t_2 is recorded as well.

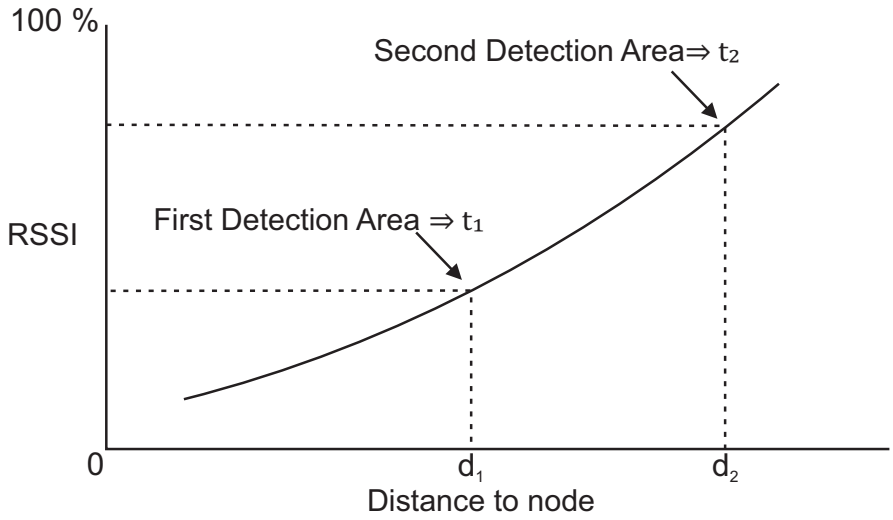


Figure 5.39: RSSI as function of the distance

Using these two constants and two variables, instantaneous speed can be calculated:

$$s = \frac{d_2 - d_1}{t_2 - t_1} \tag{5.6}$$

This speed is monitored locally at the OU and compared to the allowed in that given section to avoid over speed when approaching to a junction, crossing point or a different movement authority further in the track.

However, the RSSI denotes only the quality of the last hop that the package did and it is the summation of the loss and scattered paths. Therefore, it does not reflect the overall intensity throughout the network. Additionally, the certainty of it could be affected by elements blocking the LOS, harmful emissions near the receiver or reflection. On the other hand, considering that the distance between the train and the node is shorter that from node to node and there are the lack of elements that could block LOS between the train and track-side equipment, we can assumed that the RSSI comes from the On-board Unit.

RFID

Using RFID technology, train detection could provide an easy-to-install and non-invasive solution to incorporate to current trains and infrastructure. Passive RFID tags are attached to each of the nodes, whilst an RFID reader is on-board the train. With this configuration, only low-cost passive tags are deployed across the network.

The model utilised was the ThingMagic M6e development tool Magic, which is provided with a 6dBi antenna and a set of passive tags. This antenna has a maximum range of 9m, and allows a maximum reading rate of 750 tags/s. Features such antenna sensitivity, carrier frequency and type of tag read could be configured with the software provided.

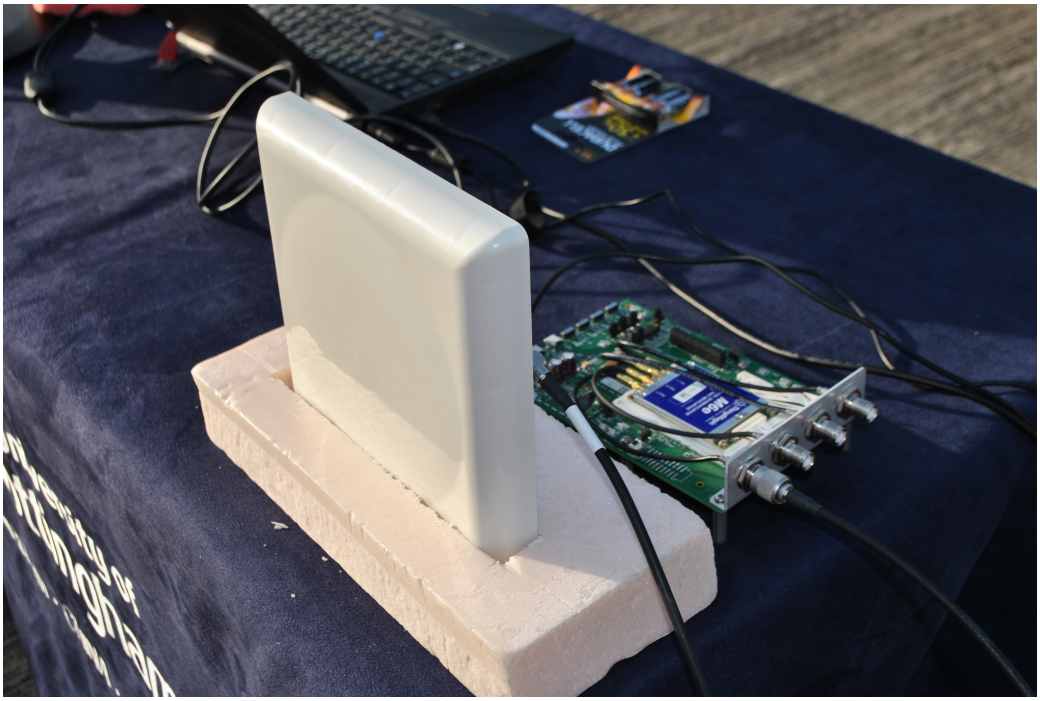


Figure 5.40: RFID antenna located at the trackside.

During the rail experiment, the performance of the tags and reader was tested. In order to facilitate the measurements, the tags were placed on the train instead: one in the front and one in the rear. The reader remained fixed next to the text track. When in operation, the reader is searching the channel to trigger the tags and receive a response. Only when the tags were in the proximity of the reader, detection was achieved. As they moved through the rail, the tags were read multiple times, proficient confidence at identifying the train. Since each tag ID is known, and then tag-to-tag distance is greater than the tag-to-reader, it is possible to know which of them passed first in front of the antenna, as a time stamp is associated to the identification. Therefore, additional information could be inferred, as direction and instantaneous speed.



Figure 5.41: One of the two RFID tags placed at the front and rear of the train

In the system proposed, this information is gathered by the OU and sent thought the network until it reaches CC to record current position of each train in a given section of the track. Unfortunately, given the nature of RFID technology, this scheme could be used as a detection technique only. Distance estimation should be conducted using an additional system.

As mentioned before, current systems such as ETCS uses eurobalises as a mean of train positioning and data transceiver which are placed in pairs (usually 3 metres apart), and follow the same principle as the method presented above: a time is associated to the detection done by the $eurobalise1$ and other time for the $eurobalise_2$. This allows to calculate speed and know train direction.

5.6.3 Train Integrity

Railway systems have to provide safety for the train itself, to the other trains and to the cargo. Train integrity systems are in charge of collecting information from

all the carriages linked to the locomotive. This is achieved by having physical connections throughout the entire train infrastructure to sense the presence of any carriage and report back in case of carriage loss. Currently, this system is considered as local as any unusual activity is reported only to the OU. However, it is important to have constant monitoring from the CC in the far end, where the traffic conditions are known and could act accordingly controlling the displacement and speed of other trains sharing the same track section.

The alternative proposed in this document is currently widely compatible with many type of sensors. Therefore, the OU could gather the information collected by this sensors and process it, and add it to the information sent to the CC constantly. This extends and allows full knowledge of the current state of each train to the system.

5.7 Conclusion

During this chapter, various testing scenarios (train detection, failure mode, SPAD, noise and interference susceptibility amongst others) and configurations (transmission power and frequency bands) were studied, presented and established, resembling realistic channel conditions and potential sources of interference that could possibly diminish the ZigBee radio's performance. The use of RC was essential to carry out the assessment, due to the EMC measurement features, where the ZigBee radios were thoroughly tested under severe EMC conditions.

Additionally, the final modular signalling system that consists on a network of smart sensors, has been presented which can be easily deployed, remotely monitored and controlled through the internet thanks to its low payload, which can be considered as part of the RIoT connectivity. This system is a potential candidate to be the backbone of a more complex wireless signalling system for traffic management, for train-ground and node-to-control centre communication. Furthermore, a detection and distance estimation method was presented that could be further explorer in future work.

Chapter 6

Conclusion

Nowadays there exists a high demand for reliable wireless technologies capable of transmitting information high bandwidth signals. These high demand implies an increase electromagnetic spectrum occupancy. Additionally, it is desired for these technologies to be low power consuming devices, which may compromise their ability to reliably process large amounts of data. During this project and throughout this thesis, the backbone for a wireless alternative for smart traffic management signalling and services system for trains has been proposed. The ZigBee protocol establishes a communication standard highly usable in vehicle-to-vehicle communications. However, since it operates in the ISM band, it shares the electromagnetic spectrum with many other devices at the same time. This could potentially diminish its capabilities, caused by unintended interference with other devices.

Alongside establishing a wireless signalling system prototype for rail track-side deployment, it has been shown how it is possible to create a range of different wireless operating conditions in the RC. The use of absorbing material and antenna configurations allowed for the control of wireless propagation channel inside the RC and the processes have been developed to control the measurement scenarios. Thus establishing a laboratory testing scheme for the proposed wireless IoT control system.

The multiple measurements show that ZigBee technology used in the XBee RF radio modules are resilient devices able to communicate even in presence of high power sources of interference, due to the DSSS modulation used. In addition, the use of its capability of switching frequency provides a higher degree of freedom, allowing it to switch across many channels to avoid the use of just one for transmission and reception. Moreover, when using one specific frequency to transmit, it proved to disregard high noise levels.

The power consumption is an important factor to consider for this system proposed, since it contemplates the total or at least partial removal of the wired infrastructure, including the power delivery. Since the literature review previous to the prototype design, ZigBee technology was contemplated because of its stated low power consumption. During the experimentation process, it was observed that in fact the power required for its operation is considerably low, even when it is taken to its maximum load.

6.1 Realistic Wireless Environments

Throughout the system assessment, various scenarios and channel conditions were addressed, studied and replicated in the RC. Although this assessment provides a confident prediction of the possible prototype behaviour, still there are many considerations to be done in order to observe the full potential of this system.

First, the test track accessed for the real-life test has several limitations. The speed top train speed is limited to 40mph due to security concerns, as the track length is limited and consists in a closed loop. Having a higher speed transport will allow to make more precise conclusions about the system's performance in a realistic operational use. Additionally, even when there was presence of stationary locomotive infrastructure, moving trains must be introduced to the scenario. This is to test communication with two or more moving trains. Taking all the metal from the immobile trains to a second plane, the facility was a clear space without trees, crossing levels, train stations, that could potentially modify, the system performance. Lately, there has been a proposal by Thales-GTS to access another

test facility located in Tuxford, England, which includes a linear 10-mile track section for testing, and it includes crossing levels, power stations and communication infrastructure.

With the use of the RC, various scenarios were created that could be potentially faced by the system when it is deployed for continuous operation. This provided a prediction of its behaviour under harsh conditions, specifically when the system is being targeted by signals with the purpose of failure. Changing the internal configuration of the RC can vary significantly the system performance.

Using the ESD gun it was possible to observe the erratic behaviour in short period of times caused by the transient disruptions present due to the use of OHL. The XBee system maintained a constant link overall and, thanks to the error correction techniques, the transmission errors were minimum. However, it will be interesting to study the actual bit errors caused by the pulses generated by the ESD. For this, a time domain analysis will be useful. The waveform produced by the spark should be characterise and analyse its effects on each of the frames sent throughout the XBee network.

6.2 Future research

Due to the fact that signalling systems are fundamental for traffic management, constant communication is of paramount importance. Moving from the current wired scheme to the wireless makes the system smarter, modular and effortless to deploy. Without this signalling, trains cannot operate until the system is re-established. Furthermore, if the system loses connectivity, it could be potentially dangerous for itself and the other trains sharing the same track.

One of the most concerning challenges is to find the optimal distance from node-to-node, in which the coverage area maintains a confident level of communication. Currently, there is not bandwidth or power level ZigBee technology for signalling system applications. However, a balance must be found between distance and power levels, that ultimately will lead to low error rate.

On the other hand, distance is not the only limitation. In case the node N fails, the previous $(N-1)$ and the following $(N+1)$ node must still be able to talk to each other. In a worse scenario, multiple consecutive noise could fail, leaving an entire section unusuable, as shown in Figure 6.1.

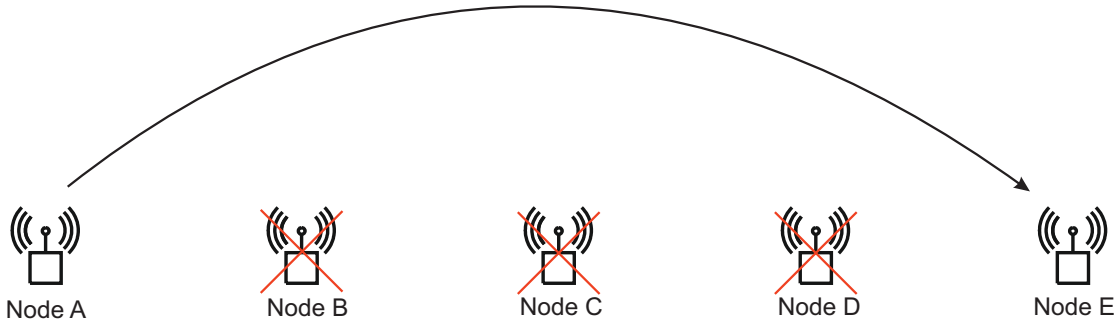


Figure 6.1: Redundancy action

Finding a coherent distance between them will provide the system with redundancy, allowing the system to accept a level of confidence enough to transmit the traffic and train conditions through the network. On the other hand, the option of increasing the coverage area of certain nodes must be explored. Using high gain antennas for reception is considered, as the transmission power should be used as established by the standards of ISM. Since the goal of the project is to provide a reliable communication system, this is not possible to install in all the nodes of the network. Therefore, a further survey of different track section scenarios must be conducted, to analyse the possible geographical locations were nodes could become unavailable by intentional or unintentional factors. Additionally to this, the RF propagation in tunnels has not been addressed yet. Tunnels are challenging for communication and location services as them block signals totally or partially. Since this system has been designed to transmit effective in a plane parallel to ground, signal propagation must be investigated as well as another scenario. Using measurements such as S_{21} could provide the propagation profile which can be recreated in the RC for laboratory tests.

6.3 Security

Throughout this project, it has been proven that ZigBee is a reliable technology that could be used to move signalling systems from a wired to wireless scheme. The lack of physical connection for data and power delivery reduces significantly the installation, maintenance and operation costs. However, any infrastructure is susceptible to intended attacks targeting its integrity to make it fail. As mentioned before, theft is a major concert to the rail industry due to the economic losses implicated.

On the other hand, any wireless device could be targeted by malicious software that could monitor the activity of the network and, furthermore fake identity and intercept the packages. In a more serious scenario, the attacker could replace the the traffic with not genuine information, causing dangerous disruptions to the whole traffic management system. Currently XBee radio modules offer 128-bit Advanced Encryption Standard (AES) encryption that does not compromise its performance. Practical susceptibility attacks to ZigBee integrity are conducted in [69], using techniques to intercept ZigBee traffic and countermeasures to resist the attacks. Similar tests must be conducted using the signalling system proposed to observe its resilience to the same type of attacks.

Appendix A

LabVIEW Interface

The Control centre is formed by the coordinator and the user interface. The interface has been developed in LabVIEW. It is able to control the lights in each node separately. Once the lights to be on or off are selected (red, amber, green or a combination), the number of the module where the information is desired to be sent is set as well, and the button "Send" must be pressed, as shown in Figure A.1. The nodes will maintain that state until a new instruction is established.

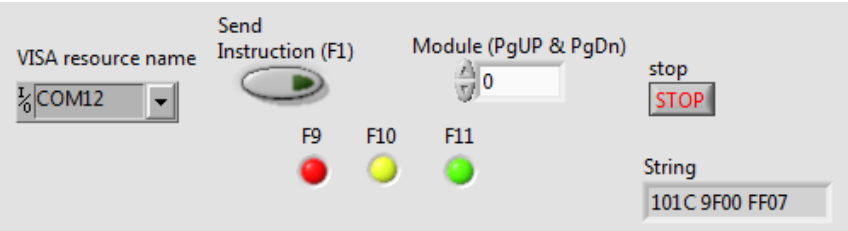


Figure A.1: Control Centre Interface

As an example, in Figure A.2 can be seen the interface that could be displayed to the driver on the train. It will give information regarding the traffic conditions ahead on the railway. The set includes the colours as follows:

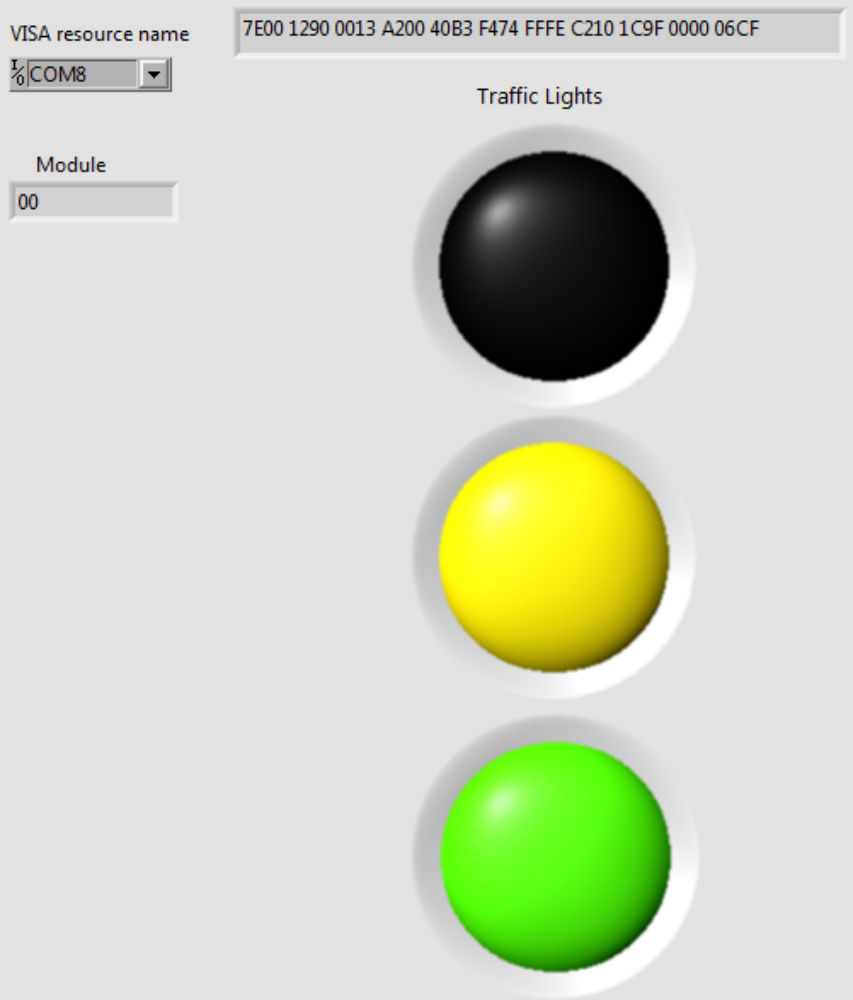


Figure A.2: On-board Unit Interface

If any other colour is needed according to the railway signalling system or Thales requirements, both interfaces and the code for the Arduino must be changed. Nonetheless, it will require minor modification and could be done on its location without taking the subsystem apart.

Bibliography

[1] J. Carr. *The Technician's EMI Handbook: Clues and Solutions*. Elsevier Science, 2000.

[2] David Weston. *Electromagnetic Compatibility: Principles and Applications, Revised and Expanded*. CRC Press, 2001.

[3] Baharak Mohajer Iravani. *Electromagnetic interference reduction using electromagnetic bandgap structures in packages, enclosures, cavities, and antennas*. University of Maryland, College Park, 2007.

[4] muRata. Emi supression filters. URL `https://www.murata.com/~/media/webrenewal/products/emc/emifil/knowhow/26to30.ashx`.

[5] Dr. Daniel Månsson Adj. Prof. Mats Bäckström Prof. Rajeev Thottappillil, Siti Jainal. Emc of railways - pantograph arcing, 2011. URL `https://www.kth.se/eme/research/topics/emc/research-projects/emc-of-railways-pantograph-arcing-1.47295`.

[6] Clayton R Paul. *Introduction to electromagnetic compatibility*, volume 184. John Wiley & Sons, 2006.

[7] Ohyun Jo, Yong-Kyu Kim, and Juyeop Kim. Internet of things for smart railway: Feasibility and applications. *IEEE Internet of Things Journal*, 5(2): 482–490, 2018.

[8] S.J. Prince. Uon emc working group - nottingham express transit: Phase 2, alstom sa, 2013.

[9] element. En 50121 railway emc standards. URL https://www.element.com/more-sectors/en-50121-railway-emc-standards.

[10] InCompliance. Emc and railway safety, 2010. URL https://incompliancemag.com/article/emc-and-railway-safety/.

[11] Stanton Lui. Railway standards en 50121, 2007. URL http://www.ee.cityu.edu.hk/~emc/EN%2050121%20Railway%20Standard.pdf.

[12] The British Standards Institution. *BS EN 50121-1:2017: Railway applications — Electromagnetic compatibility*. 2017.

[13] The British Standards Institution. *BS EN 50121-4:2016: Emission and immunity of the signalling and telecommunications apparatus*. 2016.

[14] The British Standards Institution. *Electromagnetic Compatibility (EMC) — Part 6-4: Generic standards — Emission standard for industrial environments*. 2007.

[15] Hasnain Abdullah, Juliana Md Sharif, Mohd Nasir Taib, Rusnani Ariffin, Nurul Iza Muhammad, Rohaiza Baharudin, Asmalia Zanal, Ida Rahayu Mohamed Noordin, Noorhayati Mohamad Noor, Azizah Ahmad, et al. Performance study of preliminary mini anechoic chamber fitted with coconut shell coated absorbers. In *Control System, Computing and Engineering (ICCSCE), 2013 IEEE International Conference on*, pages 602–607. IEEE, 2013.

[16] Glen Dash and LLC Ampyx. How rf anechoic chambers work. *glendash. com*, 2005.

[17] A. Goldman. *Handbook of Modern Ferromagnetic Materials*. Kluwer International Series in. Springer US, 1999. ISBN 9780412146619. URL https://books.google.co.uk/books?id=cYaQAOCuygcC.

[18] F Che Seman, R Cahill, VF Fusco, and G Goussetis. Design of a salisbury screen absorber using frequency selective surfaces to improve bandwidth and angular stability performance. *IET microwaves, antennas & propagation*, 5 (2):149–156, 2011.

[19] Y.P. Lee, J.Y. Rhee, Y.J. Yoo, and K.W. Kim. *Metamaterials for Perfect Absorption*. Springer Series in Materials Science. Springer Singapore, 2016. ISBN 9789811001055. URL https://books.google.co.uk/books?id=JgJTCwAAQBAJ.

[20] Martin D Judd and Owen Farish. A pulsed gtem system for uhf sensor calibration. *IEEE Transactions on Instrumentation and Measurement*, 47(4): 875–880, 1998.

[21] Kresimir Malaric. Electromagnetic-compatibility analysis using tem cells, 2001. URL https://www.eetimes.com/document.asp?doc_id=1255099.

[22] Siepel.

[23] Frank Leferink. High intensity electromagnetic field generation using a transportable reverberation chamber. 2008.

[24] Xiaoming Chen, Per-Simon Kildal, Charlie Orlenius, and Jan Carlsson. Channel sounding of loaded reverberation chamber for over-the-air testing of wireless devices: Coherence bandwidth versus average mode bandwidth and delay spread. *IEEE Antennas and Wireless Propagation Letters*, 8:678–681, 2009.

[25] Abdou Khadir Fall, Philippe Besnier, Christophe Lemoine, Maxim Zhadobov, and Ronan Sauleau. Determining the lowest usable frequency of a frequency-stirred reverberation chamber using modal density. In *2014 International Symposium on Electromagnetic Compatibility*, pages 263–268. IEEE, 2014.

[26] P. Besnier and B. Démoulin. *Electromagnetic Reverberation Chambers*. ISTE. Wiley, 2013. ISBN 9781118602157. URL https://books.google.co.uk/books?id=lSL8qSspsUYC.

[27] S.J. Boyes and Y. Huang. *Reverberation Chambers: Theory and Applications to EMC and Antenna Measurements*. Wiley, 2016. ISBN 9781118906248. URL https://books.google.co.uk/books?id=a-nGBwAAQBAJ.

[28] Siepel. *Recerberation Chambers - Handbook*. 2016.

[29] Department of Defence Interface Standard. Requirements for the con-

trol of electromagnetic inteference characteristics of susbsystems and equitment. URL http://quicksearch.dla.mil/qsDocDetails.aspx?ident_number=35789.

[30] Element Materials Technology. Rtca do-160 testing. URL https://www.element.com/aerospace/rtca-do-160-aerospace-environmental-testing.

[31] International Eectrotechnical Commision (IEC). *EMC-Part 4-21: Testing and measurement techniques — Reverberation chamber test methods*. 2003.

[32] David A Hill, Mark T Ma, Arthur R Ondrejka, Bill F Riddle, ML Crawford, and Robert T Johnk. Aperture excitation of electrically large, lossy cavities. *IEEE transactions on Electromagnetic Compatibility*, 36(3):169–178, 1994.

[33] Y Cui, G Wei, S Wang, and L Du. Fast calculation of reverberation chamber q-factor. *Electronics letters*, 48(18):1116–1117, 2012.

[34] Frank BJ Leferink. Using reverberation chambers for em measurements. In *Software, Telecommunications and Computer Networks (SoftCOM), 2010 International Conference on*, pages 1–5. IEEE, 2010.

[35] Comtest Engineering. Reverberation chambers. URL https://www.comtest.eu/solutions/anechoic-chambers/reverberation-chambers/.

[36] ZHAO Yang, WEI Guanghui, CUI Yaozhong, FAN Lisi, PAN Xiaodong, and WAN Haojiang. Reverberation chamber fast numerical calculation based on an improved fdtd mesh generation algorithm. *High Voltage Engineering*, 41 (3):1049–1056, 2015.

[37] Song Wang, Zhan Cheng Wu, Guang Hui Wei, Yao Zhong Cui, and Li Si Fan. A new method of evaluating reverberation chamber q-factor with experimental validation. *Progress In Electromagnetics Research*, 36:103–112, 2013.

[38] Christopher L Holloway, David A Hill, John M Ladbury, Perry F Wilson, Galen Koepke, and Jason Coder. On the use of reverberation chambers to

simulate a rician radio environment for the testing of wireless devices. *IEEE Transactions on Antennas and Propagation*, 54(11):3167–3177, 2006.

[39] Paolo Corona, Giuseppe Ferrara, and Maurizio Migliaccio. Reverberating chamber electromagnetic field in presence of an unstirred component. *IEEE Transactions on Electromagnetic Compatibility*, 42(2):111–115, 2000.

[40] Stephen O Rice. Mathematical analysis of random noise. *Bell Labs Technical Journal*, 23(3):282–332, 1944.

[41] W.C. Jakes. *Microwave mobile communications*. IEEE Press classic reissue. IEEE Press, 1974. ISBN 9780780310698. URL `https://books.google.co.uk/books?id=agpHAAAAYAAJ`.

[42] G.D. Durgin. *Space-time Wireless Channels*. Prentice Hall communications engineering and emerging technologies series. Prentice Hall PTR, 2003. ISBN 9780130656476. URL `https://books.google.co.uk/books?id=6sK3nYBoUmAC`.

[43] Marc Pous, Marco A Azpúrua, and Ferran Silva. Measurement and evaluation techniques to estimate the degradation produced by the radiated transients interference to the gsm system. *IEEE Transactions on Electromagnetic Compatibility*, 57(6):1382–1390, 2015.

[44] International Electrotechnical Commision (IEC). *EMC-Part 4-2: Testing and measurement techniques — Electrostatic discharge immunity test*. 2001.

[45] R.M. Buehrer. *Code Division Multiple Access (CDMA)*. Online access: IEEE (Institute of Electrical and Electronics Engineers) IEEE Morgan & Claypool Synthesis eBooks Library. Morgan & Claypool Publishers, 2006. ISBN 9781598290400. URL `https://books.google.co.uk/books?id=g3RRpOcLTb0C`.

[46] AY-C Wong and Victor CM Leung. Code-phase-shift keying: a power and bandwidth efficient spread spectrum signaling technique for wireless local area network applications. In *Electrical and Computer Engineering, 1997. Engi-*

neering Innovation: Voyage of Discovery. IEEE 1997 Canadian Conference on, volume 2, pages 478–481. IEEE, 1997.

[47] Axel Garcia-Pena, Daniel Salos, Olivier Julien, Lionel Ries, and Thomas Grelier. Analysis of the use of csk for future gnss signals. In *Proceedings of the 26th International Technical Meeting of The Satellite Division of the Institute of Navigation (ION GNSS 2013), Nashville TN*. Citeseer, 2013.

[48] J. Bray and C.F. Sturman. *Bluetooth 1.1: Connect Without Cables*. Pearson Education, 2001. ISBN 9780132441735.

[49] Asaduzzaman Abu, K Chidella Kishore, and F Mridha Muhammad. A time and energy efficient parking system using zigbee communication protocol. In *Proceedings of the IEEE SoutheastCon*, pages 1–5, 2015.

[50] Li Zhu, Yan Zhang, Bin Ning, and Hailin Jiang. Train-ground communication in cbtc based on 802.11 b: Design and performance research. In *Communications and Mobile Computing, 2009. CMC'09. WRI International Conference on*, volume 2, pages 368–372. IEEE, 2009.

[51] Ning Bin, Tang Tao, Qiu Kuan Min, and Gao Chun Hai. Cbtc (communication based train control): system and development.

[52] Piers Connor. Automatic train control. URL `http://www.railway-technical.com/signalling/automatic-train-control.html`.

[53] International Rail Journal. Automatic train operation takes to the main line, 2018. URL `https://www.railjournal.com/in_depth/automatic-train-control-takes-to-the-main-line`.

[54] International Association of Public Transport. A global bid for automation: Uitp observatory of automated metros confirms sustained growth rates for the coming years. URL `http://www.uitp.org/`.

[55] UNIFE. European rail traffic management system (ertms), 2009. URL `http://www.ertms.net/`.

[56] Kapsch CarrierCom. European Railway Traffic Management System - ERTMS.

[57] Office of Railand Road. Signals passed at danger. URL http://orr.gov.uk/rail/health-and-safety/infrastructure-safety/signals-passed-at-danger.

[58] Rail Safety and Standards Board Limited. Aws and tpws handbook, 2015. URL http://www.railway-technical.com/signalling/automatic-train-control.html.

[59] Network Rail. Signals explained, 2018. URL https://www.networkrail.co.uk/stories/signals-explained/.

[60] BBC-National Rail. Signal failure: The two words dreaded by every commuter, 2017.

[61] *XBee 868LP RF Modules*. Digi International Inc., 2012.

[62] Sanjay E. Sarma, Stephen A. Weis, and Daniel W. Engels. Rfid systems and security and privacy implications. In Burton S. Kaliski, çetin K. Koç, and Christof Paar, editors, *Cryptographic Hardware and Embedded Systems - CHES 2002*, pages 454–469, Berlin, Heidelberg, 2003. Springer Berlin Heidelberg. ISBN 978-3-540-36400-9.

[63] D. Sen, P. Sen, and A.M. Das. *RFID for Energy & Utility Industries*. PennWell, 2009. ISBN 9781593701055. URL https://books.google.co.uk/books?id=zSZHbngCGOOC.

[64] G. Miao, J. Zander, K.W. Sung, and S.B. Slimane. *Fundamentals of Mobile Data Networks*. Cambridge University Press, 2016. ISBN 9781316539125. URL https://books.google.co.uk/books?id=WKuzCwAAQBAJ.

[65] Rajeev Piyare and Seong-ro Lee. Performance analysis of xbee zb module based wireless sensor networks. *International Journal of Scientific & Engineering Research*, 4(4):1615–1621, 2013.

[66] Centre for Alternative Technology Charity Limited. URL http://info.cat.org.uk/solarcalculator/.

[67] Juha Meinilä, Pekka Kyösti, Tommi Jämsä, and Lassi Hentilä. Winner ii channel models. *Radio Technologies and Concepts for IMT-Advanced*, pages 39–92, 2009.

[68] Clive Kessell. Tram speed protection, 2019. URL https://www.railengineer.co.uk/2019/04/05/tram-speed-protection/.

[69] Olayemi Olawumi, Keijo Haataja, Mikko Asikainen, Niko Vidgren, and Pekka Toivanen. Three practical attacks against zigbee security: Attack scenario definitions, practical experiments, countermeasures, and lessons learned. In *Hybrid Intelligent Systems (HIS), 2014 14th International Conference on*, pages 199–206. IEEE, 2014.